



## Glass in the submarine section of the HSDP2 drill core, Hilo, Hawaii

**Edward Stolper**

*Division of Geological and Planetary Sciences, California Institute of Technology, MS 170-25, Pasadena, California 91125, USA (ems@gps.caltech.edu)*

**Sarah Sherman and Michael Garcia**

*Department of Geology and Geophysics, University of Hawaii at Manoa, 2525 Correa Road, Honolulu, Hawaii 96822, USA (bean@soest.hawaii.edu; garcia@soest.hawaii.edu)*

**Michael Baker and Caroline Seaman**

*Division of Geological and Planetary Sciences, California Institute of Technology, MS 170-25, Pasadena, California 91125, USA (mikeb@gps.caltech.edu)*

[1] The Hawaii Scientific Drilling Project recovered  $\sim 3$  km of basalt by coring into the flank of Mauna Kea volcano at Hilo, Hawaii. Rocks recovered from deeper than  $\sim 1$  km were deposited below sea level and contain considerable fresh glass. We report electron microprobe analyses of 531 glasses from the submarine section of the core, providing a high-resolution record of petrogenesis over ca. 200 Kyr of shield building of a Hawaiian volcano. Nearly all the submarine glasses are tholeiitic.  $\text{SiO}_2$  contents span a significant range but are bimodally distributed, leading to the identification of low- $\text{SiO}_2$  and high- $\text{SiO}_2$  magma series that encompass most samples. The two groups are also generally distinguishable using other major and minor elements and certain isotopic and incompatible trace element ratios. On the basis of distributions of high- and low- $\text{SiO}_2$  glasses, the submarine section of the core is divided into four zones. In zone 1 (1079– $\sim$ 1950 mbsl), most samples are degassed high- $\text{SiO}_2$  hyaloclastites and massive lavas, but there are narrow intervals of low- $\text{SiO}_2$  hyaloclastites. Zone 2 ( $\sim$ 1950–2233 mbsl), a zone of degassed pillows and hyaloclastites, displays a continuous decrease in silica content from bottom to top. In zone 3 (2233–2481 mbsl), nearly all samples are undegassed low- $\text{SiO}_2$  pillows. In zone 4 (2481–3098 mbsl), samples are mostly high- $\text{SiO}_2$  undegassed pillows and degassed hyaloclastites. This zone also contains most of the intrusive units in the core, all of which are undegassed and most of which are low- $\text{SiO}_2$ . Phase equilibrium data suggest that parental magmas of the low- $\text{SiO}_2$  suite could be produced by partial melting of fertile peridotite at 30–40 kbar. Although the high- $\text{SiO}_2$  parents could have equilibrated with harzburgite at 15–20 kbar, they could have been produced neither simply by higher degrees of melting of the sources of the low- $\text{SiO}_2$  parents nor by mixing of known dacitic melts of pyroxenite/eclogite with the low- $\text{SiO}_2$  parents. Our hypothesis for the relationship between these magma types is that as the low- $\text{SiO}_2$  magmas ascended from their sources, they interacted chemically and thermally with overlying peridotites, resulting in dissolution of orthopyroxene and clinopyroxene and precipitation of olivine, thereby generating high- $\text{SiO}_2$  magmas. There are glasses with CaO,  $\text{Al}_2\text{O}_3$ , and  $\text{SiO}_2$  contents slightly elevated relative to most low- $\text{SiO}_2$  samples; we suggest that these differences reflect involvement of pyroxene-rich lithologies in the petrogenesis of the CaO- $\text{Al}_2\text{O}_3$ -enriched glasses. There is also a small group of low- $\text{SiO}_2$  glasses distinguished by elevated  $\text{K}_2\text{O}$  and CaO contents; the sources of these samples may have been enriched in slab-derived fluid/melts. Low- $\text{SiO}_2$  glasses from the top of zone 3 (2233–2280 mbsl) are more alkaline, more fractionated, and incompatible-element-enriched relative to other glasses from zone 3. This excursion at the top of zone 3, which is abruptly overlain by more silica-rich tholeiitic magmas, is reminiscent of the end of Mauna Kea shield building higher in the core.

**Components:** 46,680 words, 24 figures, 3 tables.

**Keywords:** basaltic glass; Hawaii; HSDP; Mauna Kea; petrogenesis.

**Index Terms:** 3640 Mineralogy and Petrology: Igneous petrology; 3655 Mineralogy and Petrology: Major element composition; 8439 Volcanology: Physics and chemistry of magma bodies.

**Received** 19 March 2003; **Revised** 5 March 2004; **Accepted** 22 April 2004; **Published** 30 July 2004.

Stolper, E., S. Sherman, M. Garcia, M. Baker, and C. Seaman (2004), Glass in the submarine section of the HSDP2 drill core, Hilo, Hawaii, *Geochem. Geophys. Geosyst.*, 5, Q07G15, doi:10.1029/2003GC000553.

**Theme:** Hawaii Scientific Drilling Project      **Guest Editors:** Don DePaolo, Ed Stolper, and Don Thomas

## 1. Introduction

[2] An important feature of the lithologic section recovered by the Hawaii Scientific Drilling Project in 1999 is that its lower ~2000 m is submarine (see summary in *Hawaii Scientific Drilling Project* [2001]). Consequently, this lower part of the section contains considerable glass, reflecting rapid cooling of magmatic liquids when they come in contact with seawater. Furthermore, due to the generally low level of alteration of the core, fresh glass can usually be recovered from any given unit. From the perspective of petrological and geochemical investigations, the availability of fresh glass spanning the lower 2000 m of the HSDP2 core is advantageous in that in contrast to investigations of whole rocks, with their accumulations of phenocrysts and xenocrysts and their susceptibility to alteration, fresh glasses provide unambiguous information on the compositions of magmatic liquids. (We use the acronym HSDP to refer to the Hawaii Scientific Drilling Project. The pilot hole, or HSDP1, was drilled in 1993. The 1999 drilling is referred to as HSDP2.) Such liquid compositions provide the primary information on which petrogenetic hypotheses are constructed and tested, so studies of submarine glasses from this drill core are an important source of data on petrogenetic processes affecting erupted Hawaiian magmas over a substantial fraction of the lifetime of a single volcano. Since glass is available essentially continuously in the submarine section, it provides a particularly high-resolution record of petrogenesis. In the context of the integrated HSDP project, this high resolution record provides the framework for interpretation of the less frequently sampled whole rock samples that have been subjected to a wide range of high-precision chemical and isotopic analyses.

[3] This paper focuses on electron microprobe analyses of 531 glasses from the submarine section of the HSDP2 core, presumed to represent output from the Mauna Kea volcano [*Hawaii Scientific Drilling Project*, 2001]. There are actually two independent data sets, one from the University of Hawaii and one from Caltech, but in the interests of a coherent presentation, we have chosen to report them in a single publication. Consequently, there are considerable data and petrogenetic information, amounting to an unprecedented time series of the evolution of a Hawaiian volcanic system.

## 2. Samples

[4] Glasses were analyzed from each of the four rock types identified in the submarine section of the drill core (see Figure 1) [*Hawaii Scientific Drilling Project*, 2001]: hyaloclastites, massive basalts, pillow basalts, and intrusives. Interlayered hyaloclastites and massive basalts dominate the upper part of the submarine section from the subaerial-submarine transition at 1079 mbsl to a depth of 1883 mbsl. The first intrusive unit appears at 1883 mbsl, and from this depth to the bottom of the drill core, pillow basalts and hyaloclastites are interlayered with relatively thin intrusive units cross-cutting both pillow and hyaloclastite units.

[5] The glasses analyzed in this study represent two independent sampling and analytical programs. Most of the first suite was collected at the drill site by the core loggers. As each box of core (containing ~10 feet of core) was described petrographically, the logger selected one or two fresh, ~0.1–1 cm glass fragments from representative, interesting, and/or most easily sampled parts of the

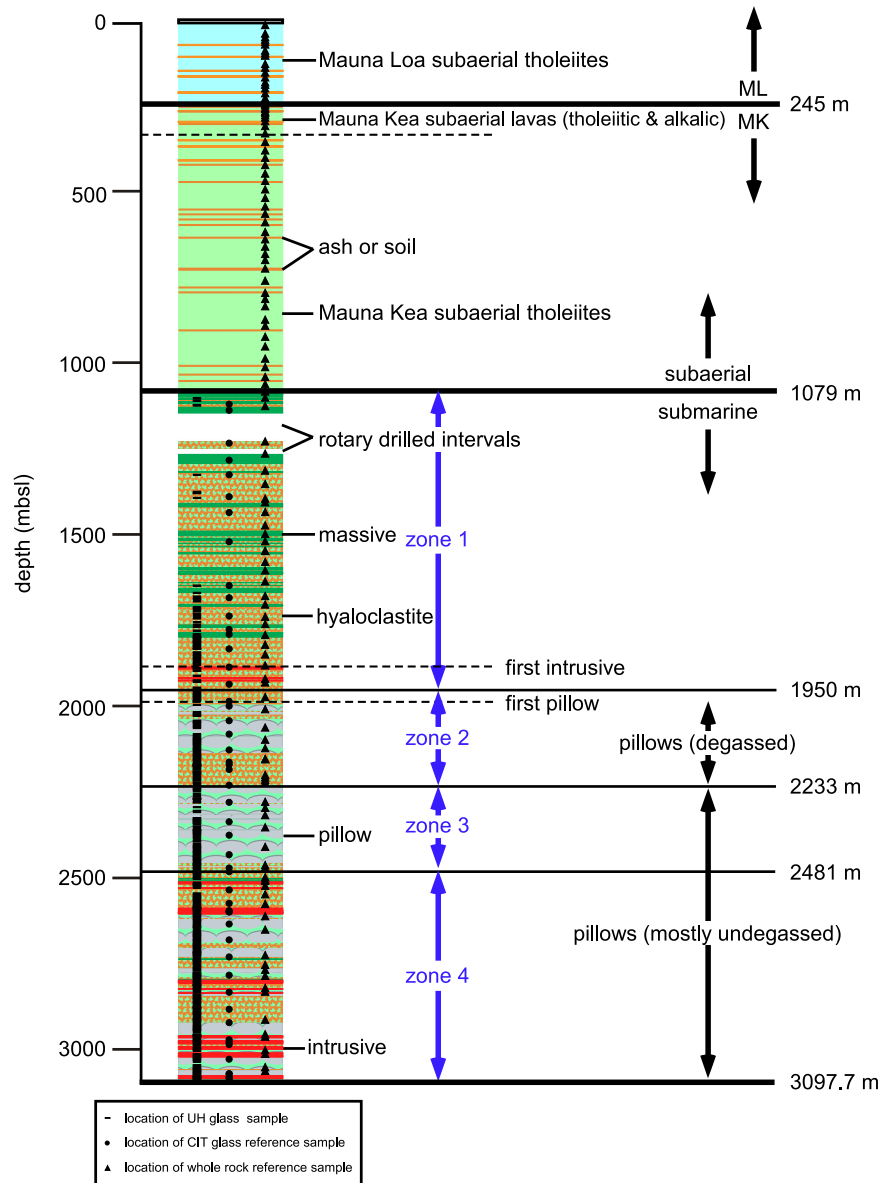


**Figure 1.** Simplified lithologic column of the HSDP2 core hole [after *Hawaii Scientific Drilling Project*, 2001]. The depths of the individual glass samples analyzed at the University of Hawaii and Caltech are indicated, as are the depths of samples in the whole rock reference suite. Key depths are also shown: the Mauna Loa-Mauna Kea boundary; the occurrence of alkalic lavas at the top of the Mauna Kea section; the subaerial-submarine boundary; the first occurrences of intrusives and pillows; and the divisions of the submarine section into zones 1–4 (see section 4.2).

core. These samples were sent to the University of Hawaii for electron microprobe analysis. The on-site sample suite was collected in a reconnaissance fashion before the overall stratigraphy of the core was known. Consequently, some sections of the core were resampled at Caltech and the glasses sent to the University of Hawaii to resolve questions about the precise locations and unit types of certain samples, and other sections were assigned revised unit types (e.g., changed from pillow to

intrusive or from hyaloclastite to intrusive breccia) on the basis of reexamination of the originally sampled section. In particular, some units (e.g., U0343, sections a–e) that were originally described as pillow basalts in the deeper parts of the submarine section are now believed to contain thin (1–10 cm) fingers of intrusive units between some of their pillow margins. These intrusive fingers have lithologies and major element chemical compositions distinct from the surrounding pillows

(e.g., SR0969-5.1 versus SR0969-5.0 and SR0975-4.95 versus SR0975-5.0), but are sufficiently thin that they were not identified at the time the samples were collected on site. In addition, some lithic fragments and glass in units identified as hyaloclastites near intrusives show lithologies and/or major element chemical compositions similar to the nearby intrusives, suggesting that they may be related to the intrusives; indeed, some of these units may be actually intrusive breccias (e.g., SR0857-20.2 from U0308c). Complexities and uncertainties of this sort are pointed out in the footnotes to Table 1.

[6] In all, 475 samples from this first suite were analyzed at the University of Hawaii. Their distribution within the core is shown in Figure 1. From these glasses, 91 were also analyzed by infrared spectroscopy for water at Caltech, and of these, 50 were also analyzed for carbon dioxide [Seaman *et al.*, 2004].

[7] The second suite, comprising 56 samples, was collected and analyzed at Caltech after drilling was completed. The principal objective was to create a reference suite of glasses (52 samples) comparable to the whole rock reference suite distributed for chemical and isotopic analyses. Most of the glass reference samples were chosen to be roughly evenly spaced ( $\sim 50$  m), and every effort was made to produce clean, fresh glass separates of 0.5–1 g. We also collected reference samples that on that basis of the stratigraphy of the core, whole rock analyses or the analyses of the on-site glass collections would be desirable to have in larger quantities. Samples for the reference suite were coarsely crushed to  $\sim 1$ –2 mm in a piston mortar, washed in deionized water, dried for several hours in a 100°C drying oven, and sorted to eliminate visibly altered fragments and fragments containing crystals. In addition, olivine separates from a number of these samples were prepared. In the case of hyaloclastite samples, all glass fragments that make up each reference sample are from the same glassy clast. In addition to the reference samples, we also collected chips from four hyaloclastites in the 1765–1810 mbsl interval for analysis at Caltech in order to extend the sampling of this “excursion” (see section 7). Electron microprobe analyses were done at Caltech along with infrared spectroscopic analyses for water and carbon dioxide [Seaman *et al.*, 2004]. Samples from this reference suite were also analyzed by laser-ablation ICP-MS at Boston

University (M. B. Baker *et al.*, Trace elements in submarine glasses from the HSDP2 core, manuscript in preparation, 2004) (hereinafter referred to as Baker *et al.*, manuscript in preparation, 2004a) and by ion microprobe for carbon at Lawrence Livermore National Laboratory [Seaman *et al.*, 2004]. Aliquots of these samples were distributed to the École Normale Supérieure de Lyon and the University of California, Berkeley for selected isotopic analyses [Bryce and DePaolo, 2000; Blichert-Toft *et al.*, 2003].

[8] Table 1 presents a complete list of the samples and analyses from this study. In addition to the 531 samples analyzed by electron microprobe, Table 1 also lists 25 additional samples that were analyzed for H<sub>2</sub>O and CO<sub>2</sub> by infrared spectroscopy but not analyzed by electron microprobe [Seaman *et al.*, 2004].

### 3. Analytical Techniques

#### 3.1. University of Hawaii

[9] Glass compositions were measured at the University of Hawaii using a five-spectrometer Cameca SX-50 electron microprobe with an accelerating voltage of 15 keV, a current of 10 nA, and a 15  $\mu$ m beam. Smithsonian VG2 and A99 glass standards were used to calibrate the major elements, and mineral standards were used to calibrate the minor elements (orthoclase for K<sub>2</sub>O, apatite for P<sub>2</sub>O<sub>5</sub>, and troilite for S). Glass standards were analyzed before and after the samples. Na<sub>2</sub>O was analyzed first in order to minimize Na loss during analyses. Counting times for the major elements were 60–130 s, except for Na<sub>2</sub>O (40 s). Counting times for minor elements were 50 s for K<sub>2</sub>O, 110 s for P<sub>2</sub>O<sub>5</sub> and 120 s for S. A PAP-ZAF matrix correction was applied to all analyses. Each analysis listed in Table 1 represents an average of 5–15 points per sample.

#### 3.2. Caltech

[10] Glass compositions were determined with a five-spectrometer JEOL 733 electron microprobe at Caltech using a 15 keV accelerating voltage, a 10 nA beam current, a 10  $\mu$ m spot size, and glass, mineral, and oxide standards (Si, VG-2; Ti, TiO<sub>2</sub>; Al, Ca, synthetic anorthite; Cr, Cr<sub>2</sub>O<sub>3</sub>; Fe, synthetic fayalite; Mn, synthetic Mn-olivine; Mg, synthetic forsterite; Na, Amelia albite; K, Asbestos microcline; P, Durango apatite; S, pyrite). Peaks were counted for 30 s, high and low backgrounds were counted for 15 s, and data were reduced using a

**Table 1 (Representative Sample).** Major Element and Volatile Concentrations<sup>a</sup> (The full Table 1, which also includes P<sub>2</sub>O<sub>5</sub>, S, H<sub>2</sub>O total, H<sub>2</sub>O molecular, CO<sub>2</sub> (IR), CO<sub>2</sub> (SIMS), Cl, and F, is available in the HTML version of this article at <http://www.g-cubed.org>)

Sample	Depth, mbsl	Unit	Rock Type	Footnote	SiO <sub>2</sub>	TiO <sub>2</sub>	Al <sub>2</sub> O <sub>3</sub>	FeO*	MnO	MgO	CaO	Na <sub>2</sub> O	K <sub>2</sub> O
SR0458-0.80	1102.9	U0180	hyaloclastite		51.13	2.65	13.51	11.71		6.46	11.12	2.27	0.38
SR0463-0.40	1109.6	U0181	massive		50.77	2.65	13.47	11.75		6.48	11.04	2.26	0.38
SR0465-2.50	1110.9	U0183	massive		51.28	2.76	13.44	11.79		6.38	10.82	2.21	0.37
SR0471-1.10	1119.8	U0184	hyaloclastite	b	51.87	2.58	13.37	11.62	0.18	6.36	10.93	2.24	0.38
SR0475-0.40	1126.4	U0185	massive		51.15	2.76	13.53	11.47		6.50	10.97	2.21	0.38
SR0475-0.40	1126.4	U0185	massive		51.55	2.47	14.98	10.62		5.90	11.16	2.34	0.35
SR0485-0.90	1138.7	U0187	hyaloclastite	b	51.74	2.59	13.29	11.55	0.16	6.51	10.89	2.31	0.39
SR0495-0.90	1234.5	U0190	hyaloclastite	b	51.83	2.73	13.37	11.44	0.17	6.21	10.91	2.30	0.46
SR0508-8.00	1283.5	U0191	massive										
SR0508-8.60	1283.7	U0192	hyaloclastite	b	51.91	2.60	13.67	10.93	0.17	6.45	11.05	2.31	0.43
SR0517-8.40	1310.8	U0195	massive										
SR0518-6.30	1313.2	U0196	hyaloclastite										
SR0523	1328.3	U0196	hyaloclastite		51.75	2.80	13.07	12.04	0.17	6.01	10.45	2.32	0.45
SR0523-6.80	1328.9	U0196	hyaloclastite	b, n	52.00	2.34	13.98	10.91		6.55	11.22	2.23	0.36
SR0539-4.30	1376.8	U0198	hyaloclastite		49.48	2.79	14.59	11.18		7.06	11.57	2.53	0.45
SR0540-6.80	1379.2	U0198	hyaloclastite		49.50	2.65	14.48	11.06		7.01	11.50	2.47	0.44
SR0541-8.10	1382.6	U0198	hyaloclastite		49.71	2.81	14.59	11.21		7.04	11.58	2.53	0.44
SR0542-7.50	1385.5	U0198	hyaloclastite										
SR0544-5.30	1391.2	U0198	hyaloclastite	b	49.50	2.88	14.20	11.15	0.17	7.05	11.49	2.60	0.46
SR0546-2.85	1396.0	U0198	hyaloclastite		49.27	3.01	14.36	11.32		6.81	11.61	2.56	0.47
SR0550-0.00	1406.1	U0199	massive										
SR0556-2.70	1421.2	U0202	hyaloclastite										
SR0561-3.30	1436.9	U0202	hyaloclastite	b	49.85	2.77	14.08	11.13	0.17	6.89	11.51	2.51	0.45
SR0572-7.30	1469.9	U0202	hyaloclastite										
SR0582-1.90	1494.9	U0205	massive										
SR0595-6.40	1523.5	U0214	hyaloclastite	b	51.51	3.29	13.00	12.24	0.16	5.93	10.28	2.33	0.53
SR0619-3.50	1570.5	U0218	hyaloclastite										
SR0631-4.30	1607.0	U0224	massive										
SR0646-6.30	1652.1	U0229	hyaloclastite		51.05	3.39	13.15	12.03		5.95	10.23	2.39	0.57
SR0646/647	1653.2	U0231	hyaloclastite	b, n	51.55	3.32	13.05	11.99	0.18	5.85	10.35	2.42	0.58
SR0653-0.75	1671.2	U0238	hyaloclastite		50.84	2.41	13.66	10.89		7.29	11.10	2.24	0.33
SR0657-8.90	1685.2	U0238	hyaloclastite		50.17	2.97	13.93	10.84		6.63	11.21	2.37	0.56
SR0658-0.90	1685.8	U0238	hyaloclastite	b	50.59	3.13	13.86	10.84	0.16	6.49	11.45	2.42	0.57
SR0659-5.50	1690.3	U0238	hyaloclastite		50.38	2.90	13.90	10.89		6.66	11.34	2.41	0.58
SR0660-1.00	1692.0	U0238	hyaloclastite		50.40	2.95	13.90	10.89		6.64	11.45	2.38	0.58
SR0661-5.20	1696.3	U0238	hyaloclastite		50.27	3.07	13.96	10.91		6.70	11.36	2.43	0.54
SR0668-2.25	1715.8	U0238	hyaloclastite		50.92	3.07	14.00	10.95		6.70	11.45	2.41	0.55
SR0668-9.95	1718.2	U0241	hyaloclastite		50.42	3.03	14.02	10.90		6.80	11.41	2.38	0.53
SR0669-2.50	1719.0	U0241	hyaloclastite		50.84	3.04	13.97	10.72		6.70	11.41	2.37	0.51
SR0672-0.95	1727.8	U0242	hyaloclastite		50.70	3.02	13.61	11.26		6.45	10.93	2.33	0.53
SR0674-3.70	1734.9	U0242	hyaloclastite		51.35	2.68	13.58	11.25		6.55	10.88	2.31	0.39
SR0675-8.80	1739.4	U0243	hyaloclastite	b	51.87	2.55	13.62	11.09	0.20	6.45	11.05	2.29	0.38

modified ZAF procedure (CITZAF [Armstrong, 1988]). In general, each probe mount consisted of 5–6 pieces of glass ( $\leq 1$  mm in size) and three analyses were collected on each of 3–4 of the pieces. Four analyses each of two USGS prepared glasses (BHVO-2g and BCR-2g; lacking an accepted analysis for each glass, we used the accepted compositions for the two powders; see [http://minerals.cr.usgs.gov/geo\\_chem\\_stand/](http://minerals.cr.usgs.gov/geo_chem_stand/)) and VG-2 [Jarosewich *et al.*, 1979] were collected at the beginning, during (generally after three to five unknowns had been analyzed; VG-2 was sometimes passed over), and at the end of each analytical session. The mean BHVO-2g composition from each session coupled with the accepted composition of this glass were used to reprocess all the k-ratios except those of S for all the analyses from that session; the mean VG-2 composition was used to reprocess the S data. The reprocessed glass compositions were averaged, and the mean compositions are listed in Table 1; individual analyses with oxide sums  $<98$  and  $>100.4\%$  (excluding  $H_2O$ ) were not included in the averages. (All concentrations are in weight percent, unless otherwise indicated.)

[11] With one exception (SR0979-1.3; this sample is a pillow margin containing an “intrusive finger”), analyses from different chips of the same sample are identical within analytical uncertainty. Glass from one of the analyzed chips

of SR0979-1.3 differs from the three other analyzed chips (5.6 versus 7.6% MgO, 51.7 versus 49.1%  $SiO_2$ ). This compositional difference is consistent with the petrographic observation that the low-MgO, high- $SiO_2$  chip contains microphenocrysts of olivine, plagioclase, and clinopyroxene, while the other chips contain only olivine microphenocrysts; it may also reflect the sampling of both the pillow and the intrusive finger. Only the average of the analyses of the higher-MgO chips is reported in the body of Table 1; the low-MgO analysis is listed in a footnote to Table 1 but is not shown in the figures or included in the various counts of samples by lava type and compositional group.

[12] The mean BCR-2g and VG-2 glass compositions based on data from all the analytical sessions are listed in Table 2 along with the sample standard deviations for each oxide. For both glasses, the mean concentrations for most oxides overlap with the accepted values at the  $1\sigma$  level. The absolute deviation between the mean MgO concentration and the accepted value for VG-2 is 0.21%, well outside the  $1\sigma$  value of 0.05%, but the deviation in MgO for BCR-2g is only 0.01%; Clague *et al.* [1990] and Dixon *et al.* [1991] report mean MgO values for VG-2 that overlap with our analyzed MgO concentration at the  $1\sigma$  level. Percent errors for each oxide (i.e.,  $100 \times 1\sigma/\text{mean concentration}$ ) based on 73 BCR-

#### Notes to Table 1.

<sup>a</sup> Unless otherwise indicated, samples are from the University of Hawaii glass suite collected during core logging in 1999. All concentrations are in weight percent, except  $CO_2$  (ppm). Numbers in parentheses for the  $H_2O$ , molecular  $H_2O$ , and  $CO_2$  analyses are  $1\sigma$  based on multiple analyses. Samples without reported errors were analyzed only once. A dash (“-”) indicates a measured concentration nominally  $<0$ .

<sup>b</sup> Samples are part of a Caltech glass reference suite collected during the summer of 2000 after core logging had been completed and revisions had been made. See text for description of sample preparation.

<sup>c</sup> Samples were collected at Caltech and analyzed at the University of Hawaii (2000–2002) to clear up ambiguity about samples collected on site in 1999.

<sup>d</sup> Rock type is different than that listed in core log, but unit number matches original lithologic unit assigned during core logging. Most of these samples are thin (2–10 cm) intrusive units that were not recognized as such when the core was logged.

<sup>e</sup> Samples were collected and analyzed at Caltech but are not part of the glass reference suite.

<sup>f</sup> CaO-K<sub>2</sub>O-rich glasses (see section 7 of the text).

<sup>g</sup> Glasses from 2233–2280 mbsl excursion (see section 6 of the text).

<sup>h</sup> CaO-Al<sub>2</sub>O<sub>3</sub>-rich glasses (MgO  $\geq 7\%$ ; both original glass compositions and those adjusted to be in equilibrium with Fo90.5 olivine form a coherent group on plots of CaO-SiO<sub>2</sub> and Al<sub>2</sub>O<sub>3</sub>-SiO<sub>2</sub>; see section 4.6 of the text).

<sup>i</sup> Suspected of alteration due to elevated Cl or molecular  $H_2O$  content; see Seaman *et al.* [2004].

<sup>j</sup> This sample has an anomalous Na<sub>2</sub>O content, attributed to alteration (see Figure 6g and Seaman *et al.* [2004]). It has been left off most figures.

<sup>k</sup> One glass chip from this sample has a distinct composition (see section 3.2 of the text):  $SiO_2$  51.67;  $TiO_2$  3.26;  $Al_2O_3$  13.16;  $FeO^*$  12.66; MnO 0.21; MgO 5.61; CaO 10.25; Na<sub>2</sub>O 2.38; K<sub>2</sub>O 0.55; P<sub>2</sub>O<sub>5</sub> 0.40; S 0.009.

<sup>l</sup> Detectable molecular  $CO_2$  based on absorption at  $2350\text{ cm}^{-1}$ .

<sup>m</sup> “Pillow breccia”; see *Hawaii Scientific Drilling Project* [2000].

<sup>n</sup> Box disturbed during handling, depth from midpoint of box.

<sup>o</sup> Close to intrusive.

<sup>p</sup> Glass from intrusive margin, originally logged as massive.

<sup>q</sup> Originally logged as hyaloclastite.

<sup>r</sup> Finger of intrusion at SR0859-1.00 not noted on original log; originally logged as pillow.

<sup>s</sup> Two lobes of aphyric basalt between SR0864-15.80 and 17.20 not noted on original log; originally logged as pillow.

<sup>t</sup> Originally logged as pillow.

<sup>u</sup> Originally logged as pillow basalt; no unit number assigned.

<sup>v</sup> Originally logged as pillow breccia (footnote m).

**Table 2.** Interlaboratory Comparison of Microprobe Data<sup>a</sup>

Sample (Number of Analyses)	Depth, mbsl	SiO <sub>2</sub>	TiO <sub>2</sub>	Al <sub>2</sub> O <sub>3</sub>	FeO*	MgO	CaO	Na <sub>2</sub> O	K <sub>2</sub> O	P <sub>2</sub> O <sub>5</sub>	S	Sum
SR0763-14.90 CIT (12)	2131.4	50.32(26)	2.59(8)	14.10(6)	10.96(13)	6.80(6)	11.88(13)	2.36(5)	0.39(2)	0.24(5)	0.015(8)	99.63
SR0763-14.90 UH (6)	2131.5	50.46(13)	2.49(8)	14.21(10)	10.78(12)	6.89(10)	11.92(4)	2.37(4)	0.36(2)	0.191(12)	0.021(7)	99.69
SR0831-2.30 CIT (12)	2438.4	49.30(23)	2.68(14)	14.18(9)	11.49(14)	6.97(10)	11.54(10)	2.50(5)	0.41(2)	0.23(4)	0.062(14)	99.36
SR0831-2.30 UH (10)	2438.5	49.63(6)	2.69(5)	14.22(5)	11.18(6)	6.98(5)	11.57(9)	2.50(4)	0.39(2)	0.20(2)	0.058(9)	99.42
SR0866-5.30 CIT (12)	2639.7	51.33(18)	2.69(17)	13.50(5)	10.94(15)	6.84(7)	11.13(10)	2.30(5)	0.42(2)	0.24(3)	0.092(18)	99.45
SR0866-5.30 UH	2639.6	51.38	2.62	13.56	11.02	6.82	11.24	2.26	0.41	0.22	0.098	99.63
SR0907-2.80 CIT (9)	2789.4	51.59(28)	2.85(11)	13.18(12)	12.36(8)	6.06(5)	10.46(5)	2.31(5)	0.47(2)	0.27(5)	0.060(15)	99.62
SR0907-2.80 UH (5)	2789.5	51.16(13)	2.83(7)	13.43(9)	12.23(13)	6.11(4)	10.64(4)	2.28(2)	0.42(3)	0.23(2)	0.078(5)	99.41
SR0949-8.20 CIT (11)	2979.7	49.43(14)	2.80(19)	14.18(7)	11.62(9)	6.63(9)	11.76(10)	2.49(4)	0.42(2)	0.26(4)	0.10(1)	99.27
SR0949-8.20 UH	2979.9	49.20	2.77	14.35	11.50	6.58	11.90	2.41	0.41	0.23	0.11	99.46
VG-2 CIT (57)		50.83(16)	1.85(9)	13.94(9)	11.84(14)	6.92(5)	11.14(10)	2.66(5)	0.20(2)	0.21(4)	0.131(13)	99.96
BCR-2g CIT (73)		54.75(35)	2.28(12)	13.63(12)	12.50(21)	3.62(5)	7.19(8)	3.12(11)	1.84(4)	0.36(5)		99.50

<sup>a</sup> Abbreviations: CIT, Caltech; UH, University of Hawaii; mbsl, meters below sea level. Values in parentheses after each oxide value are sample standard deviations; read 50.32(26) as 50.32 ± 0.26; FeO\* is all Fe as FeO. Number of analyses and oxide standard deviations are not available for SR0866-5.30 UH and SR0949-8.20 UH. Mean MnO values for VG-2 and BCR-2g are 0.21(3) and 0.21(3), respectively. Given the CIT operating conditions and counting time, sulfur in BCR-2g was below the microprobe detection limit.

2g analyses are 0.64, SiO<sub>2</sub>; 5.3, TiO<sub>2</sub>; 0.88, Al<sub>2</sub>O<sub>3</sub>; 1.7, FeO\* (i.e., total Fe as FeO), 14.3, MnO; 1.4, MgO; 1.1, CaO; 3.5, Na<sub>2</sub>O; 2.2, K<sub>2</sub>O; 13.9, P<sub>2</sub>O<sub>5</sub>.

### 3.3. Interlaboratory Comparison

[13] Five sets of pillow glasses collected independently from the same pillow margins (typically a 1–4 cm-thick glassy rind) from nominally identical depths were analyzed by both laboratories (SR0763-14.9, SR0831-2.3, SR0866-5.3, SR0907-2.8, and SR0949-8.2; see Table 2). In the three cases where the standard deviations are available for the University of Hawaii analyses, the mean concentrations for each oxide in the two sets of analyses for each sample overlap at the 1σ level, except SiO<sub>2</sub> and FeO\* in SR0831-2.3 and SiO<sub>2</sub>, Al<sub>2</sub>O<sub>3</sub>, and CaO in SR0907-2.8, all of which overlap at the 2σ level.

## 4. High- and Low-Silica Magma Types

### 4.1. Definition of the High- and Low-Silica Magma Types

[14] We begin our examination of chemical variations in the HSDP2 glass suite with a subdivision of the glasses into two groups (Figure 2). The first group, which we refer to as the low-SiO<sub>2</sub> group, is shown in all figures as blue symbols; it is defined by SiO<sub>2</sub> < 50%. The second, referred to as the high-SiO<sub>2</sub> group, is shown as pink symbols in all figures; it is defined by SiO<sub>2</sub> ≥ 50%. The high-SiO<sub>2</sub> group comprises 69% (367 of 531) of the glasses; on the basis of the spacing of the samples, we estimate that an essentially indistinguishable fraction of the submarine volume of the core (70%) is made up of high-SiO<sub>2</sub> material. The MgO contents of the two groups overlap, but the average MgO content of the high-SiO<sub>2</sub> group (6.75 ± 0.51 (1σ)%) is lower than that of the low-SiO<sub>2</sub> group (7.41 ± 0.68 (1σ)%). Comparison of histograms of MgO contents (not shown) demonstrates that the distribution of MgO contents in the low-SiO<sub>2</sub> group is shifted to higher MgO relative to the high-SiO<sub>2</sub> group.

[15] Figure 3 shows SiO<sub>2</sub> contents versus H<sub>2</sub>O and S contents of all analyzed glasses. Full discussion and interpretation of these volatile components is presented in a companion paper [Seaman *et al.*, 2004], but it is well known that H<sub>2</sub>O and S degas significantly from Hawaiian liquids only at relatively low total pressures such as those pertaining to subaerial or shallow submarine environments or to high-level magma chambers connected to the

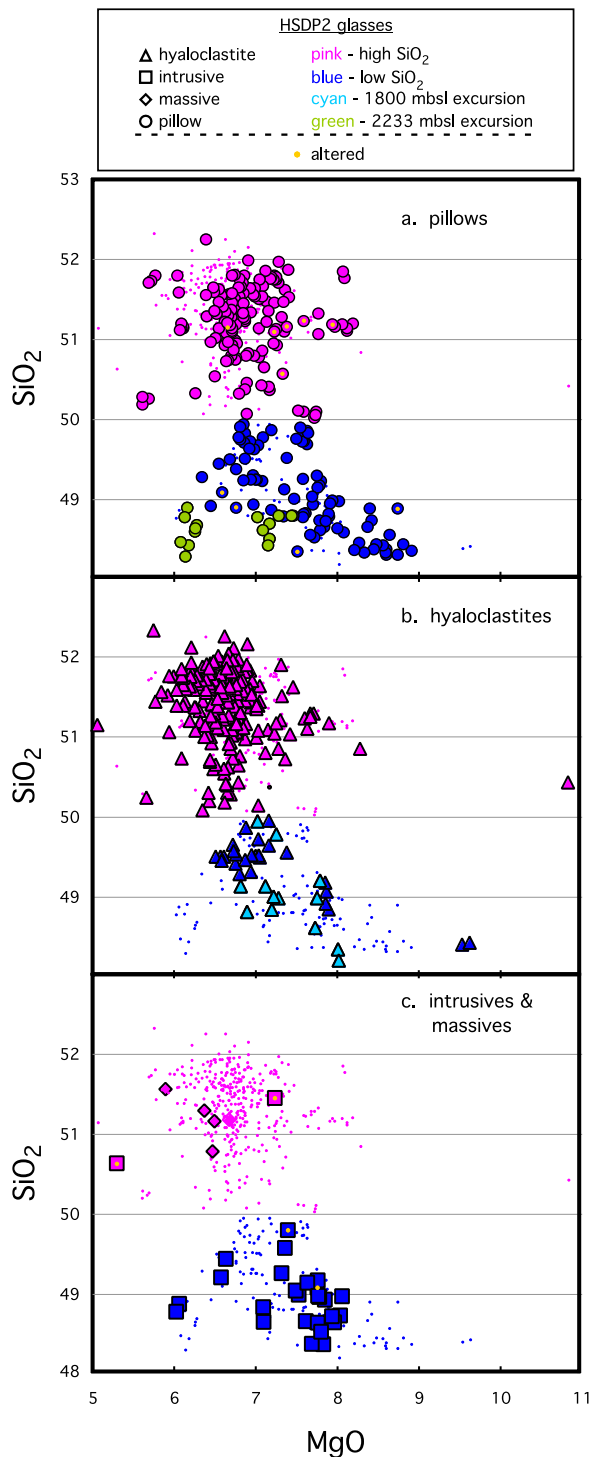


**Figure 2.** MgO versus SiO<sub>2</sub> (wt.%) for glasses from the HSDP2 core: (a) pillow-rim glasses; (b) hyaloclastite glasses; (c) glasses from intrusive and massive units. In each panel, the small dots are all samples not assigned to the group being emphasized with the large symbols. Altered samples, based on elevated molecular water or Cl contents [Seaman *et al.*, 2004], are indicated by superimposed gold-colored dots.

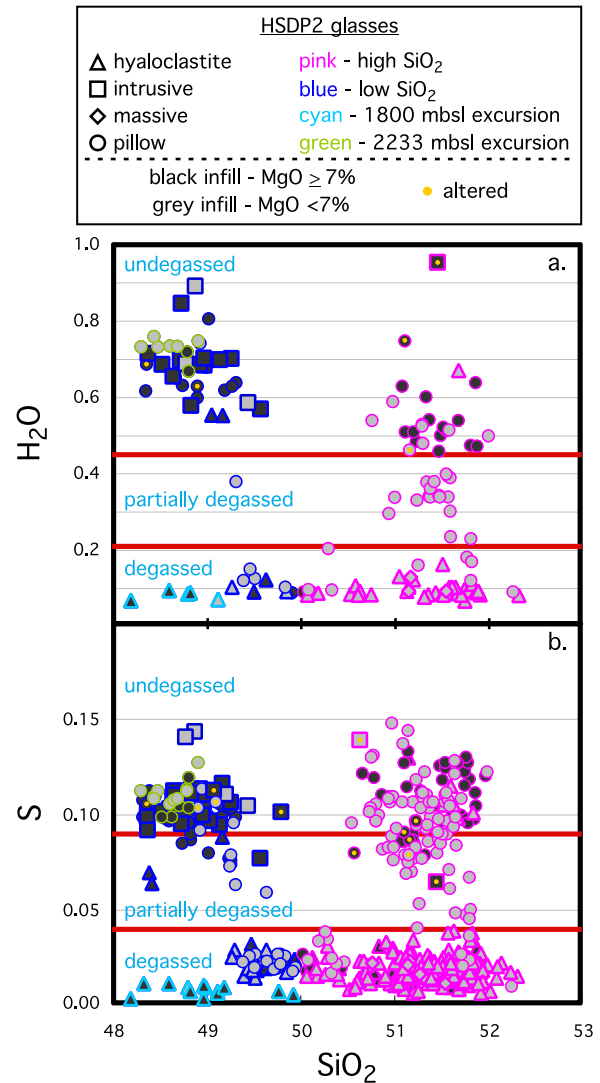


**Figure 3.** (a) H<sub>2</sub>O and (b) S contents (wt.%) versus SiO<sub>2</sub> (wt.%) for HSDP2 glasses. The definitions of undegassed, partially degassed, and degassed samples are given in section 4.1. Symbol shapes indicate rock types, and colors indicate the chemical group to which the glasses are assigned (see the legend). Gray-filled symbols represent glasses with <7% MgO; black-filled symbols represent glasses with ≥7% MgO. Altered samples, based on elevated molecular water or Cl contents [Seaman *et al.*, 2004], are indicated by superimposed gold-colored dots.

atmosphere. For example, on the basis of the results of Dixon and Stolper [1995], basaltic magmas with ~0.7% H<sub>2</sub>O (i.e., corresponding roughly to the upper end of the distribution of water contents shown in Figure 3) would only degas significant amounts of water at pressures less than ~45 bars; samples with 0.5 and 0.2% H<sub>2</sub>O would only degas significant amounts of water at pressures less than ~25 and 5 bars, respectively.

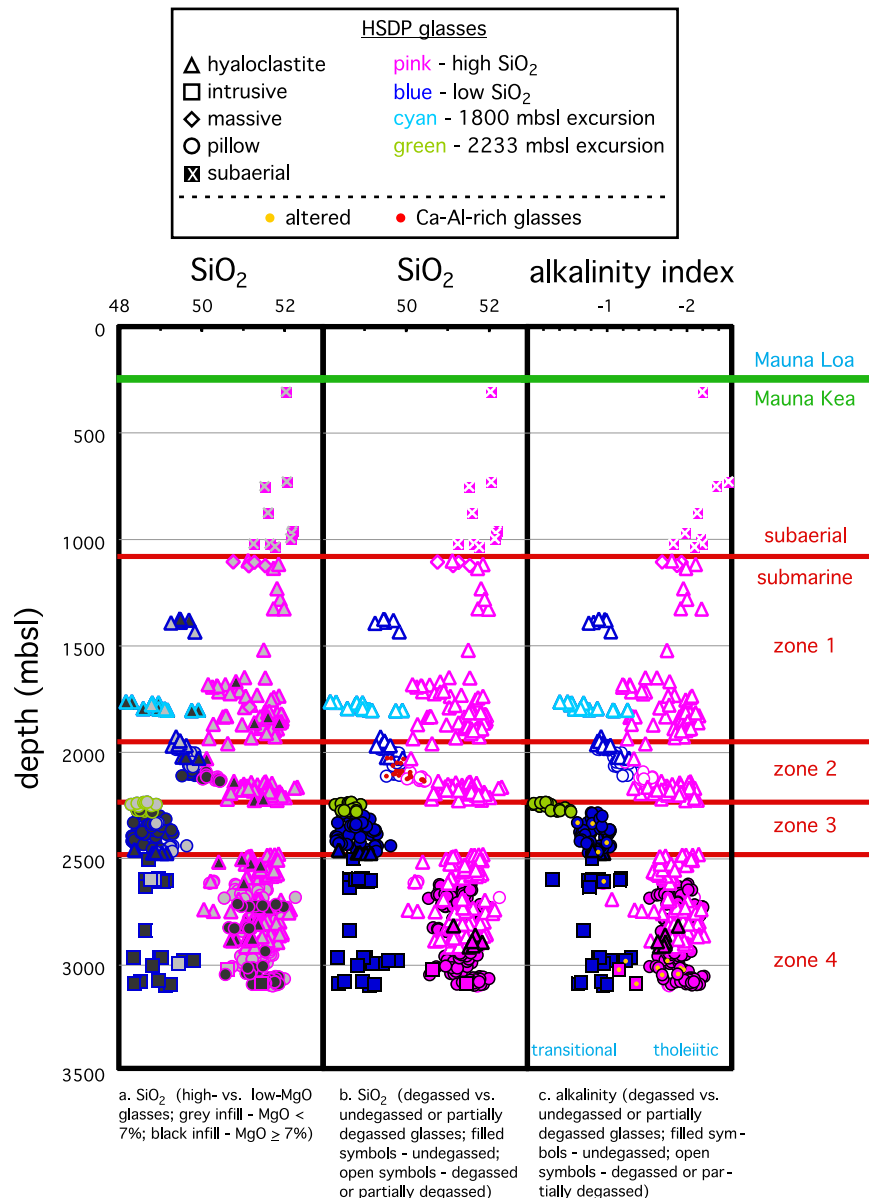


**Figure 4.** (a and b) SiO<sub>2</sub> (wt.%) and (c) alkalinity versus depth (mbsl) for glasses from the HSDP2 core and the HSDP pilot hole [Garcia, 1996]. The horizontal green line shows the position of the unconformity between Mauna Loa and Mauna Kea subaerial lavas. Horizontal red lines show divisions of the core into subaerial samples and zones 1–4 (see section 4.2). Symbol shapes indicate rock types, and colors indicate the chemical group to which the glasses are assigned (see the legend). In Figure 4a, gray-filled symbols represent glasses with <7% MgO; black-filled symbols represent glasses with ≥7% MgO. Filled symbols in Figures 4b and 4c represent partially degassed or undegassed glasses; open symbols represent degassed glasses; see section 4.1 for the definitions of degassed versus partially degassed and undegassed glasses. In Figure 4b, superimposed red dots indicate Ca-Al-rich glasses (see section 4.6). In Figure 4c, superimposed gold-colored dots indicate altered samples [Seaman *et al.*, 2004].

Following Moore and Clague [1992], Garcia and Davis [2001], and Sherman *et al.* [2002], we divide our samples into an “undegassed” group ( $H_2O \geq 0.45\%$  and  $S \geq 0.09\%$ ), a “partially degassed” group ( $0.45 > H_2O \geq 0.21\%$ ;  $0.09 > S \geq 0.04\%$ ), and a “degassed” group ( $H_2O < 0.21\%$  and  $S < 0.04\%$ ). Although the exact boundaries of this

classification scheme are arbitrary, the point is that the “degassed” samples lost water and sulfur at pressures approaching atmospheric, whereas the “undegassed” samples did not experience pressures of less than ~40–50 bars for sufficient time to vesiculate significantly. Figure 3 shows that the undegassed and partially degassed glass samples

define a low-SiO<sub>2</sub> group (106 samples; 48.3–49.8% SiO<sub>2</sub>) and a high-SiO<sub>2</sub> group (135 samples; 50.5–52.0% SiO<sub>2</sub>) separated by a gap in SiO<sub>2</sub> in which there are no undegassed or partially degassed samples. In contrast, degassed samples span the full range of SiO<sub>2</sub> content and, in particular, fill the gap in SiO<sub>2</sub> content defined by the undegassed samples.

[16] Figure 4 shows SiO<sub>2</sub> content and alkalinity versus depth for the HSDP2 glasses (alkalinity is defined as the vertical distance of a sample to the Macdonald-Katsura line on a silica-alkalies diagram [Carmichael *et al.*, 1974]). Figures 4a and 4b show SiO<sub>2</sub> contents of the glasses using distinct symbols for the different sample types (pillows; hyaloclastites; massives; intrusives; “excursions”; see below). In Figure 4a, light gray versus black filled symbols indicate glasses with <7% and ≥7% MgO; in Figures 4b and 4c, open symbols indicate degassed glasses, and filled symbols indicate undegassed/partially degassed samples. Note that all of the glasses plot on the tholeiitic side of the Macdonald-Katsura line (i.e., the alkalinity is negative). (We refer to most of these glasses as tholeiites since they plot below the Macdonald-Katsura line. Some authors would define most (or all) of the low-SiO<sub>2</sub> glasses as “transitional” [Wolfe *et al.*, 1995; Sisson *et al.*, 2002], but we restrict use the term “transitional” to compositions essentially on the Macdonald-Katsura line. Note that all glasses from this study have normative hypersthene (CIPW norms were calculated assuming 5–10% of the Fe is Fe<sup>3+</sup>.)

[17] Figure 5 shows the distributions of SiO<sub>2</sub> contents in histogram form by rock type, distinguishing degassed and partially degassed from undegassed samples. Figure 5a shows that the pillow-rim glasses are mostly undegassed and have a bimodal distribution of SiO<sub>2</sub> contents; this figure also shows clearly that degassed pillows nearly all have intermediate SiO<sub>2</sub> contents. Figure 5b shows that although the hyaloclastite glasses span the full range of silica contents in the core, most are in the high-SiO<sub>2</sub> group (and degassed) and, in contrast to the pillow-rim glasses, the distribution of SiO<sub>2</sub> contents in the hyaloclastite glasses is not as clearly bimodal (i.e., low- and intermediate-SiO<sub>2</sub> glasses are roughly equally abundant). Figure 5c shows that all of the glasses we analyzed from the massive flows in the upper submarine section are degassed and have high SiO<sub>2</sub>. Figure 5c also illustrates the predominance of

undegassed, low-SiO<sub>2</sub> glasses among the intrusive glasses in this study.

[18] Figure 6 shows on SiO<sub>2</sub> variation diagrams the concentrations of several major and minor elements in glasses from this study. In this figure and several others we restrict our comparison to glasses with ≥7% MgO to minimize the effects of the fractionation of phases other than olivine [Seaman *et al.*, 2004]. Glasses from different depth intervals and degassed versus undegassed/partially degassed glasses are distinguished by different symbols in Figure 6. This figure shows clearly that the distinction between the high- and low-SiO<sub>2</sub> groups extends to several other chemical components in addition to silica. Relative to the high-SiO<sub>2</sub> group, the low-SiO<sub>2</sub> group is higher in Al<sub>2</sub>O<sub>3</sub> and FeO\*. Although the differences are small, the low-SiO<sub>2</sub> group is also systematically higher in Na<sub>2</sub>O and TiO<sub>2</sub>. The low-SiO<sub>2</sub> group is also slightly higher in H<sub>2</sub>O and perhaps slightly lower in S. The CaO, K<sub>2</sub>O, or P<sub>2</sub>O<sub>5</sub> contents of the two groups are not distinguishable.

[19] Figure 7 shows variations with depth of several isotopic and elemental ratios in the HSDP2 samples. Most of the analyses shown are of whole rocks, but several are for glasses, including some from the reference suite from this paper. Isotopic and trace element data on the HSDP2 samples are fully interpreted elsewhere by the authors who report them [Bryce and DePaolo, 2000; Blichert-Toft *et al.*, 2003; Eisele *et al.*, 2003; Feigenson *et al.*, 2003; Huang and Frey, 2003; Kurz *et al.*, 2004; Rhodes and Vollinger, 2004], and some details of the comparison to our data set are presented in Appendix A2. The point we want to emphasize here is that the high- and low-SiO<sub>2</sub> groups are generally distinguishable isotopically and using certain elemental ratios. This is particularly evident for He isotope ratios (Figure 7a). The low-SiO<sub>2</sub> samples typically have higher <sup>3</sup>He/<sup>4</sup>He, and the range of <sup>3</sup>He/<sup>4</sup>He of the low-SiO<sub>2</sub> group (~14–25 RA) is larger than that of the high-SiO<sub>2</sub> group (~10–17 RA). There is, however, overlap in the He isotope ratios of these groups in that some of the low-SiO<sub>2</sub> samples do not have elevated <sup>3</sup>He/<sup>4</sup>He. Although the effects in other isotopic ratios are not as large, ε<sub>Nd</sub> (Figure 7b), <sup>176</sup>Hf/<sup>177</sup>Hf (Figure 7c), and <sup>206</sup>Pb/<sup>204</sup>Pb (Figure 7e) are all typically lower and <sup>87</sup>Sr/<sup>86</sup>Sr (Figure 7d) is typically higher in low-SiO<sub>2</sub> samples relative to high-SiO<sub>2</sub> samples. As with He isotopic ratios,

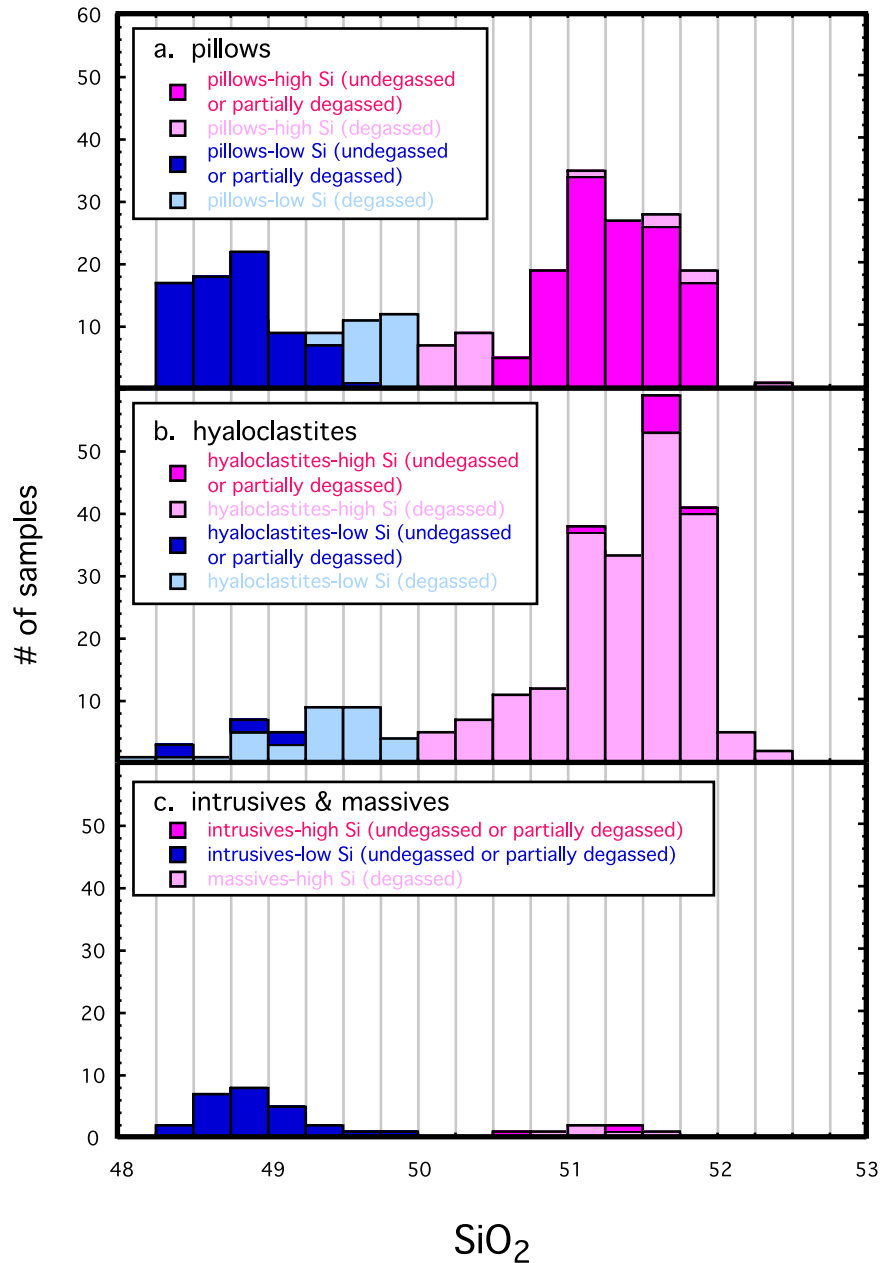


**Figure 5.** Histograms of SiO<sub>2</sub> contents of HSDP2 glasses by rock type: (a) pillow-rim glasses; (b) hyaloclastite glasses; (c) glasses from intrusive and massive units. Samples assigned to the high-SiO<sub>2</sub> group are pink; samples in the low-SiO<sub>2</sub> group are blue. Lighter shading indicates degassed samples; the solid histogram bars indicate undegassed or partially degassed glasses (see section 4.1 for the definitions of degassed versus partially degassed and undegassed glasses).

however, there is overlap in the isotopic characteristics of the two groups. The Zr/Nb ratios of the low-SiO<sub>2</sub> samples are also typically lower than those of the high-SiO<sub>2</sub> samples (Figure 7f) [Huang and Frey, 2003], although there is again some overlap. Although some ratios of incom-

patible elements (e.g., La/Yb, Ce/Pb, K<sub>2</sub>O/P<sub>2</sub>O<sub>5</sub>) are not distinguishable in these two groups [Huang and Frey, 2003; Baker et al., manuscript in preparation, 2004a], as a whole, the isotopic and incompatible trace element ratios require that formation of the high- and low-SiO<sub>2</sub> magmatic

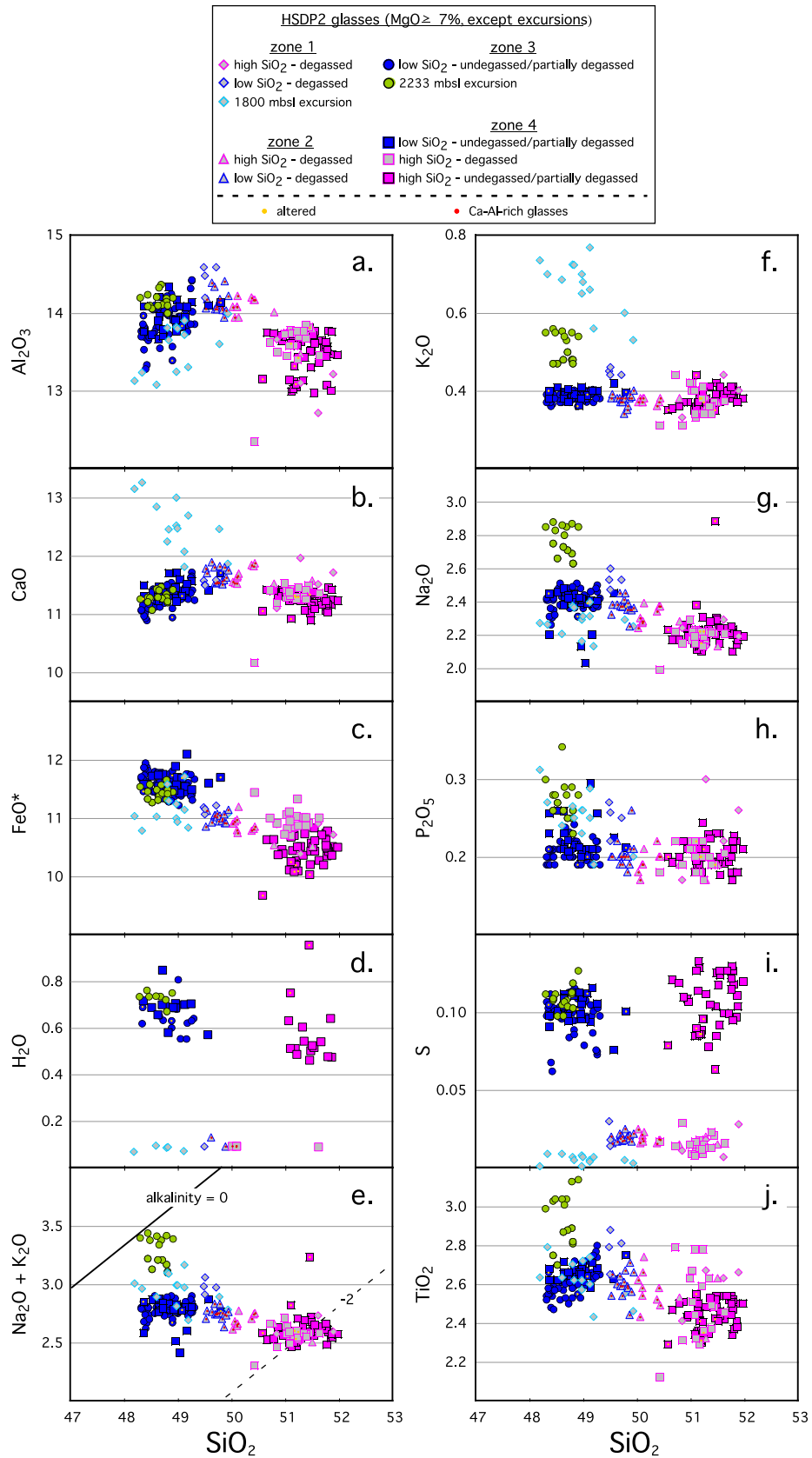


Figure 6

groups involved compositionally distinguishable mantle sources.

## 4.2. Distribution of the High- and Low-Silica Magma Types

[20] The submarine section of the core can be divided into the four depth intervals shown in Figure 4 on the basis of the silica contents or alkalinities of the glasses. These zones provide a convenient basis for much of the discussion of the magmatic history recorded by the HSDP2 samples.

### 4.2.1. Zone 1 (1079–~1950 mbsl)

[21] The upper boundary of this zone is defined by the subaerial-submarine transition, and the lower boundary is defined by a transition with increasing depth from high- to low-SiO<sub>2</sub> hyaloclastites. We have relatively few glass samples from shallower than ~1650 mbsl, so our characterization of zone 1 is incomplete. All of the samples are degassed and most (67 of 88 samples) are high-SiO<sub>2</sub> glasses. Some of the samples (~10%) are intermediate in silica content (i.e., they fall in the gap (49.8–50.5%; see Figure 3) in silica content between the undegassed high- and low-SiO<sub>2</sub> glasses). There is a group of six low-SiO<sub>2</sub> glasses at 1376–1437 mbsl; no high-SiO<sub>2</sub> glasses are present in this interval, but coverage is insufficient to characterize in detail the transitions between these low-SiO<sub>2</sub> glasses and the high-SiO<sub>2</sub> glasses immediately above and below them.

[22] There is a significant excursion to low-SiO<sub>2</sub> hyaloclastite glasses at ~1765–1810 mbsl. Although high-SiO<sub>2</sub> glasses are also present in this depth interval (i.e., three glasses from massive and hyaloclastite units in the 1781–1794 mbsl interval have >50% SiO<sub>2</sub>), the 13 low-SiO<sub>2</sub>

glasses in the ~1765–1810 mbsl interval are a coherent group, compositionally distinct from all other low-SiO<sub>2</sub> glasses in the core; these samples are shown with distinctive cyan symbols in all figures. This compositional excursion is discussed in detail in section 7.

[23] Overall, although we have few glass samples from zone 1, comparison with whole rock analyses (see section 4.3 and Appendix A1) supports the generally high-SiO<sub>2</sub> nature of this zone and the presence of several relatively narrow low-SiO<sub>2</sub> excursions.

### 4.2.2. Zone 2 (~1950–2233 mbsl)

[24] This zone extends from ~1950 to 2233 mbsl. All samples from this interval are degassed. Its base is defined by an abrupt transition from high-SiO<sub>2</sub> hyaloclastites above to low-SiO<sub>2</sub> pillows below. Samples from the lower ~100 m of this zone are high-SiO<sub>2</sub> hyaloclastites; samples from the middle ~100 m are intermediate-SiO<sub>2</sub> pillows (i.e., they fall in the gap in silica content between the undegassed high- and low-SiO<sub>2</sub> glasses); and the upper ~80 m contains dominantly low-SiO<sub>2</sub> pillows and hyaloclastites. The upper boundary is arbitrarily defined as a transition from high-SiO<sub>2</sub> hyaloclastites above to low-SiO<sub>2</sub> hyaloclastites below; this boundary is not as abrupt as the lower boundary, as both magma types are present as glasses over a ~30 m interval. What is most distinctive about zone 2 is the continuous decrease in silica contents of glasses from its bottom to its top (Figure 4; detail in Figure 20).

[25] The hyaloclastites (thought to be derived by slumping of debris from subaerial magmas that fragmented on reaching the shore line [*Hawaii Scientific Drilling Project*, 2001; *Seaman et al.*, 2004]) and pillows (emplaced by submarine erup-

**Figure 6.** SiO<sub>2</sub> versus various oxides/elements (wt.%) for glasses from the HSDP2 core. Except for glasses from the excursions at 2233–2280 and 1765–1810 mbsl, all of which are shown for comparison, only glasses with ≥7% MgO are plotted. Symbol shapes distinguish samples from zones 1–4 (see section 4.2). Colors indicate the chemical group to which the glasses are assigned (see the legend). Gray-filled symbols represent degassed glasses; color-filled symbols represent partially degassed and undegassed glasses (see section 4.1 for the definitions of degassed versus partially degassed and undegassed glasses). (a) Al<sub>2</sub>O<sub>3</sub>; (b) CaO; (c) FeO\*; (d) H<sub>2</sub>O; (e) Na<sub>2</sub>O + K<sub>2</sub>O; (f) K<sub>2</sub>O; (g) Na<sub>2</sub>O; (h) P<sub>2</sub>O<sub>5</sub>; (i) S; and (j) TiO<sub>2</sub>. The contours of alkalinity in Figure 6e are based on the expression in the footnote on p. 412 of *Carmichael et al.* [1974]; the line for alkalinity = 0 (the “Macdonald-Katsura line”) is taken as the boundary between tholeiitic (alkalinity ≤ 0) and alkalic (alkalinity > 0) lavas. Superimposed red dots indicate Ca-Al-rich glasses (see section 4.6); superimposed gold-colored dots indicate altered samples [*Seaman et al.*, 2004]. Note that in Figure 6g one altered, high-SiO<sub>2</sub> intrusive glass (SR0972-15.7) has a significantly elevated Na<sub>2</sub>O content relative to other high-SiO<sub>2</sub> glasses with comparable MgO contents.

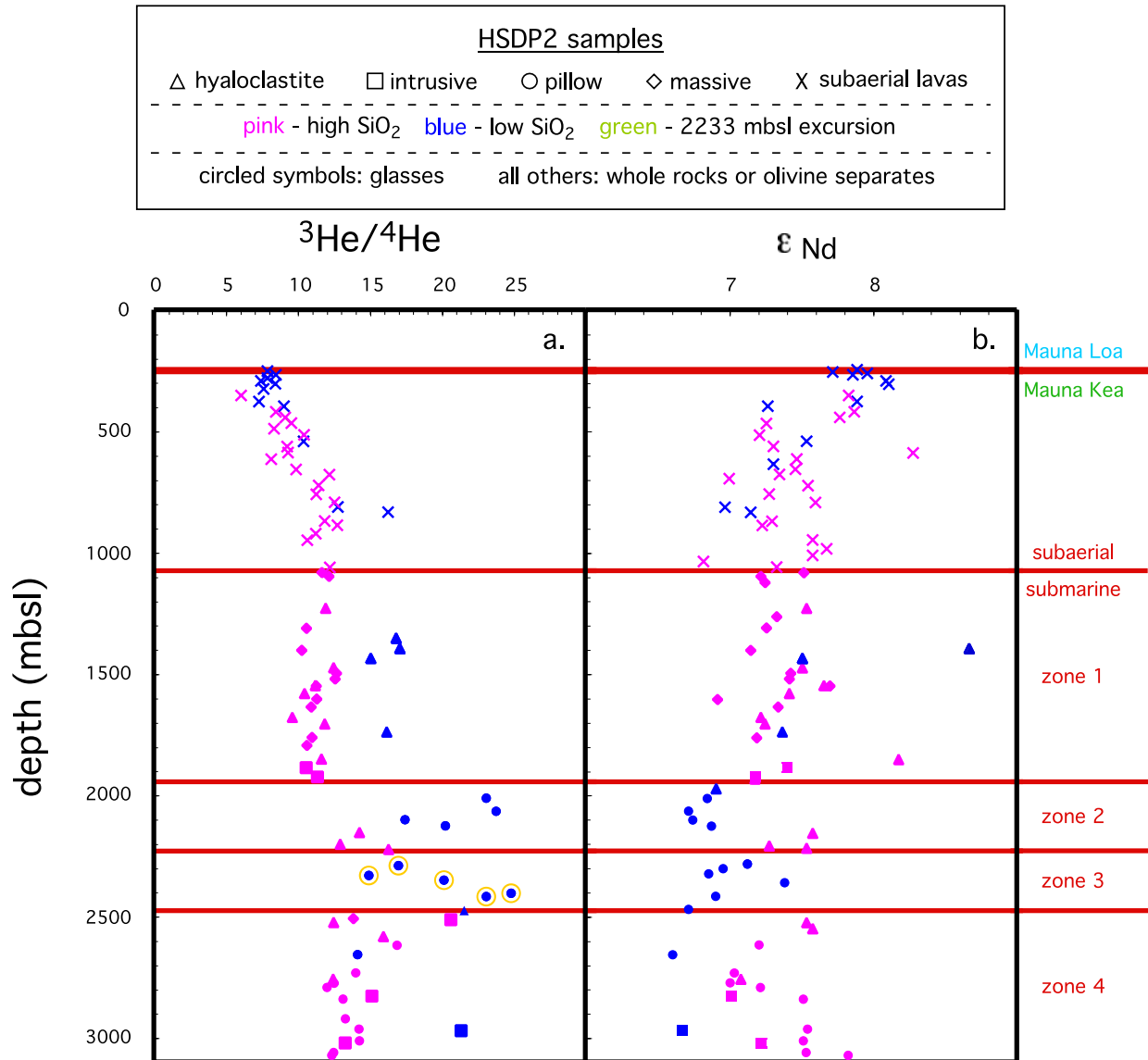


**Figure 7.** Depth (mbsl) versus isotopic and trace element ratios in HSDP2 samples. Data are for whole rocks, except for the few data points (He and Hf isotopes) enclosed in orange circles, which were obtained on glasses. Symbol shapes indicate rock types, and colors indicate the chemical groups to which the samples are assigned (see the legend). (a)  $^3\text{He}/^4\text{He}$  [Kurz *et al.*, 2004]. (b)  $\epsilon_{\text{Nd}}$  [Bryce and DePaolo, 2000]. (c)  $^{176}\text{Hf}/^{177}\text{Hf}$  [Blichert-Toft *et al.*, 2003]. (d)  $^{87}\text{Sr}/^{86}\text{Sr}$  [Bryce and DePaolo, 2000]. (e)  $^{206}\text{Pb}/^{204}\text{Pb}$  [Eisele *et al.*, 2003]. (f) Zr/Nb [Rhodes and Vollinger, 2004].

tions) from zone 2 define the same long-term trend, indicating that subaerial and submarine magmas delivered to the drill site are coupled in this time interval. Moreover, in contrast to pillows, hyaloclastites collect material from more than a single lobe of a single flow (e.g., perhaps from multiple flows at a single nearshore site that are mixed during the slumping event or by long-shore drift of glass fragments to the nearshore site from which the slump originated), and thus it

would not have been surprising if hyaloclastite glasses were variable compositionally over short depth intervals, perhaps even containing samples from multiple volcanoes. Such highly variable glass compositions have been observed in other submarine Hawaiian volcanoclastic deposits, although the variability appears to correlate with the distance from the source [Clague *et al.*, 2002; Naka *et al.*, 2002; Sherman *et al.*, 2002; Shinozaki *et al.*, 2002]. The well-defined compositional

trend in zone 2 hyaloclastites and their similarity  
 $^{176}\text{Hf}/^{177}\text{Hf}$

undegassed or partially degassed low-SiO<sub>2</sub> lavas.  
 $^{87}\text{Sr}/^{86}\text{Sr}$

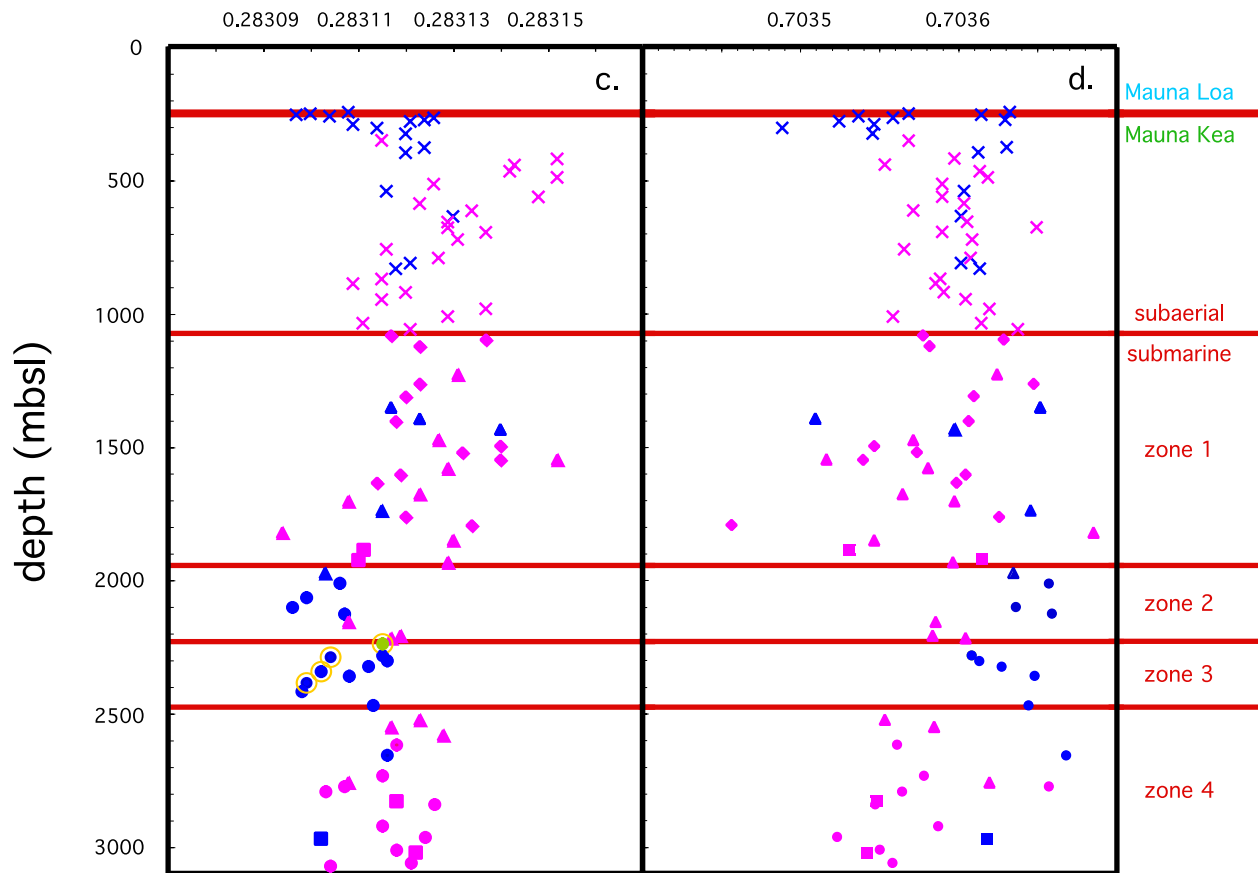


Figure 7. (continued)

to pillows in the same part of the core demonstrate that glasses in hyaloclastites can be reasonable recorders of magmas erupting over relatively short time intervals from a single volcano, especially when the hyaloclastites are deposited near the shoreline, as is likely to be the case for these HSDP2 samples (M. B. Baker et al., Growth models for Hawaiian volcanoes, manuscript in preparation, 2004) (hereinafter referred to as Baker et al., manuscript in preparation, 2004b). On the other hand, the 30 m transitional interval at the top of zone 2 containing low-SiO<sub>2</sub> glasses corresponding to the top of zone 2 and high-SiO<sub>2</sub> glasses corresponding to the bottom of zone 1 may likewise indicate that mixing of multiple flows can occur in the process of forming hyaloclastites.

#### 4.2.3. Zone 3 (2233–2481 mbsl)

[26] This zone extends from 2233 to 2481 mbsl. All of the 80 samples in the interval are from

Except for two relatively thin hyaloclastite units (unit 294, ~7 m thick, and unit 296, ~11 m thick) at or near its bottom, all of the samples in this interval are pillows. This zone contains 50% of the low-SiO<sub>2</sub> glasses in our sample suite. The top and bottom of this interval are abrupt compositionally. The upper boundary defines a transition between this pillow-dominated low-SiO<sub>2</sub> interval and overlying hyaloclastites; the lower boundary coincides with the boundary between two hyaloclastite units (unit 296 above and unit 297 below).

[27] From the bottom of zone 3 to 2280 mbsl, silica contents decrease slightly (from ~49.2 to ~48.6%; although this is indistinguishable at the 2  $\sigma$  level, the decrease is systematic), and there is a small complementary increase in alkalinity. However, in the narrow interval from 2280 mbsl to the top of zone 3 at 2233 mbsl, although the silica content is roughly constant, there is a significant increase in the alkalinity of the samples (Figure 4c); samples from

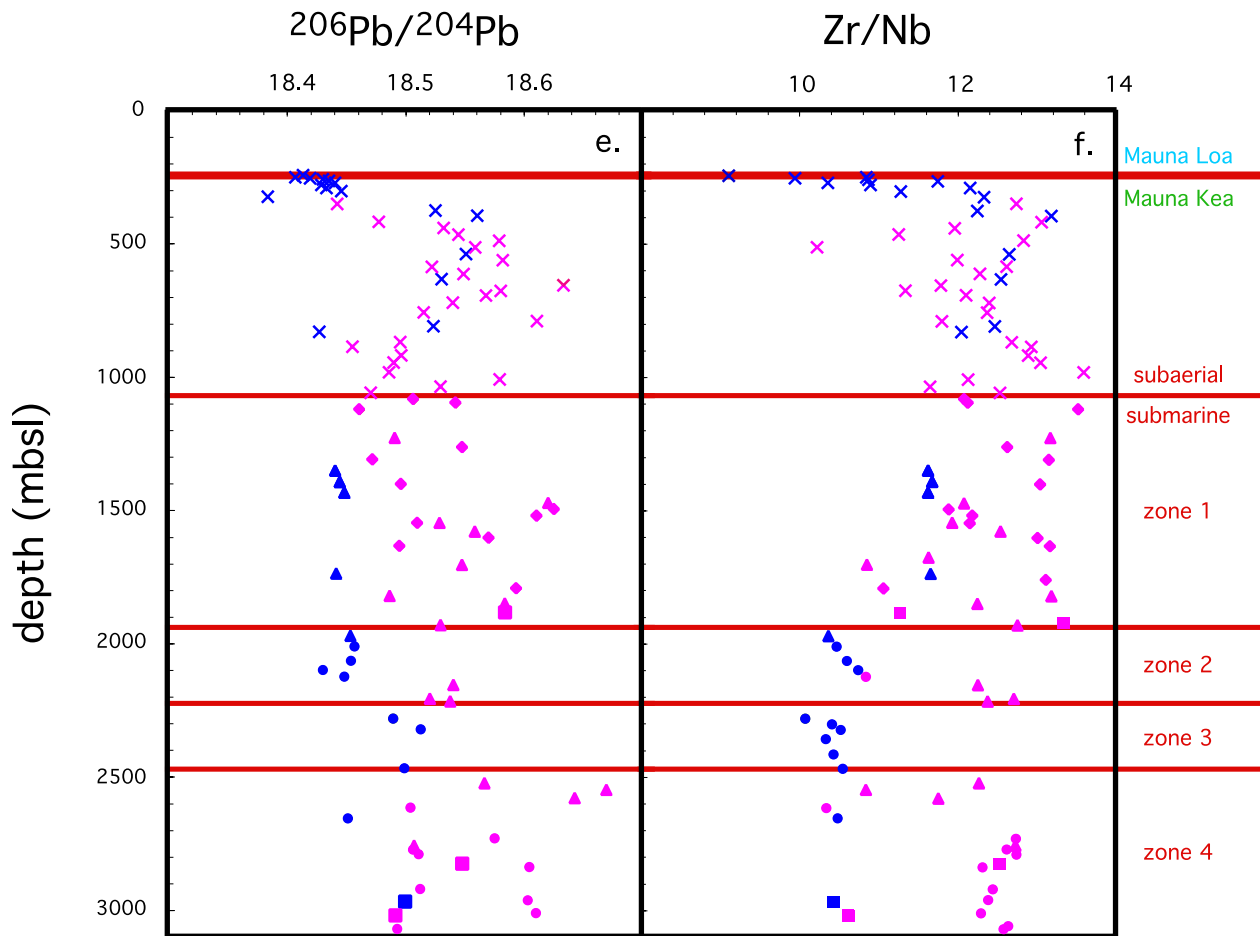


Figure 7. (continued)

2233–2280 mbsl are shown with distinctive green symbols in all figures. The samples at the top of this ~50 m interval are transitional between alkalic and tholeiitic, extending to the Macdonald-Katsura line; note that all have normative hypersthene, although the amount decreases slightly (i.e., from ~7–11% to ~5–8%) from the base to the top of this interval, consistent with the increase in alkalinity. This “excursion” in the upper ~50 m of zone 3 is also manifested in the concentrations of other major elements and minor and trace elements. The petrological and geochemical significance of the glasses in this narrow interval are discussed in section 6.

[28] Although it is not apparent in Figure 4, there is a thin interval at the base of zone 3 (2438–2481 mbsl) in which S and H<sub>2</sub>O contents of the glasses from hyaloclastites and pillows vary by about a factor of 2, in contrast to a total variability of only a few tens of percent at higher levels in this zone [Seaman *et al.*, 2004]. The

major and minor element compositions of glasses in this interval do not vary systematically and are not distinguishable from the middle section of zone 3.

#### 4.2.4. Zone 4 (2481–3098 mbsl)

[29] We define zone 4 as the interval extending from 2481 mbsl to the base of the core (3098 mbsl). The glasses in this interval are overwhelmingly high in SiO<sub>2</sub>. The exceptions are a single low-SiO<sub>2</sub> hyaloclastite from near the top of the zone (SR839-5.5 at 2486.2 m; the S content of this sample is 0.105%, perhaps suggesting an affinity with the undegassed and partially degassed, low-SiO<sub>2</sub> hyaloclastites from zone 3 units 294 and 296, only ~6 m higher in the section); all but two of the 28 intrusive glasses (including samples of the numbered intrusive units and the unnumbered intrusive fingers at pillow margins; see section 2); and seven degassed pillow and hyaloclastite glasses

with intermediate  $\text{SiO}_2$  contents. As described above for zone 2, interlayered pillows and hyaloclastites in zone 4 overlap compositionally (except for the extent of degassing), indicating, that pillows (submarine lavas) and hyaloclastites (subaerial magmas) erupting in this interval provide similar information on the temporal evolution of magmatic sources. Although not apparent in Figure 4, there is a thin sub-zone (2763–2841 mbsl) over which S and  $\text{H}_2\text{O}$  contents of the pillows decrease systematically with decreasing depth [Seaman *et al.*, 2004].

### 4.3. Comparison of Subaerial and Submarine HSDP Samples

[30] Although our focus is on the suite of glasses from the submarine section, there are complementary whole rock analyses at intervals of typically 10–40 m over the entire length of the HSDP2 core [Rhodes and Vollinger, 2004] and from the  $\sim 1$  km long HSDP1 core [Rhodes, 1996]. Figure 8 compares  $\text{SiO}_2$  content versus depth and alkalinity versus depth for our suite of glasses from the HSDP2 core with whole rocks from the HSDP1 and HSDP2 cores (whole rock analyses were adjusted to 7% MgO; see Appendix A1 for the procedure). Figure A1 shows  $\text{SiO}_2$  variation diagrams comparing concentrations of several oxides in glasses from this study (only glasses with  $\geq 7\%$  MgO are shown) with whole rocks (adjusted to 7% MgO) from the two HSDP cores.

[31] The comparisons shown in Figure 8 and Figure A1 demonstrate that the glass data and the whole rock data are generally similar in the regions of the core in which they overlap. Moreover, the key observations from our evaluation of the glass data (the subdivision of the submarine section into distinct zones and the characteristics and trends in those zones; the subdivision of the submarine samples into high- and low- $\text{SiO}_2$  groups; and the paucity of intermediate  $\text{SiO}_2$  content samples in the submarine section) are all confirmed by the less densely sampled whole rocks. Note that the whole rock analyses in the hyaloclastite intervals are of lithic fragments (typically  $\sim 10$ – $30$  cm in length) within the hyaloclastites, *not* the hyaloclastite whole rocks. That the trends defined by analyses of these clasts are similar to those defined by the hyaloclastite glasses suggests that most lithic clasts are more slowly cooled equivalents of the same magmas sampled as glass in the hyaloclastites. This observation also supports the inference based on the similarity of hyaloclastite glasses from sample to sample over short depth intervals (see section 4.2) that the hyaloclastite-

forming slumps that delivered nearshore fragmental deposits to the location of the drill site usually sampled closely related materials.

[32] The whole rock analyses extend the sample suite up through the subaerial section and include trace element and isotopic analyses (Figure 7). The chemical trends observed in the HSDP2 and HSDP1 subaerial samples have been described by Feigenson *et al.* [2003], Huang and Frey [2003], Rhodes and Vollinger [2004], Albarède [1996], Rhodes [1996], and Yang *et al.* [1996a]. The most significant aspect is the shift toward low-silica, alkalic lavas in the upper 50–150 m of the Mauna Kea section; it is important to emphasize that these alkalic lavas, although low in  $\text{SiO}_2$ , are distinct compositionally and isotopically from the low- $\text{SiO}_2$  magma type defined in the submarine section and represent a separate phenomenon related to the end of shield building [Huang and Frey, 2003]. Moreover, the significant compositional shift in the upper 50–150 m of the Mauna Kea section is superimposed on a longer term shift in isotopic ratios (e.g.,  $^3\text{He}/^4\text{He}$ ,  $\epsilon_{\text{Nd}}$ ) and highly and moderately incompatible trace element ratios (e.g., Zr/Nb, La/Yb) that occurs over the upper 1000 m of the core, i.e., over essentially the entire subaerial portion of the section (see Figure 7) [DePaolo *et al.*, 1996].

[33] We discuss here two features of the subaerial section that contrast with the trends observed in the submarine section. First, the low- $\text{SiO}_2$  magma type that is such an important feature of the deeper parts of the submarine section is far less abundant in the subaerial section. In fact, Huang and Frey [2003] identified only one subaerial low- $\text{SiO}_2$  sample (SR354-7.75 at 833.9 mbsl) they considered based on He and Pb isotopes to be comparable to the low- $\text{SiO}_2$  samples from the submarine section; i.e., they concluded that all other subaerial low- $\text{SiO}_2$  samples (all of which occur shallower than  $\sim 800$  mbsl) are distinct geochemically from the submarine low- $\text{SiO}_2$  group and are instead associated with the trend to low- $\text{SiO}_2$  alkalic magmas at the end of shield building. The paucity of low- $\text{SiO}_2$  magmas in the subaerial section (other than the alkalic ones near the very top of the section) is emphasized in the histogram shown in Figure 9b. Second, the mode of the distribution of silica contents in the subaerial lavas is offset from that of the high- $\text{SiO}_2$  magma type defined in the submarine section. This is observable in Figure 8, where in the subaerial section, and particularly shallower than  $\sim 850$  mbsl, most of the whole rocks have  $\text{SiO}_2 < 51\%$  (adjusted to 7% MgO), whereas most of the high- $\text{SiO}_2$  mag-

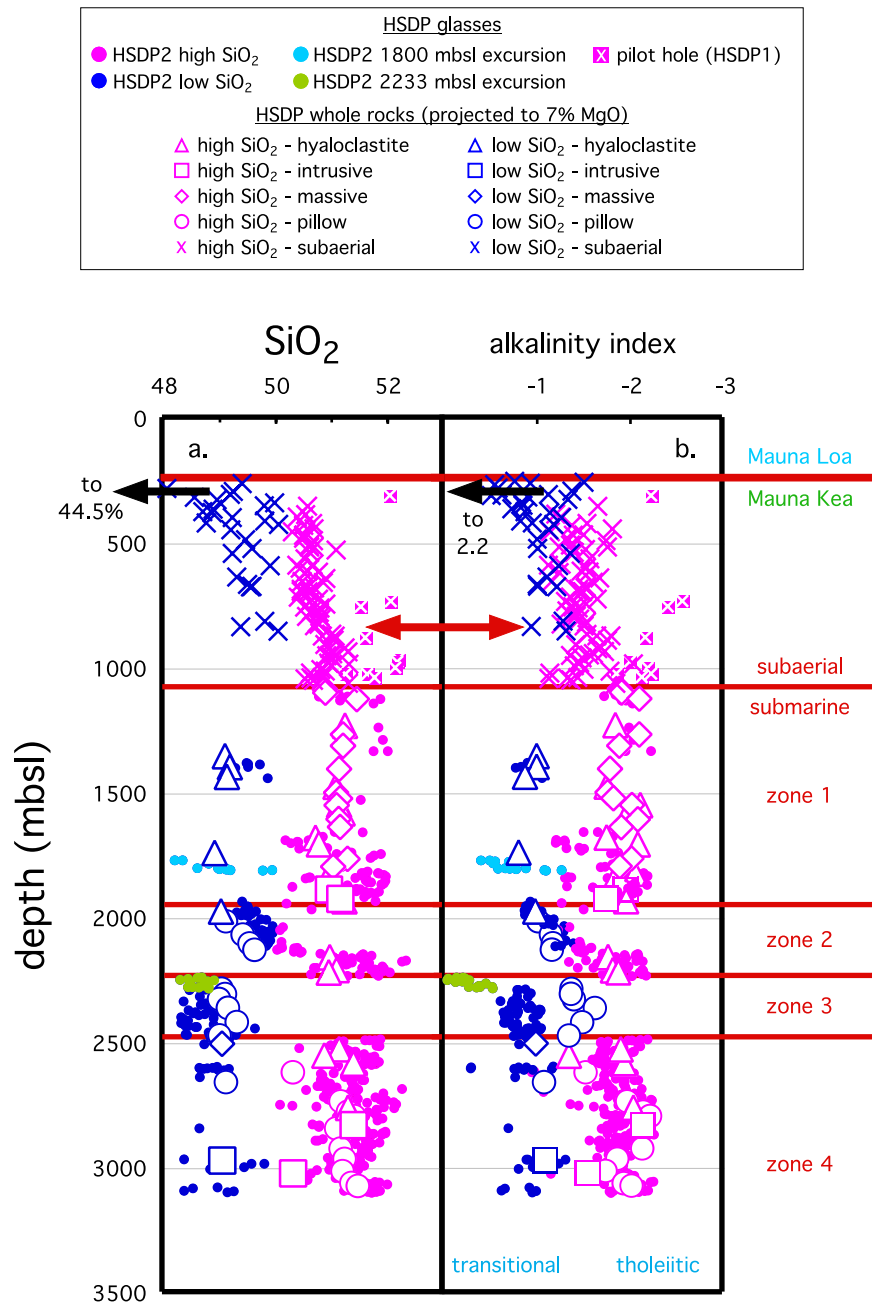


**Figure 8.** Depth (mbsl) versus (a)  $\text{SiO}_2$  content and (b) alkalinity for HSDP1 and HSDP2 whole rocks [Rhodes, 1996; Rhodes and Vollinger, 2004] projected to 7% MgO (as described in Appendix A1). HSDP2 glasses from this work are shown for comparison. The heavy horizontal red line shows the position of the unconformity between Mauna Loa and Mauna Kea subaerial lavas. Other horizontal red lines show divisions of the core into subaerial samples and zones 1–4 (see section 4.2). HSDP2 glasses are shown as the small, filled dots; the larger symbols are HSDP whole rocks with rock type distinguished by symbol shape as indicated in the legend. Note that the hyaloclastite whole rock analyses are of lithic clasts from hyaloclastites. Colors indicate the chemical groups to which the glasses and whole rocks are assigned (see the legend). The heavy black arrows point toward the alkaline lavas (not shown) from near the top of the Mauna Kea section. The double-headed red arrow indicates the depth of the shallowest subaerial whole rock sample related to the submarine low- $\text{SiO}_2$  magma type [Huang and Frey, 2003].

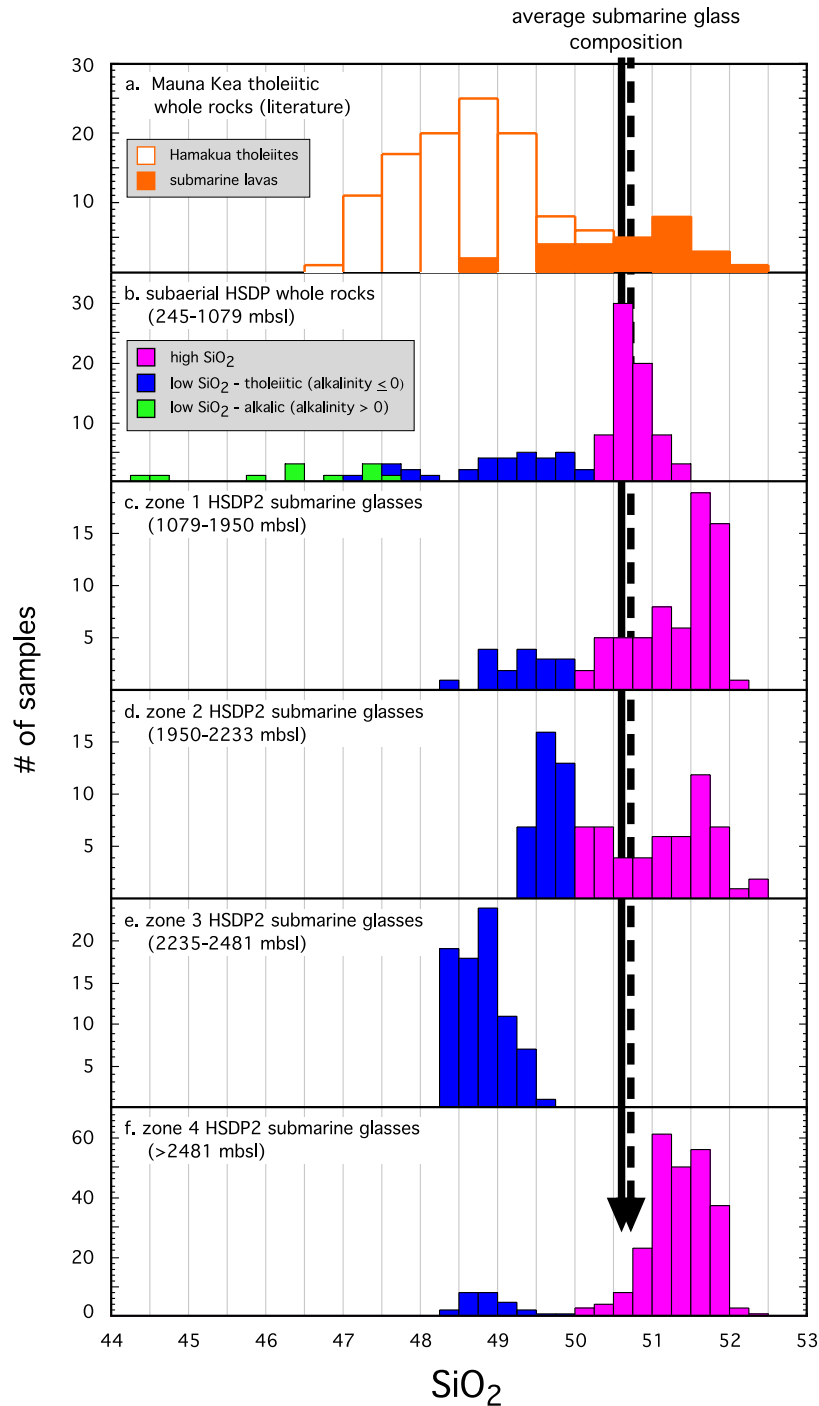


**Figure 9.** Histograms of SiO<sub>2</sub> contents of Mauna Kea and HSDP samples by depth interval: (a) Mauna Kea subaerial [Muir and Tilley, 1963; Macdonald and Katsura, 1964; Basaltic Volcanism Study Project, 1981; Frey et al., 1990, 1991; Wolfe et al., 1995] and submarine [Moore and Clague, 1992; Yang et al., 1994; Wolfe et al., 1995; Norman and Garcia, 1999; Holcomb et al., 2000] tholeiitic (i.e., alkalinity  $\leq 0$ ) whole rocks from the literature (projected to 7% MgO as described in Appendix A3); (b) subaerial HSDP whole rocks [Rhodes, 1996; Rhodes and Vollinger, 2004] (projected to 7% MgO as described in Appendix A1); (c–f) HSDP2 glasses from submarine zones 1–4. Samples assigned to the high-SiO<sub>2</sub> group are pink; samples in the low-SiO<sub>2</sub> group are blue; subaerial alkalic samples (i.e., alkalinity  $> 0$ ) are green. Two essentially indistinguishable average submarine glass compositions are shown: one is the average of all glasses from this study (solid black arrow at 50.61% SiO<sub>2</sub>); the other is a weighted average based on the spacing of the samples (dashed black arrow at 50.72% SiO<sub>2</sub>).

mas in the submarine section have  $\text{SiO}_2 > 51\%$ . This shift to lower silica contents in the high- $\text{SiO}_2$  subaerial samples can be seen clearly in the histograms in Figure 9. Oxygen isotope ratios of phenocrysts and groundmass of the HSDP2 lavas also shift in the vicinity of the subaerial-submarine boundary [Wang *et al.*, 2003].

[34] The paucity of the low- $\text{SiO}_2$  magma type in the shallower parts of the section (i.e., both in zone 1 of the submarine section and in the subaerial lavas) may signify a change in source materials, conditions of melting, and/or magmatic plumbing such that the low- $\text{SiO}_2$  magma type so important in the deeper parts of the submarine section is simply no longer being produced or delivered to the volcanic edifice in significant quantities after a certain point. Likewise, the shift to lower average  $\text{SiO}_2$  content in the high- $\text{SiO}_2$  rocks of the subaerial section could reflect related temporal changes in mantle processes or source compositions that resulted in a change in the characteristics of high- $\text{SiO}_2$  magmas extracted from the mantle sources of Mauna Kea magmas as the volcano reached the end of its lifetime. This could represent an anticipation (i.e., in terms of changes in source composition or in conditions of melt generation) of the more extreme shift to low-silica, alkalic magmas at the end of shield building [Huang and Frey, 2003; Rhodes and Vollinger, 2004], in which case the shift in  $\text{SiO}_2$  content would be coupled to the long-term trends in other chemical and isotopic parameters that extend over the full range of the subaerial section and culminate in the alkalic lavas in the upper 50 m of the Mauna Kea section (see summary by DePaolo *et al.* [1996]).

[35] Rhodes and Vollinger [2004] emphasized the abrupt change in HSDP2 magmas at the subaerial-submarine boundary, and they focused in particular on the decrease in the MgO contents of whole rocks passing upward through this horizon. They interpreted this as a reflection of a fundamental change in the plumbing system of the volcano, and although they preferred the hypothesis that the magma supply rate decreased significantly at this time, they also considered the possibility that a steady state magma chamber did not develop until this stage in the volcano's history. This second possibility offers an alternative explanation of our observation of a shift in the subaerial section toward a unimodal distribution of silica contents with a modal silica content intermediate between the high- and low- $\text{SiO}_2$  magma types of the

submarine section: i.e., perhaps both magma types were produced and delivered to the volcanic edifice both before and after the timing of the submarine-subaerial transition at the drill site, but whereas in the submarine part of section, particularly in its deeper reaches, the two magma types could avoid mixing because there was not a steady state magma chamber, in the higher, subaerial section, the efficiency of magma chambers at capturing and mixing the magmatic output was such that no subaerial magmas bypassed the mixing process and all erupted magmas were mixed. A test of this is whether the modal silica content of the subaerial magmas corresponds to the average submarine magma, and Figure 9 shows that this is indeed the case. Although the shift in other oxides from bimodal distributions in the submarine samples to unimodal distributions in the subaerial magmas is not as dramatic as for silica, the modal concentrations in the subaerial magmas of all other oxides analyzed here also correspond to the average submarine magma. However, as pointed out by Rhodes and Vollinger [2004], it is not obvious why there should be an increase rather than a decrease in the efficiency of mixing as the volcano ages, nor do we have an explanation for why this change would have occurred precisely at the time that the subaerial-submarine transition (which occurs at different times at different places on the volcano) occurred at the drill site. Finally, even if magma chamber dynamics were responsible for the shift from bimodal to unimodal  $\text{SiO}_2$  contents near the submarine-subaerial transition, this would in any case have to have been superimposed on the gradual shift in trace element and isotopic ratios and major element chemistry of the magmas (culminating in the alkalic lavas at the top of the section) that occurred as Mauna Kea's magmatic system wound down toward the end of its lifetime.

#### 4.4. Comparison of the Compositions of HSDP2 Glasses to Those From Mauna Kea and Other Hawaiian Volcanoes

[36] In this section we briefly compare our analyses of HSDP2 glasses with previously reported analyses of Mauna Kea glasses and glasses from other Hawaiian volcanoes and emphasize those respects in which they are either similar or distinctive. We present in Appendices A3 and A4 additional details of these comparisons.

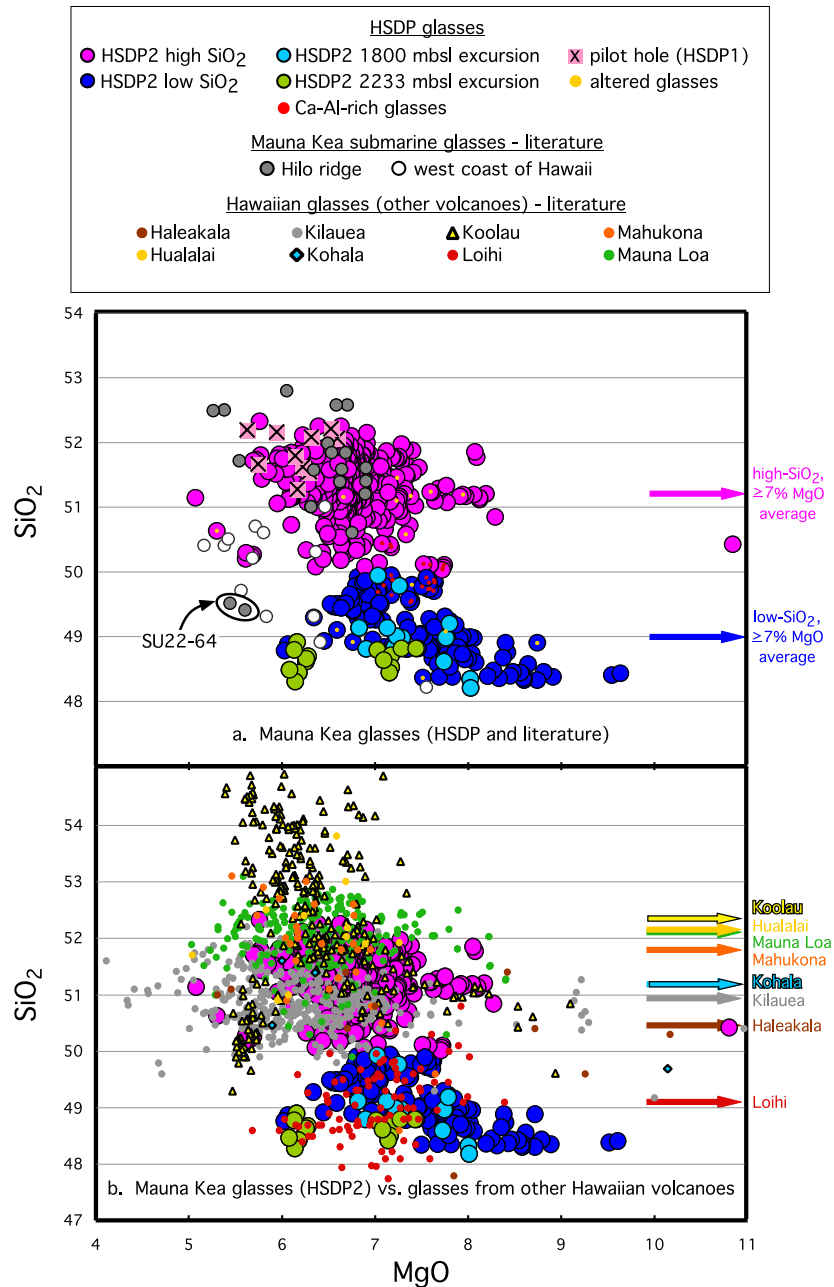


**Figure 10.** MgO versus SiO<sub>2</sub> (wt.%) for glasses from the HSDP2 core compared with (a) other glasses from the Mauna Kea volcano and (b) glasses from other Hawaiian volcanoes [Tilley and Scoon, 1960; Anderson and Wright, 1972; Moore et al., 1982, 1985, 1990a, 1995; Hawkins and Melchior, 1983; Byers et al., 1985; Moore and Clague, 1987, 1992; Garcia et al., 1989, 1990, 1993, 1995a, 1995b; Jambon and Zimmermann, 1990; Clague et al., 1991, 1995, 2000, 2002; Dixon et al., 1991; Honda et al., 1993; Helz et al., 1995; Mangan et al., 1995; Garcia, 1996; Wright and Helz, 1996; Kent et al., 1999; Burkhard, 2001; Dixon and Clague, 2001; Johnson et al., 2002; Shinozaki et al., 2002; Davis et al., 2003]. Only tholeiitic glasses (i.e., alkalinity ≤ 0) are plotted. Glasses shown in Figure 10a include subaerial glasses from the HSDP1 pilot hole [Garcia, 1996], submarine glasses from the Hilo ridge [Garcia et al., 1989; Moore and Clague, 1992; Yang et al., 1994; Holcomb et al., 2000], and submarine glasses from offshore of the west coast of Hawaii [Moore and Clague, 1992], some of which were erupted subaerially. Symbols are color coded as indicated in the legend. Arrows at the right edge of Figure 10a are the average SiO<sub>2</sub> contents of high-SiO<sub>2</sub> and low-SiO<sub>2</sub> HSDP2 glasses with ≥ 7% MgO. Averages of tholeiitic glasses from other Hawaiian volcanoes (all MgO contents) are shown at the right edge of Figure 10b. In Figure 10a, superimposed red dots indicate Ca-Al-rich glasses (see section 4.6) and superimposed gold-colored dots indicate altered samples [Seaman et al., 2004].

[37] Figure 10a compares MgO and SiO<sub>2</sub> contents of tholeiitic Mauna Kea glasses reported in the literature with those of glasses from the HSDP2 core. The range of SiO<sub>2</sub> contents of tholeiitic Mauna Kea glasses from the literature is comparable to that of the HSDP2 glasses, but there is no indication of bimodality and the silica contents of most of these glasses overlap the high-SiO<sub>2</sub> HSDP2 glasses. Subaerial glasses from the HSDP1 core and submarine glasses dredged from the Hilo ridge (except glass from one sample, SU-22-64 [Moore and Clague, 1992; Yang et al., 1994]) correspond compositionally to the high-SiO<sub>2</sub> group of HSDP2 glasses. In contrast, submarine Mauna Kea glasses from off the west coast of Hawaii [Moore and Clague, 1992] are nearly all lower in SiO<sub>2</sub> than the bulk of the dredged Hilo ridge glasses, and about half of these samples plus glasses from one sample dredged from the Hilo ridge (SU-22-64) have silica contents that overlap those of the low-SiO<sub>2</sub> group. Finally, we note that the literature Mauna Kea glasses tend to be more fractionated than the typical HSDP2 glasses; i.e., most have <7% MgO.

[38] Figure 10b compares MgO and SiO<sub>2</sub> contents of the HSDP2 glasses with those of tholeiitic glasses from other Hawaiian volcanoes. The typically relatively narrow range in SiO<sub>2</sub> in the output of a single Hawaiian volcano (usually ~2%) is apparent in Figure 10b and is the reason why silica content has often been regarded as a diagnostic feature of the lavas of an individual Hawaiian volcano [Garcia et al., 1989; Frey and Rhodes, 1993; Frey et al., 1994; Hauri, 1996]. The HSDP2 glasses and the Mauna Kea glasses from the literature (Figure 10a) are clearly unusual in spanning a range in SiO<sub>2</sub> of ~4% and suggest that this conventional wisdom may be invalid (although the possibility that the HSDP2 samples come from more than one volcano must be considered; see section A6 and Rhodes and Vollinger [2004]). Thus an important result of the HSDP2 project is that if we assume that the HSDP2 samples are all eruptive products from Mauna Kea, then SiO<sub>2</sub> is not a robust fingerprint of tholeiites from an individual volcano when sampled over a sufficient time interval, and in some time periods almost the full range in SiO<sub>2</sub> contents known for Hawaiian tholeiites can erupt from a single volcano in rapid succession. These results complement other recent demonstrations of greater variability in the output of Hawaiian volcanoes during shield building than has been generally believed to be the norm. For example,

although related to a relatively rare explosive eruption, Kilauea's Uwekahuna Ash Member (~2–3 Ka) also demonstrates that magmas spanning nearly the full range of SiO<sub>2</sub> contents shown in Figure 10 can erupt over a narrow time interval from Hawaiian shield volcanoes [Dzurisin et al., 1995]. Similarly, recent studies of subsurface and submarine samples from Koolau volcano [Jackson et al., 1999; Shinozaki et al., 2002; Tanaka et al., 2002; Haskins and Garcia, 2004] indicate a range in SiO<sub>2</sub> contents comparable to that found here for HSDP2 glasses and show that what had been regarded as the diagnostic high SiO<sub>2</sub> of Koolau subaerial lavas is not representative of the entire shield-building stage of this volcano. Likewise, volcanoclastic sediments associated with the Nuuanu and Wailau landslides can show compositional ranges comparable to those observed for HSDP2 samples [Clague et al., 2002; Sherman et al., 2002; Shinozaki et al., 2002], although the jumbling of materials from multiple sources and ambiguities about their provenance make these results difficult to interpret in any detail.

[39] In addition to the large range in SiO<sub>2</sub> content, the abrupt changes in silica content with depth observed in the HSDP2 core (Figure 4) appear atypical for a single volcano in its tholeiitic shield-building phase on the basis of previous results for Hawaiian volcanoes. For example, Mauna Loa shows no significant change in the SiO<sub>2</sub> contents of glasses over a 250 Kyr interval [Garcia et al., 1995b]; likewise, although possibly showing a slight decrease in SiO<sub>2</sub> with depth over 350 Kyr, Kilauea does not display abrupt changes comparable to those observed in the HSDP2 core [Quane et al., 2000]. However, there are other recent results suggesting rapid variability in the output of Hawaiian shield volcanoes, even those with high-level magmatic plumbing systems. For example, as mentioned above, Kilauea's Uwekahuna Ash Member demonstrates that magmas spanning a wide range of SiO<sub>2</sub> contents can erupt over a short time interval from a mature Hawaiian shield volcano [Dzurisin et al., 1995], and several recent studies suggest a relatively rapid transition from lower-SiO<sub>2</sub> to higher-SiO<sub>2</sub> magmas late in the shield-building phase of Koolau volcano [Shinozaki et al., 2002; Tanaka et al., 2002; Haskins and Garcia, 2004]. Note, however, that if our characterization of Mauna Kea were restricted to the subaerial and upper submarine portions of the HSDP1 and HSDP2 cores (i.e., spanning the ~150–500 Ka age range (W. D. Sharp and D. J. DePaolo, Dating of the HSDP2 core, manuscript in

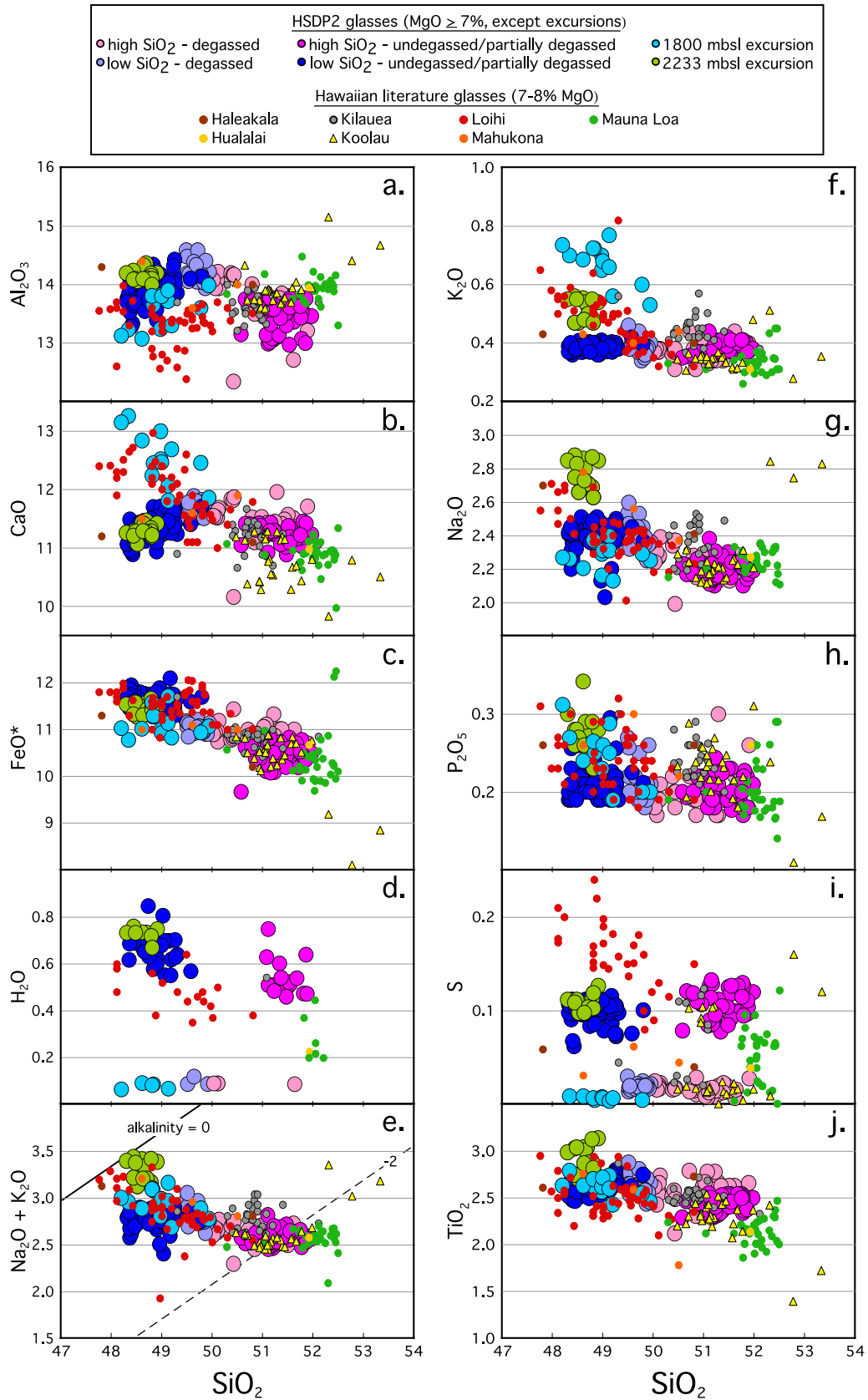


Figure 11

preparation, 2004) (hereinafter referred to as Sharp and DePaolo, manuscript in preparation, 2004)), we might conclude that except for the shift to transitional and alkalic low-SiO<sub>2</sub> magmas at the end of shield building, Mauna Kea also erupted magmas covering only a narrow range of silica contents; i.e., aside from samples in narrow intervals at 800, 1350–1400, and 1760–1810 mbsl that could easily be missed, large fluctuations in SiO<sub>2</sub> contents unassociated with the end of shield building only occur at depths of ~2–3 km in the HSDP2 drill core.

[40] Figure 11 (see also Appendix A4) shows major and minor elements in HSDP2 glasses (all ≥7% MgO) and glasses from other Hawaiian volcanoes (all 7–8% MgO) on SiO<sub>2</sub> variation diagrams. A similar comparison between HSDP2 glasses and whole rocks from other Hawaiian volcanoes is shown in Figure 12. The principal results of these comparisons are as follows:

[41] • In terms of silica content, Loihi tholeiites and the low-SiO<sub>2</sub> HSDP2 glasses form a well-defined group generally distinct from all the other volcanoes (although a few Kilauea, Mahukona, and Haleakala tholeiitic glasses overlap with the low-silica group). This similarity between low-SiO<sub>2</sub> HSDP2 lavas and Loihi tholeiites has been pointed out in several other studies and extends to some trace element and isotopic ratios [Eisele *et al.*, 2003; Huang and Frey, 2003; Kurz *et al.*, 2004; Rhodes and Vollinger, 2004]. However, as shown in Figures 11 and 12, although the FeO\*, Na<sub>2</sub>O, and TiO<sub>2</sub> contents of Loihi tholeiites also overlap precisely with those of the low-SiO<sub>2</sub> HSDP2 glasses, Loihi samples are distinctly lower in some components (Al<sub>2</sub>O<sub>3</sub>, H<sub>2</sub>O) and typically higher in several others (CaO, K<sub>2</sub>O, P<sub>2</sub>O<sub>5</sub>, and S). Despite these differences, the low-SiO<sub>2</sub> HSDP2 samples are most similar overall to Loihi tholeiites among other known Hawaiian magmas.

[42] • Kilauea glasses, although on average lower in MgO (and somewhat lower in SiO<sub>2</sub>; Figure 10), have a distribution of SiO<sub>2</sub> contents similar to the high-SiO<sub>2</sub> HSDP2 glasses; the same is true for the Haleakala and Kohala glasses, but the sample suites for these volcanoes are much smaller. The similarity between high-SiO<sub>2</sub> HSDP2 samples and Kilauea tholeiites also extends to some isotopic and incompatible trace element ratios [Eisele *et al.*, 2003; Rhodes and Vollinger, 2004]. Figures 11 and 12 show that HSDP2 high-SiO<sub>2</sub> glasses and Kilauea samples are also similar in most major and minor chemical components, but the K<sub>2</sub>O, Na<sub>2</sub>O, and P<sub>2</sub>O<sub>5</sub> contents of Kilauea lavas tend to be higher. Despite these differences, the high-SiO<sub>2</sub> HSDP2 glasses are most similar overall to Kilauea tholeiites among other known magmas from the island of Hawaii.

[43] • Mauna Loa glasses overlap the upper end of the distribution of SiO<sub>2</sub> contents of the high-SiO<sub>2</sub> HSDP2 glasses; Hualalai and Mahukona glasses are also typically at this end of the distribution, although their sample suites are small. However, Mauna Loa lavas have higher Al<sub>2</sub>O<sub>3</sub> and somewhat lower CaO, K<sub>2</sub>O, TiO<sub>2</sub> contents, and they are distinctly different in several isotopic and incompatible trace element ratios [DePaolo *et al.*, 1996; Blichert-Toft *et al.*, 2003; Huang and Frey, 2003; Kurz *et al.*, 2004; Rhodes and Vollinger, 2004].

[44] • Subaerially exposed Koolau lavas span a wide compositional range, but typically have SiO<sub>2</sub> contents higher than those of the high-SiO<sub>2</sub> HSDP2 glasses (52–54% SiO<sub>2</sub> after adjustment to 7% MgO; Figure 12). Relative to the high-SiO<sub>2</sub> HSDP2 glasses, these subaerial Koolau lavas also have higher Al<sub>2</sub>O<sub>3</sub>, Na<sub>2</sub>O, K<sub>2</sub>O, and P<sub>2</sub>O<sub>5</sub> and lower CaO; they are also distinctive isotopically and in terms of many ratios of incompatible trace elements [Blichert-Toft *et al.*, 2003; Huang and Frey, 2003]. Glasses with these characteristics have also been identified in what are believed to be

**Figure 11.** Comparison of SiO<sub>2</sub> versus various oxides/elements (wt.%) in HSDP2 glasses and in glasses from other Hawaiian volcanoes from the literature [Anderson and Wright, 1972; Moore *et al.*, 1982, 1990a, 1995; Hawkins and Melchior, 1983; Byers *et al.*, 1985; Garcia *et al.*, 1989, 1993, 1995a, 1995b; Clague and Moore, 1991; Clague *et al.*, 1991, 2000, 2002; Helz *et al.*, 1995; Mangan *et al.*, 1995; Garcia, 1996; Burkhard, 2001; Dixon and Clague, 2001; Johnson *et al.*, 2002; Shinozaki *et al.*, 2002; Davis *et al.*, 2003]: (a) Al<sub>2</sub>O<sub>3</sub>; (b) CaO; (c) FeO\*; (d) H<sub>2</sub>O; (e) Na<sub>2</sub>O + K<sub>2</sub>O; (f) K<sub>2</sub>O; (g) Na<sub>2</sub>O; (h) P<sub>2</sub>O<sub>5</sub>; (i) S; and (j) TiO<sub>2</sub>. For HSDP2 glasses, only samples with ≥7% MgO are shown (excepting the excursions at 1800 and 2233 mbsl, for which all glasses are shown); for glasses from the literature, only tholeiitic glasses with 7–8% MgO are shown. Symbols and color coding are explained in the legend. Degassed, partially degassed, and undegassed glasses are defined in section 4.1. Note that one altered, high-SiO<sub>2</sub> intrusive glass (SR0972-15.7) has a significantly elevated Na<sub>2</sub>O content relative to other high-SiO<sub>2</sub> glasses with comparable MgO contents; although shown on all previous figures, it is not shown on this or subsequent figures (except Figures 14 and 15).

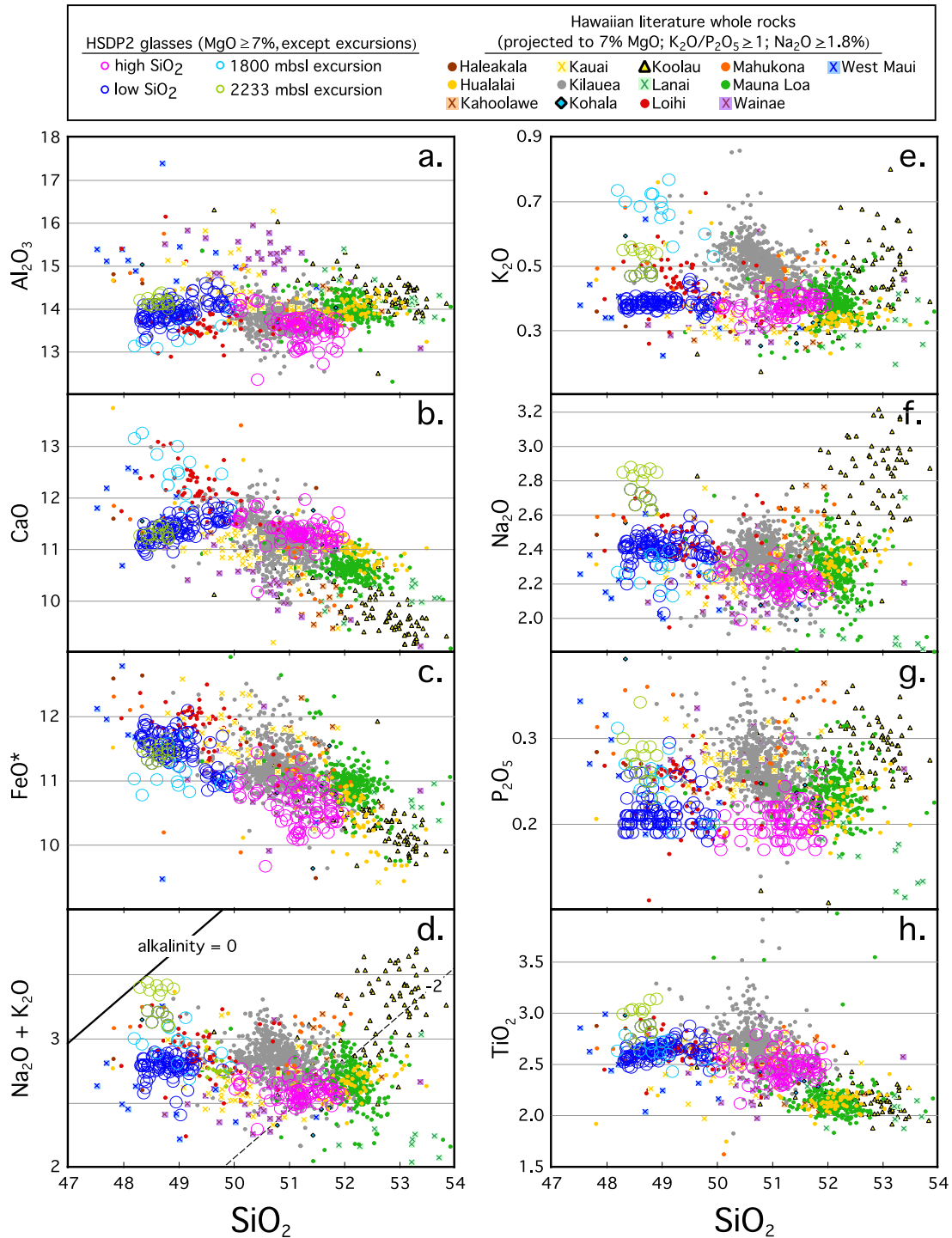


**Figure 12.** Comparison of  $\text{SiO}_2$  versus various oxides (wt.%) in HSDP2 glasses ( $\geq 7\%$  MgO; excepting excursions) and in tholeiitic whole rocks (i.e., alkalinity  $\leq 0$ ) from other Hawaiian volcanoes from the literature. Most whole rock analyses were downloaded from the GEOROC database (<http://georoc.mpch-mainz.gwdg.de/Entry.html>). Analyses shown in these Figures represent a subset of records in the precompiled database for the Hawaiian islands plus analyses for Kauai lavas from *Mukhopadhyay et al.* [2003]. In order to minimize the effects of alteration, whole rock analyses with  $\text{K}_2\text{O}/\text{P}_2\text{O}_5 < 1$  or  $\text{Na}_2\text{O} < 1.8\%$  were excluded from the compilation. Whole rock compositions for each volcano were separately fit to lines versus MgO and projected to 7% MgO as described in Appendix A4. Symbols and color coding are explained in the legend. (a)  $\text{Al}_2\text{O}_3$ ; (b) CaO; (c)  $\text{FeO}^*$ ; (d)  $\text{Na}_2\text{O} + \text{K}_2\text{O}$ ; (e)  $\text{K}_2\text{O}$ ; (f)  $\text{Na}_2\text{O}$ ; (g)  $\text{P}_2\text{O}_5$ ; and (h)  $\text{TiO}_2$ .

Koolau-derived submarine materials from the flank of Oahu [Clague *et al.*, 2002; Shinozaki *et al.*, 2002], and they are readily identified in Figures 10b and 11 as those samples with  $>52\%$   $\text{SiO}_2$ . In addition, recent studies of subsurface and submarine samples thought to represent an earlier phase of shield building of Koolau volcano [Jackson *et al.*, 1999; Shinozaki *et al.*, 2002; Tanaka *et al.*, 2002; Haskins and Garcia, 2004] have identified magma compositions that differ from the distinctive subaerially exposed Koolau lavas. Glasses from this “main shield stage” of the Koolau volcano [Tanaka *et al.*, 2002] typically have 50–52%  $\text{SiO}_2$  and comprise most of the Koolau glasses plotted in Figure 11. Although described as similar to Mauna Loa and Kilauea [Shinozaki *et al.*, 2002; Tanaka *et al.*, 2002], it is clear from Figure 11 that these lower- $\text{SiO}_2$  Koolau-derived glasses are most similar to the HSDP2 high- $\text{SiO}_2$  glasses. Indeed, of all well-characterized Hawaiian volcanoes, the high- $\text{SiO}_2$  HSDP2 glasses are most like those of Koolau’s “main shield phase” in terms of major elements; although there are some differences (e.g.,  $^{206}\text{Pb}/^{204}\text{Pb}$ ), this correspondence also extends to several trace element and isotopic ratios (e.g., compare results in Figure 7 with Tanaka *et al.* [2002]).

#### 4.5. Estimates of the Compositions of Mantle-Derived Magmas in the HSDP2 Core

[45] An important question raised by the range and distribution of  $\text{SiO}_2$  contents of the HSDP2 glasses and the complex pattern of  $\text{SiO}_2$  content as a function of depth in the core is whether the continuous range in  $\text{SiO}_2$  content reflects a continuum of mantle-derived magmas or the mixing of two discrete magma series within the volcanic edifice. How this question is answered influences strongly how to approach understanding the petrogenesis of the magmas sampled by the HSDP2 core. For example, at one extreme there could be a continuous range of source compositions and/or conditions of melting, such that each  $\text{SiO}_2$  content (after correction for fractionation, but this effect is not large over the observed range of fractionation of the HSDP2 glasses [see Seaman *et al.*, 2004]) in the observed range of glasses maps onto this range of mantle compositions and processes. At the other extreme, there might be only two parental magma compositions, one high- $\text{SiO}_2$  and the other low- $\text{SiO}_2$ , and samples with intermediate silica contents give information on mixing of magmas

rather than on source compositions or melting processes. It is in general difficult to distinguish between these end-member interpretations of a continuous compositional suite of magmas, but an argument can be made in the case of the HSDP2 glasses for two distinct magma series.

[46] The key observations that allow us to adopt as a working hypothesis that there are two dominant and distinct magma series in the HSDP2 core derive from Figure 3, which shows  $\text{SiO}_2$  contents versus the concentrations of  $\text{H}_2\text{O}$  and S. The distinction between the high- and low-silica groups may at first appear arbitrary because there is a continuous distribution of chemical composition between them; however, the volatile contents of these glasses suggest that there are two non-overlapping magma series for the HSDP2 rocks, not a continuum, because if we restrict our consideration to undegassed glasses, there are unambiguously two distinct, non-overlapping groups of glasses. Although more complex explanations could be advanced for the patterns shown in Figure 3, for the remainder of this paper we adopt the simple hypothesis that there are distinct high- and low- $\text{SiO}_2$  magma series and that intermediate- $\text{SiO}_2$  glasses either formed by mixing and degassing at high levels in the volcanic edifice or represent samples of the Ca-Al-rich glasses described in section 4.6 (most of which are degassed because they occur primarily in the shallower parts of the core.) The bimodal distribution of silica contents of the submarine HSDP2 glasses, particularly in zones 2–4 (Figure 9) and among glasses with  $\geq 7\%$  MgO (Figure 6), is consistent with this hypothesis. Seaman *et al.* [2004] discuss in detail additional evidence for interrelationships between mixing, degassing, and fractionation in the petrogenesis of HSDP2 lavas.

[47] In order to compare the low- and high- $\text{SiO}_2$  glasses to potential partial melts of mantle peridotite, we reconstructed a model parental liquid for each glass with  $\geq 7\%$  MgO from zones 3 and 4 by incremental addition of equilibrium olivine until the reconstructed liquid could equilibrate with  $\text{Fo}_{90.5}$  olivine (the most magnesian olivine found in HSDP1 Mauna Kea lavas [Baker *et al.*, 1996]). We then averaged all the reconstructed parental melts from each magma series to obtain model parent magmas for the low- and high- $\text{SiO}_2$  magma series; these model compositions are listed in Table 3. The average amount of olivine fractionation from these model parental magmas is 24.4%

for the low-SiO<sub>2</sub> series and 21.6% for the high-SiO<sub>2</sub> series.

#### 4.6. CaO-Al<sub>2</sub>O<sub>3</sub>-Enriched Glasses

[48] For the most part, there are no systematic variations in composition with SiO<sub>2</sub> within the high- and low-SiO<sub>2</sub> compositional groups. However, as shown in Figure 6, there is an elongation of the low-SiO<sub>2</sub> group toward a group of mostly degassed glasses with intermediate SiO<sub>2</sub> contents (i.e., between the well-defined undegassed low-SiO<sub>2</sub> and high-SiO<sub>2</sub> groups) and elevated CaO and Al<sub>2</sub>O<sub>3</sub> contents. Glasses with these characteristics are identified in Table 1. Most of these high-CaO-Al<sub>2</sub>O<sub>3</sub> glasses have <50% SiO<sub>2</sub> and thus are shown in blue, but some have higher SiO<sub>2</sub> contents and are shown in pink. In addition to their high CaO and Al<sub>2</sub>O<sub>3</sub> contents, these samples have lower FeO\* contents, slightly higher TiO<sub>2</sub> contents, and subtly different trace element patterns (Baker et al., manuscript in preparation, 2004a) relative to the main group of low-SiO<sub>2</sub> glasses. The sense of the variation from the dominant low-SiO<sub>2</sub> glasses to these distinctive CaO-Al<sub>2</sub>O<sub>3</sub>-enriched glasses does not point toward the main high-SiO<sub>2</sub> group (Figure 6). Note that the slightly elevated CaO and Al<sub>2</sub>O<sub>3</sub> contents are only apparent in glasses with greater than ~7% MgO; HSDP2 glasses with lower MgO contents have generally experienced pyroxene and plagioclase fractionation [Seaman et al., 2004], and thus even if they were derived from liquids with these characteristics, they would not preserve them.

[49] All of the CaO-Al<sub>2</sub>O<sub>3</sub>-enriched glasses identified in Table 1 are from zone 2, and all of the zone 2 low-SiO<sub>2</sub> glasses are plausibly identified with this group. However, in addition to the CaO-Al<sub>2</sub>O<sub>3</sub>-enriched samples identified in Table 1, three degassed low-SiO<sub>2</sub> hyaloclastite glasses from zone 1 (SR539-4.3, SR540-6.8, and SR541-8.1; i.e., all of the low-SiO<sub>2</sub> glasses from zone 1 other than the excursion at ~1800 mbsl; see section 7), three partially degassed pillows from near the base of zone 3 (SR831-15.7, SR833-3.1, SR833-9.0), and two undegassed intrusive glasses from near the base of zone 4 (SR944-11.3, SR944-11.6) have generally similar characteristics, but have been excluded because of slight differences from the majority of the members of this group (e.g, the two intrusives from near the base of zone 4 have CaO, Al<sub>2</sub>O<sub>3</sub>, and SiO<sub>2</sub> contents similar to the bulk of the CaO-Al<sub>2</sub>O<sub>3</sub>-enriched glasses, but they have distinctly higher FeO\* contents). One other zone 3 pillow glass (SR0831-2.3) and one other zone 4 intrusive glass (SR0949-8.2) also have similar char-

acteristics, but they are not included in the CaO-Al<sub>2</sub>O<sub>3</sub>-enriched group because they have <7% MgO. The key point here is that although the CaO-Al<sub>2</sub>O<sub>3</sub>-enriched glasses are a clearly defined subgroup of the HSDP2 samples, for some samples the criteria for including them or not in this group is subjective.

[50] Although it is tempting to equate this group of HSDP2 glasses with the type 2 low-SiO<sub>2</sub> whole rocks identified by Rhodes and Vollinger [2004] because both occur preferentially in the shallow parts of the core, this cannot be the case since Rhodes and Vollinger did not classify the zone 2 low-SiO<sub>2</sub> samples as type 2, yet this is the most extensive occurrence of Ca-Al-rich glasses in the core; we conclude that the distinguishing characteristics of the Ca-Al-rich glass type appear to be sufficiently small that they are not recognizable from the whole rock analyses.

[51] The differences between these CaO-Al<sub>2</sub>O<sub>3</sub>-enriched glasses and the more abundant low-SiO<sub>2</sub> HSDP2 glasses are subtle, but we nevertheless conclude that they represent a distinctive compositional subgroup because their compositions cannot be explained by low-pressure fractionation of either the high- or low-SiO<sub>2</sub> groups [Seaman et al., 2004] or by magma mixing between these groups. Consequently, we infer that the trend from the more typical low-SiO<sub>2</sub> glasses to these CaO-Al<sub>2</sub>O<sub>3</sub>-rich glasses at slightly higher SiO<sub>2</sub> contents represents a mantle-derived signature. As developed below, our preferred explanation for the petrogenesis of their parental liquids is that they contain contributions from pyroxene-rich lithologies in their mantle sources (see section 5.4).

[52] As we did for the low- and high-SiO<sub>2</sub> glasses, a model parental liquid was calculated for each CaO-Al<sub>2</sub>O<sub>3</sub>-rich glass by incremental addition of liquidus olivine until the liquid composition could coexist with Fo<sub>90.5</sub> olivine. The average of eight of the most silica-rich of these reconstructed liquid compositions is listed in Table 3. The average amount of olivine fractionation from this model parental magma is 23.0%.

### 5. Constraints on Petrogenesis

[53] The ultimate goals of our petrological and geochemical investigations are to constrain the compositions of the mantle sources of magmas sampled in the HSDP core, the variability in processes and conditions of melting leading to the observed magma compositions, and the tem-

**Table 3.** Phase Compositions Used in Mass Balance Calculations

Phase	SiO <sub>2</sub>	TiO <sub>2</sub>	Al <sub>2</sub> O <sub>3</sub>	FeO*	MnO	MgO	CaO	Na <sub>2</sub> O	K <sub>2</sub> O	P <sub>2</sub> O <sub>5</sub>	Fit A <sup>a</sup>	Fit B <sup>b</sup>	Fit C <sup>c</sup>
low-Si <sup>d</sup>	46.72	1.98	10.52	11.76	0.17	17.42	8.62	1.81	0.29	0.16	0.918(11)	0.942(17)	0.948(16)
1 sigma <sup>d</sup>	0.18	0.04	0.11	0.12	—	0.19	0.08	0.06	0.01	0.01			
oliv <sup>e</sup>	40.68	0.01	0.12	9.46	0.13	48.85	0.44	0	0	0	-0.116(9)	-0.064(10)	-0.063(10)
opx <sup>e</sup>	54.37	0.19	5.44	5.58	0.11	31.46	2.19	0.13	0	0	0.119(17)	0.023(20)	0.062(16)
cpx <sup>e</sup>	54.19	0.24	4.24	5.41	0.11	24.88	9.77	0.56	0	0	0.079(14)	0.076(18)	
cpx <sup>f</sup>	51.2	0.28	9.8	3.9	0.11	18.9	15.1	0.8	0.03	0.02			0.048(11)
gt <sup>f</sup>	43.2	0.42	23.07	6.1	0.18	20.9	6.1	0.01	0.02	0.02		0.022(8)	0.004(6)
high-Si <sup>g</sup>	48.99	1.91	10.56	10.79	0.17	15.95	8.86	1.74	0.30	0.16	1.000		
1 sigma <sup>g</sup>	0.30	0.04	0.15	0.26	—	0.40	0.21	0.09	0.02	0.01			
model A <sup>a</sup>	48.92	1.86	10.63	10.79	0.16	16.03	8.9	1.72	0.27	0.15			
% error A <sup>a</sup>	0.14	2.7	0.66	0.01	3.1	0.46	0.39	0.92	11.0	7.6			
high-Ca,Al <sup>h</sup>	47.94	1.97	10.89	11.18	0.15	16.52	9.05	1.78	0.29	0.15		1.000	1.000
1 sigma <sup>h</sup>	0.06	0.06	0.09	0.06	—	0.10	0.06	0.02	0.01	0.01			
model B <sup>b</sup>	47.76	1.90	10.86	11.16	0.16	16.39	9.02	1.75	0.28	0.15			
% error B <sup>b</sup>	0.37	3.4	0.25	0.12	7.1	0.79	0.35	1.28	4.3	2.2			
model C <sup>c</sup>	47.77	1.91	10.86	11.12	0.16	16.41	9.03	1.77	0.28	0.15			
% error C <sup>c</sup>	0.35	3.1	0.22	0.45	6.5	0.66	0.28	0.62	3.3	3.2			

<sup>a</sup>Weighted mass balance fit to the mean high-SiO<sub>2</sub> glass composition; chi-squared = 5.17;  $Q = 0.64$  (where  $Q$  is the chi-squared distribution for a specified number of degrees of freedom). Calculated glass composition and phase proportions (as weight fractions and one sigma uncertainties in parentheses). Percent error is 100 times the absolute value of the difference for each oxide between the high-SiO<sub>2</sub> composition and the calculated model A composition divided by the actual oxide value. The sigma values used to weight the mass balance are 0.23 SiO<sub>2</sub>, 0.10 TiO<sub>2</sub>, 0.08 Al<sub>2</sub>O<sub>3</sub>, 0.15 FeO\*, 0.02 MnO, 0.17 MgO, 0.09 CaO, 0.05 Na<sub>2</sub>O, 0.02 K<sub>2</sub>O, and 0.03 P<sub>2</sub>O<sub>5</sub> and were calculated by multiplying the mean of the two sets of percent errors calculated for the average BCR-2g and VG-2 microprobe analyses (see Table 2) by each oxide value in the high-SiO<sub>2</sub> composition listed above. This approach was used so as to provide a consistent set of weights for all the mass balance calculations, e.g., the 1 sigma values based on the mean of the high-CaO, Al<sub>2</sub>O<sub>3</sub> samples are small due to the small number of samples included in that average (see footnote h).

<sup>b</sup>Mass balance fit to the mean high-CaO, Al<sub>2</sub>O<sub>3</sub> glass composition; chi-squared = 2.88;  $Q = 0.82$ . Fit uses the residual olivine, orthopyroxene, and clinopyroxene compositions from the peridotite melting calculation and the residual garnet composition from the garnet pyroxenite melting experiment of *Hirschmann et al.* [2003]. Percent error is as defined in footnote a. Sigma values used as weights in the mass balance (0.23 SiO<sub>2</sub>, 0.10 TiO<sub>2</sub>, 0.08 Al<sub>2</sub>O<sub>3</sub>, 0.16 FeO\*, 0.02 MnO, 0.17 MgO, 0.09 CaO, 0.05 Na<sub>2</sub>O, 0.02 K<sub>2</sub>O, 0.02 P<sub>2</sub>O<sub>5</sub>) were calculated as described in footnote a.

<sup>c</sup>Mass balance fit to the mean high-CaO, Al<sub>2</sub>O<sub>3</sub> glass composition; chi-squared = 2.17;  $Q = 0.90$ . Fit uses the residual olivine and orthopyroxene compositions from the peridotite melting calculation and the residual clinopyroxene and garnet compositions from the garnet pyroxenite melting experiment of *Hirschmann et al.* [2003]. Percent error as defined in footnote a. Sigma values used to weight the fit are listed in footnote b.

<sup>d</sup>Mean of 76 low-SiO<sub>2</sub> zone 3 and zone 4 undegassed or partially degassed glasses (with  $\geq 7$  wt.% MgO) recalculated to be in equilibrium with Fo<sub>90.5</sub> olivine using an oliv-liqu  $K_{D,Fe+2-Mg}$  of  $0.32 \pm 0.02$  ( $1\sigma$ ) and an  $fO_2$  of QFM. Not included in the calculation were SR0944-11.3 and SR0944-11.6 (zone 4); these two glasses plot within the field of the raw high-Ca-Al glasses (they plot outside the high-Ca-Al field after both sets are adjusted back to Fo<sub>90.5</sub>). The  $K_D$  value represents the mean of 170 oliv-liqu  $K_D$  values from one-atmosphere experiments on picritic to andesitic compositions [*Kinzler and Grove*, 1985; *Tormey et al.*, 1987; *Longhi and Pan*, 1988; *Grove and Juster*, 1989; *Thy et al.*, 1991, 1998, 1999; *Thy*, 1995; *Toplis and Carroll*, 1995; *Yang et al.*, 1996b] calculated after partitioning total Fe in the liquid into FeO and Fe<sub>2</sub>O<sub>3</sub> using the expression of *Kress and Carmichael* [1991]. Starting with each glass with  $\geq 7$  wt.% MgO, 0.0001 weight fraction of equilibrium olivine was repeatedly added to each composition until that evolving composition was in equilibrium with Fo<sub>90.5</sub> olivine; the minor element composition of the olivine was held constant throughout the calculation, and the abundances of Al, Cr, Mn, and Ca represent the mean concentration of these elements found in MK olivine phenocrysts [*Baker et al.*, 1996]. The 1 sigma values are the sample standard deviations for each oxide value in the mean of the olivine-adjusted low-SiO<sub>2</sub> glasses; only 10 of the glasses were analyzed for MnO (CIT analyses), and thus no standard deviation is given.

<sup>e</sup>Olivine, orthopyroxene, and clinopyroxene compositions calculated using BATCH [*Longhi*, 2002], the following mantle composition (44.9 SiO<sub>2</sub>, 0.38 TiO<sub>2</sub>, 3.94 Al<sub>2</sub>O<sub>3</sub>, 0.384 Cr<sub>2</sub>O<sub>3</sub>, 8.55 FeO\*, 0.135 MnO, 38.3 MgO, 3.04 CaO, 0.36 Na<sub>2</sub>O, 0.029 K<sub>2</sub>O), and the following pressure-melting path: 10% melting at 30 kbar; removal of 9.5% melt; 30 to 25 kbar continuous polybaric melting of the resulting residue (2% melting per kbar with 1.5% melt removal); total amount of melt removed is 16.1%; calculated temperature at 25 kbar is 1524°C. The residual mantle mode (in weight fraction) is 0.676 olivine, 0.185 orthopyroxene, 0.119 clinopyroxene.

<sup>f</sup>Residual phases of run 95MMH23 [*Hirschmann et al.*, 2003], a 25 kbar melting experiment at 1500°C on a garnet pyroxenite bulk composition.

<sup>g</sup>Mean high-SiO<sub>2</sub> glass composition; the average of 47 olivine-adjusted (in equilibrium with Fo<sub>90.5</sub> olivine, see footnote d) zone 4 undegassed or partially degassed high-SiO<sub>2</sub> glasses (with  $\geq 7$  wt.% MgO). The 1 sigma values are the sample standard deviations for each oxide value in the mean of the olivine-adjusted high-SiO<sub>2</sub> glasses; only three of the glasses were analyzed for MnO (CIT analyses), and thus no standard deviation is given.

<sup>h</sup>Mean high-CaO, Al<sub>2</sub>O<sub>3</sub> glass composition (average of eight zone 2 degassed high-SiO<sub>2</sub> glasses with  $\geq 7$  wt.% MgO after adjusting for olivine addition; samples included in average: SR0755-4.6, SR0758-3.1, SR0759-18.8, SR0761-1.0, SR0762-9.1, SR0763-2.7, SR0763-6.1, and SR0764-11.8). The 1 sigma values are the sample standard deviations for each oxide value in the mean of these olivine-adjusted glasses. MnO value is based on one CIT analysis; no standard deviation is reported.

poral and spatial variations of these parameters and processes. The compositional differences between the high- and low-SiO<sub>2</sub> magma series must reflect to some degree differences in source composition based on ratios of highly incompatible trace elements and in isotopic ratios (see section 4.1).

Although separation of the effects of varying source composition, the pressure and degree of melting, and the effects of mixing and magma-mantle interactions during ascent is difficult and generally requires assumptions about the nature and/or origin of the compositional variability in

the source, we nevertheless evaluate here several simple hypotheses for the observed range of primitive magma compositions from the HSDP2 core. We defer discussion of the excursions at 2233–2280 and 1765–1810 mbsl to sections 6 and 7.

### 5.1. Direct Partial Melts of Peridotite

[54] Figure 13 compares the average reconstructed primitive high- and low-SiO<sub>2</sub> liquid compositions with fields encompassing experimental partial melts of lherzolites or mixtures of basalt and peridotite minerals under nominally dry conditions. Although the results of such experiments depend upon the starting composition and it is unlikely that Hawaiian magmas represent single stage melts (i.e., as opposed to blends of melts from sources

spanning a range of compositions, pressures, and temperatures), it is nevertheless clear that the reconstructed parental liquid of the low-SiO<sub>2</sub> series is broadly consistent with melting of a lherzolitic source at 30–40 kbar. Note that our analysis cannot distinguish between harzburgitic and lherzolitic residues in the sources of the parents of the low-SiO<sub>2</sub> magmas, and indeed this distinction would be difficult if the degree of melting were approximately that required to exhaust clinopyroxene from these sources. A similar estimate of 28–30 kbar for the

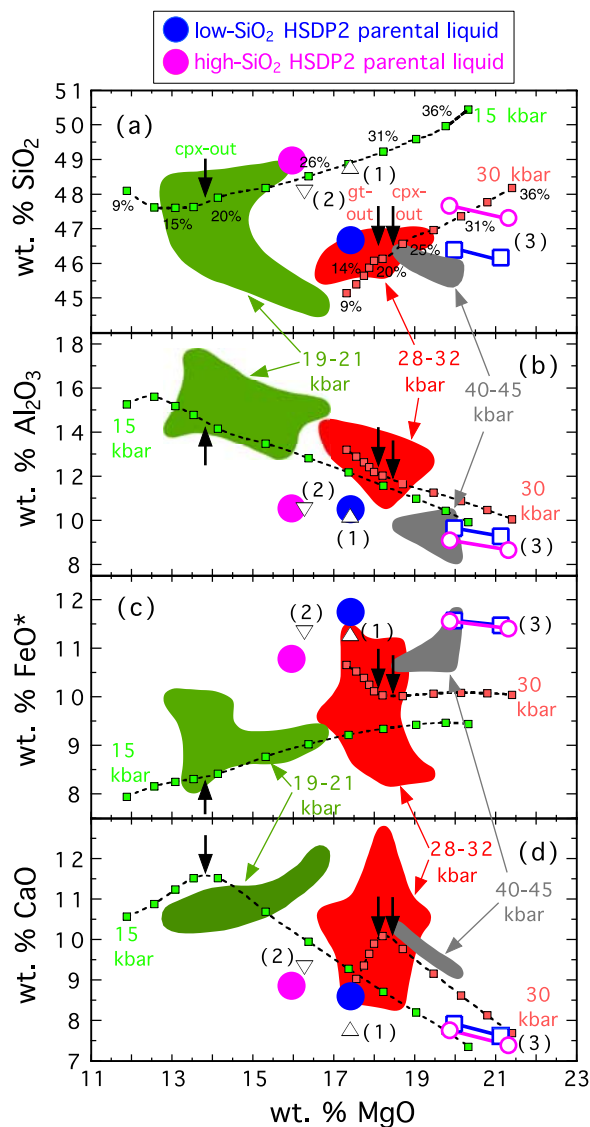


**Figure 13.** Variation diagrams comparing high- and low-SiO<sub>2</sub> HSDP2 parental liquids with high-pressure experimental liquids at 19–21 kbar (green field), 28–32 kbar (red field), and 40–45 kbar (gray field). Only experimental liquids that meet the following criteria were used to define these fields: the experimental starting materials were either peridotites or mixtures of basalt and peridotite minerals; Na<sub>2</sub>O contents of 1.0–2.6%; K<sub>2</sub>O contents  $\leq$ 1.0%; mg#  $\geq$ 0.7; for experiments at  $P \leq 30$  kbar, an equilibrium solid assemblage of olivine + orthopyroxene + clinopyroxene  $\pm$  spinel and/or garnet; for  $P > 30$  kbar, a solid assemblage of olivine + clinopyroxene  $\pm$  orthopyroxene  $\pm$  garnet. Data sources: Falloon and Green [1988], Hirose and Kushiro [1993], Kinzler [1997], Kushiro [1996], Salters et al. [2002], and Walter [1998]. HSDP2 parental liquid compositions were calculated as follows: low-SiO<sub>2</sub> glasses with  $\geq$ 7% MgO from zone 3 and zone 4 were recalculated to be in equilibrium with Fo<sub>90.5</sub> olivine and then averaged to give the low-SiO<sub>2</sub> parent liquid; the high-SiO<sub>2</sub> parent liquid represents the mean of zone 4 high-SiO<sub>2</sub> glasses with  $\geq$ 7% MgO after recalculation to equilibrium with Fo<sub>90.5</sub> olivine (the olivine addition calculations are described in section 4.5 and Table 3). The open triangles labeled (1) and (2) are the starting compositions for the experiments on Kilauea magmas of Wagner and Grove [1998] and Eggins [1992], respectively. The pink open circles and blue open squares labeled (3) are the calculated high- and low-SiO<sub>2</sub> HSDP2 parent liquids of Feigenson et al. [2003]. A 15 kbar batch melting path using the mantle composition reported in Table 3 and the algorithm of Longhi [2002] is shown by the small green squares; the degree of melting varies from 8.8 to 38.8% (the numbers next to every other point in Figure 13a indicate the degree of melting); the black vertical arrow in each panel indicates clinopyroxene-out (at  $\sim$ 17–20% melting). The small red squares show the 30 kbar melting path calculated using the same bulk mantle composition and algorithm; the degree of melting varies from 8.5 to 35.9% (the numbers next to every other point in Figure 13a indicate the degree of melting), and the vertical black arrows indicate garnet-out and clinopyroxene-out (at  $\sim$ 20–23% and 23–25% melting, respectively). (a) MgO versus SiO<sub>2</sub>; (b) MgO versus Al<sub>2</sub>O<sub>3</sub>; (c) MgO versus FeO\*; (d) MgO versus CaO.

pressure at which the low-SiO<sub>2</sub> parental liquid could equilibrate with lherzolitic or harzburgitic assemblages is obtained using the approach of Wang *et al.* [2002]. Likewise, Feigenson *et al.* [2003] concluded on the basis of comparison with projected high-pressure phase relations that a model parental liquid for the low-SiO<sub>2</sub> magma series equilibrated with a harzburgitic residue at 30–35 kbar and represents 12–13% melting; our low-SiO<sub>2</sub> parent composition (Table 3) projects just within the harzburgite field at ~27 kbar (very close to harzburgite-lherzolite boundary) on the pseudoternary phase diagram of Feigenson *et al.* [2003]. Finally, Figure 13 shows the calculated sequence of partial melts of a peridotitic source (see Table 3) at 30 kbar based on the parameterization of Longhi [2002]; comparison of the average low-SiO<sub>2</sub> parental liquid to this calculated trend illustrates its overall consistency with lherzolite- or harzburgite-saturated partial melts under these conditions. Although these inferences of the pressure at which the parental liquids of the low-SiO<sub>2</sub> magma series could have been generated are based on similar experimental data sets, the data treatments are largely independent, so we consider it significant that all suggest equilibration with a harzburgitic or lherzolitic residue at ~30–40 kbar. Experiments specifically directed at testing or refining this statement will be required, but we accept as a working hypothesis that the low-SiO<sub>2</sub> series derives from parental liquids produced under these conditions.

[55] We are unable to determine on the basis of Figure 13 whether garnet would have been present in the residual sources of the melts parental to the low-SiO<sub>2</sub> magmas, but Feigenson *et al.* [2003] and Huang and Frey [2003] concluded on the basis of trace element abundances that garnet was absent from these residues. However, these suggestions contrast with analysis of trace element abundances in other Hawaiian magmas [Hofmann *et al.*, 1984; Budahn and Schmitt, 1985; Sims *et al.*, 1995], which have been used to infer that the residues of Hawaiian primary magmas contain garnet.

[56] In contrast to the parental liquid of the low-SiO<sub>2</sub> series, Figure 13 suggests that the parental liquid of the high-SiO<sub>2</sub> series is unlikely to be saturated with a lherzolitic assemblage under dry conditions at any pressure. In particular, at the MgO content of the reconstructed parental liquid composition, the high SiO<sub>2</sub> content of this parental liquid could only be consistent with olivine +

orthopyroxene-saturation at pressures of ~15–20 kbar, yet the CaO contents are far too low to be consistent with clinopyroxene saturation under these conditions. Again, these inferences must be tested directly by experimentation on the reconstructed parental high-SiO<sub>2</sub> liquid composition. Nevertheless, they are consistent with the conclusions of Feigenson *et al.* [2003], although they estimate harzburgite equilibration pressures of 20–30 kbar for their more MgO-rich estimate of the composition of the high-SiO<sub>2</sub> parental liquid. Olivine + orthopyroxene-saturation for the HSDP2 high-SiO<sub>2</sub> parental melt is also consistent with the experiments of Wagner and Grove [1998] and Eggins [1992], which suggest that the parental liquids of Hawaiian magmas from Kilauea (which as shown in Figure 13 are similar in composition to the reconstructed high-SiO<sub>2</sub> HSDP2 parent liquid) are saturated with harzburgitic assemblages at 14 and 20 kbar (1425 and 1450°C, respectively), but are not saturated with lherzolitic assemblages under any conditions. Comparison of the estimated high-SiO<sub>2</sub> parental liquid with calculated partial melts of a fertile peridotitic source at 15 kbar based on the parameterization of Longhi [2002] reinforces this conclusion. Note, however, that the FeO\* contents of both the reconstructed high- and low-SiO<sub>2</sub> parent liquids are significantly higher than expected for peridotite melting on the basis of the Longhi [2002] calculations; this probably signifies that the FeO\* contents of the sources of HSDP2 magmas are higher than estimates for relatively primitive upper mantle.

[57] Could the high-SiO<sub>2</sub> liquids simply represent higher degrees of isentropic melting to lower pressures of the same (or similar) sources that produced the low-SiO<sub>2</sub> liquids, such that clinopyroxene was exhausted between the degree of melting of the low-SiO<sub>2</sub> melts (leaving a lherzolitic residue) and the high-silica melts (leaving a harzburgitic residue)? Although this could explain the nearly identical CaO contents of the high- and low-SiO<sub>2</sub> parental melts (i.e., the maximum in CaO content of partial melts of peridotite that corresponds to clinopyroxene-out could be bracketed by the degrees of melting that produced the high- and low-SiO<sub>2</sub> parental melts), it cannot be reconciled with their nearly identical Al<sub>2</sub>O<sub>3</sub> (Figure 13), Na<sub>2</sub>O, K<sub>2</sub>O, and P<sub>2</sub>O<sub>5</sub> contents (see Table 3). The details of the trace element and isotopic geochemistry of the two magma types are also inconsistent with the two magma types representing different degrees of melting of identical sources [Bryce and DePaolo,

2000; Blichert-Toft *et al.*, 2003; Eisele *et al.*, 2003; Huang and Frey, 2003; Kurz *et al.*, 2004].

## 5.2. Mixing of Melts of Peridotite and Eclogite/Pyroxenite

[58] Hauri [1996] proposed that the overall trend in magma composition among Hawaiian volcanoes could be understood by mixing between basaltic melts of peridotitic source components (resulting in the low-SiO<sub>2</sub>, high-FeO\* end of the trend shown in Figures 11c and 12c) and dacitic melts of eclogitic source components (producing the high-SiO<sub>2</sub>, low-FeO\* end of the trend). He argued that this trend cannot represent variable degrees of melting of a single source because of the correlations between major elements and isotopic ratios and the fact that the SiO<sub>2</sub> and FeO\* contents of lavas from most Hawaiian volcanoes (even after correction for olivine fractionation) do not overlap with experimentally determined trends defined by clinopyroxene ± garnet-saturated partial melts of mantle peridotite at any pressure. Jackson *et al.* [1999], Takahashi and Nakajima [2002], and Norman *et al.* [2002] developed these ideas further with specific reference to the SiO<sub>2</sub>- and Na<sub>2</sub>O-rich tholeiites from Koolau. In addition, Reiners [2002] suggested that melting of pyroxenite or eclogite results in enrichments in SiO<sub>2</sub> in magmas from Hawaii and elsewhere, and Lassiter *et al.* [2000] proposed that silica enrichment results from the involvement of pyroxenites from the Pacific lithosphere in the formation of post-erosional lavas from Oahu and Kauai.

[59] The high- and low-SiO<sub>2</sub> glasses from the HSDP2 core fall on the FeO\*-SiO<sub>2</sub> trend defined by most Hawaiian lavas (see Figures 11c and 12c), so if only FeO\* and SiO<sub>2</sub> were considered, their compositions might be explained by the hypothesis of mixing of dacitic melts of eclogite with basaltic melts of peridotite if this were the explanation of this overall trend in Hawaiian magmas. This hypothesis could also be consistent with the conclusion of Eisele *et al.* [2003] that recycled oceanic crust could explain aspects of the HSDP Pb isotope data. However, as described in section A4, although the high-SiO<sub>2</sub> HSDP2 glasses fall on the overall trends of Hawaiian lavas in Figures 11 and 12, the low-SiO<sub>2</sub> HSDP2 glasses fall off the trends for several major elements (e.g., in CaO-SiO<sub>2</sub> and Al<sub>2</sub>O<sub>3</sub>-SiO<sub>2</sub> space); they also define trace element trends at high angle to those of the high-SiO<sub>2</sub> magma series [Huang and Frey, 2003]. Consequently, neither

this nor any other hypothesis that explains the overall inter-volcano trend of Hawaiian magmas can be applied without modification to explaining the differences between the high- and low-SiO<sub>2</sub> HSDP2 magma series.

[60] Rigorous testing of a generic role for eclogite or pyroxenite in the petrogenesis of the HSDP2 glasses is difficult because of the wide range of possible pyroxene-rich lithologies, bulk compositions, and melting behaviors [e.g., Hirschmann and Stolper, 1996; Schiano *et al.*, 2000] and because of intrinsic complexities in the melting behavior of sources containing multiple lithologies [Hirschmann and Stolper, 1996; Phipps Morgan, 1999]. However, the specific hypothesis presented by Hauri [1996] is readily testable because he provided an estimate of the composition of the dacitic melt that he proposed as an end-member to the array of Hawaiian magma compositions. As shown in Figure 14, although successful in FeO\*-SiO<sub>2</sub> space, this hypothesis cannot explain trends in any other major oxides among the two HSDP2 glass groups (or among Hawaiian magmas as a whole). Other objections to this hypothesis as applied to Hawaiian magmas as a whole are that more SiO<sub>2</sub>-rich Hawaiian magmas do not have systematically elevated Sr/Y ratios [Norman and Garcia, 1999]; that models of aggregated melts of average pyroxenite and eclogite have Sm/Yb and Na/Ti ratios inconsistent with the trend of Hawaiian lavas [Putirka, 1999]; and that combined Hf-Nd-Th isotope and trace element systematics of Hawaiian basalts, and in particular the lack of dependence of isotope ratios on degree of melting, argue against a significant role for garnet pyroxenite or eclogite in their sources [Stracke *et al.*, 1999].

[61] Although we conclude that the high-SiO<sub>2</sub> and low-SiO<sub>2</sub> HSDP2 magmas cannot be related by the involvement of melts of eclogite or pyroxenite in the specific form proposed by Hauri [1996], we emphasize again that there are many potential free parameters for such a process. We describe below (section 5.4) a model that invokes pyroxene-rich lithologies to explain the trend from the low-SiO<sub>2</sub> HSDP2 glasses toward the slightly CaO-Al<sub>2</sub>O<sub>3</sub>-enriched glasses described in section 4.6.

## 5.3. Thermal and Chemical Interaction Between Ascending Melt and Mantle Peridotite

[62] An alternative to relating the high- and low-SiO<sub>2</sub> magma types by different degrees of peridotite

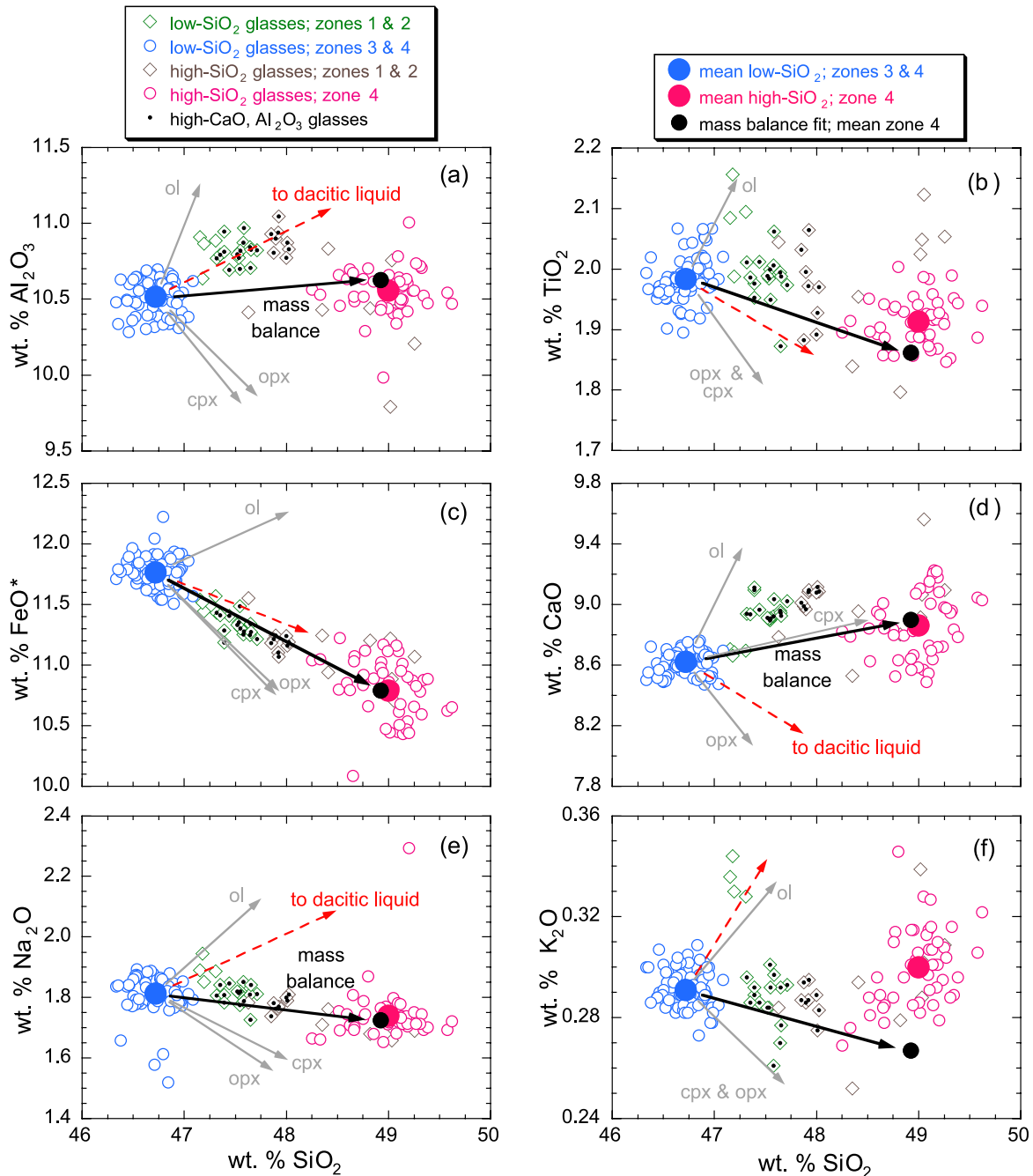


**Figure 14.** Results of the mass balance calculations relating the average recalculated low-SiO<sub>2</sub> parent liquid (filled blue circle) to the average recalculated high-SiO<sub>2</sub> parent liquid (filled pink circle) by addition/subtraction of residual peridotite minerals. Individual HSDP2 glasses with  $\geq 7\%$  MgO (small open circles and diamonds) were corrected to equilibrium with Fo<sub>90.5</sub> olivine at QFM and 1 bar. Open diamonds with small black circles denote the CaO-Al<sub>2</sub>O<sub>3</sub>-enriched glasses. The large filled black circle represents the best-fit high-SiO<sub>2</sub> parent liquid composition based on the mass balance calculation, and the heavy black arrow shows the vector between the average low-SiO<sub>2</sub> parent liquid and this best-fit composition. The gray arrows labeled “ol,” “opx,” and “cpx” show the compositional effects of olivine crystallization and pyroxene dissolution and only one arrow is shown. Phase compositions and details of this mass balance calculation are given in Table 3 and in the text. The red dashed arrow labeled “to dacitic liquid” shows a mixing line between the low-SiO<sub>2</sub> parent liquid and the dacitic partial melt of *Hauri* [1996]. SiO<sub>2</sub> versus (a) Al<sub>2</sub>O<sub>3</sub>, (b) TiO<sub>2</sub>, (c) FeO\*, (d) CaO, (e) Na<sub>2</sub>O, (f) K<sub>2</sub>O.

melting over a range of pressures or mixing between melts of distinct sources is a class of hypothesis relating the two magma types through the interaction of ascending melts with the solid matrix of the overlying mantle [e.g., Kelemen, 1986, 1990; Kelemen *et al.*, 1990, 1995; Eggins, 1992; Wagner and Grove, 1998; Asimow and Stolper, 1999; Asimow, 2002]. The simplest view of this process is that a temperature difference develops between adiabatically ascending liquid and the peridotite through which it ascends, which is cooler either because it is on its partially molten adiabat or because it has been cooled by conductive cooling through the overlying lithosphere. If the ascending liquid and cooler peridotite are allowed to interact thermally on ascent, this leads to extra melting of the peridotite as heat is transferred from the liquid (assuming the peridotite is at or near its solidus). If the liquid and peridotite interact chemically as well as thermally, trends in liquid composition different from those accompanying simple batch or fractional fusion can result. In particular, resorption of orthopyroxene and clinopyroxene and precipitation of olivine are typical results of this process. Although no one, to our knowledge, has rigorously modeled the trace element signature of this process, simplified models of the interaction between ascending melts and mantle peridotite suggest that this type of interaction can produce complex trace element patterns in the evolving liquid [e.g., Navon and Stolper, 1987; Kelemen *et al.*, 1990; Spiegelman and Kelemen, 2003].

[63] This kind of interaction can be readily envisioned in the context of an ascending plume beneath Hawaii. Although the details are complex, as the material in the ascending plume encounters the overlying lithosphere, it begins to flow horizontally and is dragged in the direction of movement of the overlying Pacific plate. Thus the high-temperature material undergoing decompression melting in the central part of the ascending plume is overlain by horizontally moving material from the leading edge of the plume that may have already undergone some degree of melting [see Ribe and Christensen, 1999], and ascending melts can be expected to interact with these overlying residues [Ribe and Smooke, 1987]. Eggins [1992] and Wagner and Grove [1998] envisioned such a process when they proposed that melts from depth interacted with shallow, plume-derived, harzburgitic residues to produce the high-SiO<sub>2</sub> magmas of Kilauea. Rhodes and Hart [1995] invoked a similar process to explain the presence of a Kilauea-like isotopic signature in Mauna Loa lavas. As devel-

oped by Kelemen and his colleagues for mid-ocean ridges and island arcs, this process of reactive melt migration beneath Hawaii could lead to the development of high-porosity, olivine-rich channels through which liquids from depth ascend [e.g., Kelemen, 1986, 1990; Kelemen *et al.*, 1995].

[64] Detailed modeling of this process is complex, requiring energy and mass balances, parameterization of phase equilibria, and specifications of ratios of melt and rock fluxes [Asimow and Stolper, 1999; Asimow, 2002]. We have evaluated this hypothesis from the perspective of mass balance: that is, we ask whether the parental magmas of the high- and low-SiO<sub>2</sub> series could be related by addition and/or subtraction of olivine ± orthopyroxene ± clinopyroxene. The low- and high-SiO<sub>2</sub> parent liquids used in this mass balance calculation are the same reconstructed compositions shown in Figure 13. The phase compositions used in the mass balance and the resulting fits are reported in Table 3. A least squares mass balance involving these phases produces an excellent match to the high-SiO<sub>2</sub> magma series by coupled crystallization of olivine and resorption of orthopyroxene and clinopyroxene by the low-SiO<sub>2</sub> magma series. On the basis of a weighted fit, the balanced equation required for this match is

$$\begin{aligned}
 &0.918(11)(\text{low-SiO}_2\text{melt}) - 0.116(9)(\text{olivine}) \\
 &\quad + 0.119(17)(\text{orthopyroxene}) + 0.079(14)(\text{clinopyroxene}) \\
 &= 1(\text{high-SiO}_2\text{melt})
 \end{aligned}$$

The coefficients are weight fractions and the values in parentheses are one-sigma uncertainties. The mean of the absolute values of the ten oxide residuals in the above fit is 0.036%; not including clinopyroxene in the mass balance results in a significantly poorer fit.

[65] Figure 14 shows the vector in composition space corresponding to the reaction defined by this mass balance and illustrates graphically the degree to which the chemical composition of the average high-SiO<sub>2</sub> magma can be matched by this reaction. It is important to emphasize that although this mass balance has three free parameters (i.e., the coefficient for high-SiO<sub>2</sub> melt is set to 1 and the sum of the other four coefficients must sum to 1), it successfully accounts for 10 major and minor elements in the high-SiO<sub>2</sub> parent magma. Note that this mass balance requires an increase in the amount of melt in the production of the high-SiO<sub>2</sub> magma from the low-SiO<sub>2</sub> magma, consistent with the conceptual framework of thermal and chemical interaction between ascending melt and

overlying near-solidus peridotite. Moreover, the sense of the mass balanced reaction (resorption of orthopyroxene and clinopyroxene accompanied by precipitation of olivine) is consistent with known phase equilibria and thermodynamic analysis of the interactions between peridotite and ascending melt [Kelemen, 1990].

[66] It is noteworthy that clinopyroxene is a significant component of the mass balanced reaction (i.e., the ratio of resorbed orthopyroxene to clinopyroxene is  $\sim 1.5:1$ ). Thus resorption of lherzolite would be required to generate the high-SiO<sub>2</sub> magma from the low-SiO<sub>2</sub> magma rather than resorption of harzburgite as proposed by Eggin [1992] and Wagner and Grove [1998]. However, interaction of lherzolite with progressively larger amounts of low-SiO<sub>2</sub> melt would first exhaust clinopyroxene and then orthopyroxene from the peridotite (and the reaction coefficients would change discontinuously with each phase exhaustion). Thus, even if low-SiO<sub>2</sub> melts were to interact with lherzolites, as the mass balance coefficients imply, harzburgites and dunites are plausible products of this reaction, consistent with the phase equilibrium constraints presented in section 5.1 that suggest the high-SiO<sub>2</sub> magmas are harzburgite-saturated rather than lherzolite-saturated.

[67] One observation that may appear to be difficult to reconcile with the hypothesis that the high-SiO<sub>2</sub> magma series is produced by interaction between ascending low-SiO<sub>2</sub> magmas and overlying lherzolite is the bimodality of rock types observed in the HSDP2 core. However, if melt-peridotite interaction occurred from the top of the melting zone in the plume (i.e., from the depth at which the streamlines of ascending peridotite in the plume become dominantly horizontal) to the base of the lithosphere, the interaction could occur over a reproducible depth range and could proceed to a well-defined extent and cease at a well-defined final pressure. Provided that the melt:rock ratio were not high enough to have exhausted orthopyroxene from the peridotite with which the ascending melt interacts, the SiO<sub>2</sub> content of the melt at the top of the zone of interaction would be fixed by its saturation with olivine + orthopyroxene, resulting in a roughly invariant SiO<sub>2</sub> content (i.e., a continuum in SiO<sub>2</sub> content could only result if the pressure at which the melt-peridotite interaction ceased were highly variable). If interaction always proceeded to roughly the base of the lithosphere, it is thus possible that a reproducible high-SiO<sub>2</sub> product could dominate the output of the plume. Note that in this context,

the eruption of low-SiO<sub>2</sub> magmas would be the anomaly; i.e., eruption of magmas that escaped melt-peridotite interaction would be the exception, perhaps facilitated by the flow of magma through olivine-rich conduits developed by previous melt-peridotite interaction [Kelemen, 1986, 1990; Kelemen et al., 1995].

[68] Further development of this hypothesis for the relationship between the low- and high-SiO<sub>2</sub> magma series would require an energy balance to determine if the coefficients implied by the successful mass balance are consistent with available thermochemical data and phase equilibria. Moreover, it remains to be seen whether the isotopic and trace element differences between the high- and low-SiO<sub>2</sub> magmas can be rationalized via this hypothesis; given the mass balance required to account for the major elements in the two magma series, their differences in trace elements and isotopes can be used to solve for the implied characteristics of the assimilated peridotite, which can in turn be compared with known or plausible sources. Although full development of a model for the interactions between ascending melt and overlying peridotite is beyond the scope of this paper, we emphasize that the simple mass balance calculation summarized above and illustrated in Figure 14 successfully accounts for the major element differences between the high- and low-SiO<sub>2</sub> magma series and thus represents a promising start to explaining the primary petrological observations of the HSDP2 project.

#### 5.4. Origin of the CaO- and Al<sub>2</sub>O<sub>3</sub>-Rich, Intermediate SiO<sub>2</sub> Glasses: A Possible Signature of Pyroxene-Rich Source Rocks

[69] Although reaction between low-SiO<sub>2</sub> HSDP2 melt and peridotite can reproduce the compositions of high-SiO<sub>2</sub> HSDP2 magmas, Figure 14 shows that the same mass balance coefficients cannot explain the zone 2 glasses with SiO<sub>2</sub>, Al<sub>2</sub>O<sub>3</sub>, and CaO contents slightly elevated relative to the more abundant low-SiO<sub>2</sub> glasses from zones 3 and 4 (see section 4.6). Likewise, the trend of these glasses toward increasing CaO and Al<sub>2</sub>O<sub>3</sub> cannot be explained simply by variations in the pressure and/or degree of lherzolite melting, since CaO is expected to increase while Al<sub>2</sub>O<sub>3</sub> decreases with increasing melt fraction under these conditions (Figure 13). In addition to their slight elevations in CaO, Al<sub>2</sub>O<sub>3</sub>, and SiO<sub>2</sub>, these glasses tend to have higher TiO<sub>2</sub> contents and they are enriched by up to  $\sim 10\%$  relative to the more abundant low-SiO<sub>2</sub> glasses in moderately incompatible elements

such as the REE from Nd to Yb, Hf, Zr, and Y (Baker et al., manuscript in preparation, 2004a). Taken together, these major and trace element characteristics of these slightly CaO-, Al<sub>2</sub>O<sub>3</sub>-enriched glasses are consistent with a pyroxene-rich component, so in this section we briefly evaluate the hypothesis that the deviations of these glasses from the main group of low-SiO<sub>2</sub> HSDP2 magmas reflects involvement of pyroxene-rich rocks in their petrogenesis.

[70] It has in recent years become popular to ascribe a role for pyroxenite or eclogite in the sources of Hawaiian magmas, motivated by particular aspects of their major element (see section 5.2), minor and trace element, and/or isotopic characteristics [e.g., Hauri, 1996; Hofmann and Jochum, 1996; Lassiter and Hauri, 1998; Jackson et al., 1999; Lassiter et al., 2000; Sobolev et al., 2000; Norman et al., 2002; Reiners, 2002; Takahashi and Nakajima, 2002]. As emphasized above, such hypotheses are generally difficult to evaluate or quantify. Nevertheless, simple mixing of known partial melts of pyroxenites with the low-SiO<sub>2</sub> group of magmas cannot explain the observed trend toward CaO-Al<sub>2</sub>O<sub>3</sub>-rich glasses. For example, as shown in Figure 14, mixing of the dacitic liquid proposed by Hauri [1996] as a partial melt of eclogite with the more abundant zone 3 and zone 4 low-SiO<sub>2</sub> magmas cannot explain the trend toward the high CaO-Al<sub>2</sub>O<sub>3</sub> glasses. Similarly, mixing of experimentally produced, SiO<sub>2</sub>-rich partial melts of pyroxenites [Kogiso and Hirschmann, 2001; Pertermann and Hirschmann, 2003] cannot account for the observed trends. We emphasize, however, that mantle pyroxenites cover a wide range of chemical composition, and it is not possible to rule out that some might produce partial or total melts that on mixing with low-SiO<sub>2</sub> HSDP2 magmas could produce the observed trend toward CaO-Al<sub>2</sub>O<sub>3</sub>-rich glasses, although there is at present no way to test this hypothesis. Note that many pyroxenites lie on the SiO<sub>2</sub>-poor side of the garnet-pyroxene thermal divide; these generate SiO<sub>2</sub>-poor partial melts [Schiano et al., 2000; Hirschmann et al., 2003] that would not produce silica-enrichment on mixing with low-SiO<sub>2</sub> HSDP2 magmas.

[71] We focus here, as we did in the previous section for the high-SiO<sub>2</sub> glasses, on evaluating the potential of a simple mass balance to explain the observed trend from the main group of low-SiO<sub>2</sub> glasses to the most silica-rich of the CaO-Al<sub>2</sub>O<sub>3</sub>-enriched glasses from zone 2. The idea of these calculations is to assess the possibility of explaining the observed compositional trend

toward this group of glasses by interaction with pyroxene-rich assemblages. Given the large number of degrees of freedom needed to evaluate the possible role of pyroxene-rich lithologies in petrogenesis, this is necessarily incomplete, but these mass balance calculations can be envisioned as evaluating a process similar to the thermal and chemical interaction described in section 5.3 that would occur between ascending melt and overlying peridotite, except the overlying rocks in this case could be pyroxene-rich peridotite or pyroxenite ± peridotite rather than peridotite alone.

[72] As in the previous section, all mass balance calculations were done on an average reconstructed high-CaO-Al<sub>2</sub>O<sub>3</sub> parental liquid (shown in Figure 15 as a brown diamond). In the mass balance to produce the CaO-Al<sub>2</sub>O<sub>3</sub>-rich glasses from the low-SiO<sub>2</sub> glasses, we included olivine, orthopyroxene, clinopyroxene, and garnet. The rationale for including all of these phases rather than just clinopyroxene and garnet is that if there is a successful mass balance in producing the CaO-Al<sub>2</sub>O<sub>3</sub>-rich glasses from low-SiO<sub>2</sub> liquids by addition and/or subtraction of these phases in some combination, the relative amounts of these phases will allow us to distinguish the relative roles of peridotite and pyroxenite (i.e., dominantly olivine and orthopyroxene for peridotite versus dominantly clinopyroxene ± garnet for pyroxenite or eclogite) in relating these two groups of magmas. Two sets of calculations were done: one using the composition of clinopyroxene from a model lherzolitic residue and the other using clinopyroxene from a melting experiment on pyroxenite (see Table 3 for all phase compositions used in these calculations).

[73] The best-fit mass balance utilizing the lherzolitic clinopyroxene composition is

$$\begin{aligned}
 &0.942(17)(\text{low-SiO}_2\text{melt}) - 0.064(10)(\text{olivine}) \\
 &\quad + 0.023(20)(\text{orthopyroxene}) \\
 &\quad + 0.076(18)(\text{peridotitic clinopyroxene}) \\
 &\quad + 0.022(8)(\text{garnet}) \\
 &= 1(\text{Ca-Al-rich melt}).
 \end{aligned}$$

The best fit utilizing the pyroxenitic clinopyroxene composition is

$$\begin{aligned}
 &0.948(16)(\text{low-SiO}_2\text{melt}) - 0.063(10)(\text{olivine}) \\
 &\quad + 0.062(16)(\text{orthopyroxene}) \\
 &\quad + 0.058(11)(\text{pyroxenitic clinopyroxene}) \\
 &\quad + 0.004(6)(\text{garnet}) = 1(\text{Ca-Al-rich melt}).
 \end{aligned}$$

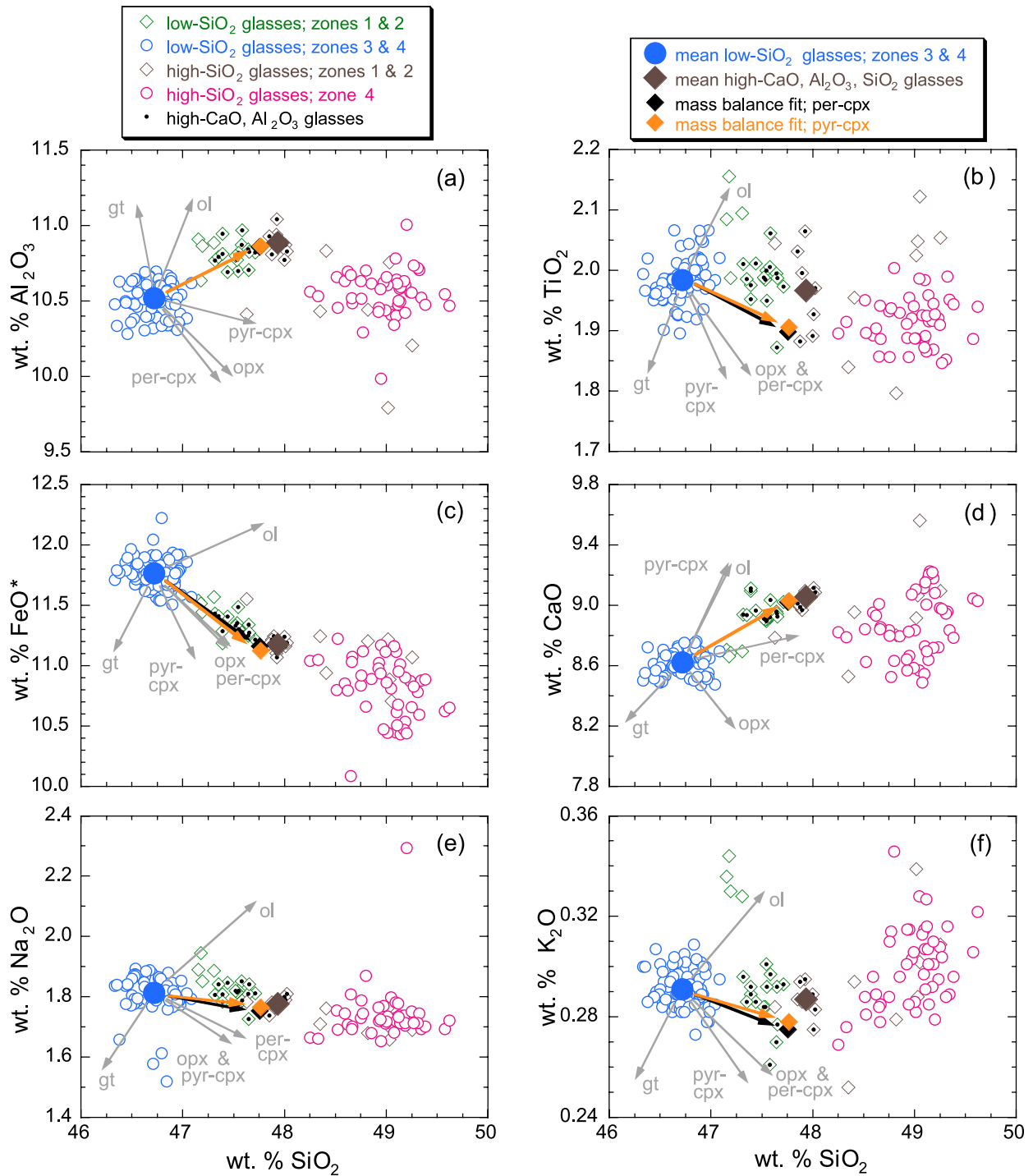


Figure 15

Details of the two fits are reported in Table 3. The differences between them reflect the higher  $\text{Al}_2\text{O}_3$  and CaO contents of the residual pyroxenitic clinopyroxene compared to the residual lherzolitic clinopyroxene. Note, however, that the sum of the orthopyroxene and clinopyroxene coefficients in both fits are similar (0.10–0.12). Compared to the mass balance fit for the high- $\text{SiO}_2$  parent liquid, which has a clinopyroxene/olivine ratio of  $\sim 0.7$ , the two mass balance fits for the CaO- $\text{Al}_2\text{O}_3$ -rich parental liquid have clinopyroxene/olivine ratios of  $\sim 1$ , emphasizing the low- $\text{SiO}_2$  liquid would have to interact with more clinopyroxene-rich material to produce the CaO- $\text{Al}_2\text{O}_3$ -rich magmas. As with the mass balance needed to produce the high- $\text{SiO}_2$  magma from the low- $\text{SiO}_2$  magma, these mass balances for the CaO- $\text{Al}_2\text{O}_3$ -rich magma require an increase in the amount of melt in the production of the CaO- $\text{Al}_2\text{O}_3$ -rich magma from the low- $\text{SiO}_2$  magma and precipitation of olivine, consistent with thermal and chemical interaction between ascending melt and overlying near-solidus mantle materials. The coefficients for garnet in the mass balances are much lower than olivine and pyroxenes and the garnet coefficient is indistinguishable from zero in the fit using pyroxenitic clinopyroxene.

[74] Figure 15 shows the vectors in composition space corresponding to these mass balances and demonstrates graphically that the chemical composition of the average high-CaO- $\text{Al}_2\text{O}_3$  magma can be well matched by these reactions. We emphasize that although this mass balance has four free parameters (i.e., the coefficient for high- $\text{SiO}_2$  melt is set to 1 and the sum of the other five coefficients must sum to 1), it successfully accounts for 10 major and minor elements in the average high-CaO- $\text{Al}_2\text{O}_3$  magma.

[75] We have also explored mass balance fits with other combinations of phases. Garnet is not an

essential phase: acceptable mass balances were obtained using olivine, orthopyroxene, and either of the clinopyroxene compositions. The only other acceptable solution involved olivine, the peridotitic clinopyroxene, and garnet; the same set of phases but using the pyroxenitic clinopyroxene produced a marginal fit. Marginal or poor results were obtained for all fits that did not include olivine (e.g., clinopyroxene + garnet) and for mass balances with olivine + clinopyroxene or olivine + garnet.

[76] The mass balances presented in this section demonstrate that the CaO- $\text{Al}_2\text{O}_3$ -rich magmas could have evolved from the more abundant low- $\text{SiO}_2$  magmas by resorption of clinopyroxene  $\pm$  orthopyroxene  $\pm$  garnet accompanied by precipitation of olivine. Thus one possibility is that thermal and chemical interaction of low- $\text{SiO}_2$  magmas with overlying regions containing pyroxenites or eclogites and peridotite or containing pyroxene-rich peridotites resulted in this trend. If so, the greater abundance of CaO- $\text{Al}_2\text{O}_3$ -rich glasses in zone 2 (i.e., relative to zones 3 and 4, which have few, if any, such glasses) might suggest that such pyroxene-rich lithologies are more abundant in the plume or the regions above the segregation of melt from the plume as the volcano begins to move off the central, most productive regions of the plume. As in section 5.3, we emphasize that further development of this kind of hypothesis would require an energy balance to determine if the coefficients implied by the successful mass balances are consistent with available thermochemical data and phase equilibria. Moreover, although we favor an involvement of pyroxene-rich lithologies to explain the CaO- $\text{Al}_2\text{O}_3$ -rich glasses and have shown that chemical and thermal interaction between low- $\text{SiO}_2$  magmas and clinopyroxene-rich mantle rocks is at least a permissible process, as emphasized above, the large range in compositions of candidate

**Figure 15.** Results of the mass balance calculations relating the average low- $\text{SiO}_2$  parent liquid (filled blue circle) to the average of the most silica-rich recalculated high-CaO- $\text{Al}_2\text{O}_3$  parent liquid (filled brown diamond) by addition/subtraction of residual peridotite and residual pyroxenite minerals. Individual HSDP2 glasses with  $\geq 7\%$  MgO (small open circles and diamonds) were corrected to equilibrium with  $\text{Fo}_{90.5}$  olivine at QFM and 1 bar. Open diamonds with small black circles denote the CaO- $\text{Al}_2\text{O}_3$ -enriched glasses. The filled orange and black diamonds represent the two best-fit high-CaO- $\text{Al}_2\text{O}_3$  parent liquid compositions based on the mass balance calculations, and the heavy orange and black arrows show the vectors between the average low- $\text{SiO}_2$  parent liquid and these best-fit compositions. The orange diamond is the best-fit for model B given in Table 3: i.e., using the following minerals in the mass balance: olivine, orthopyroxene, and clinopyroxene (“per-cpx”) from residual peridotite, and garnet from residual pyroxenite. The black diamond is the best-fit for model C given in Table 3: i.e., using the following minerals in the mass balance: olivine and orthopyroxene from residual peridotite, and clinopyroxene (“pyr-cpx”) and garnet (gt) from residual pyroxenite. The gray arrows show the compositional effects of olivine crystallization and pyroxene and garnet dissolution on the mean low- $\text{SiO}_2$  parent liquid. Phase compositions and details of these mass balance calculations are given in the text and Table 3.  $\text{SiO}_2$  versus (a)  $\text{Al}_2\text{O}_3$ , (b)  $\text{TiO}_2$ , (c)  $\text{FeO}^*$ , (d) CaO, (e)  $\text{Na}_2\text{O}$ , (f)  $\text{K}_2\text{O}$ .

pyroxene-rich lithologies means it is difficult to be more precise at this point or to rule out other processes by which pyroxene-rich rocks might lead to the distinctive CaO-Al<sub>2</sub>O<sub>3</sub>-rich glasses.

## 6. Excursion to Transitional Glasses at 2233–2280 mbsl

[77] We have mentioned several times two “excursions” in the core to unusual glass compositions. The deeper one occurs in the top ~50 m of zone 3, as indicated by the alkalinity changes in this interval (Figure 4c). In addition to the change in alkalinity, there are increases in K<sub>2</sub>O, P<sub>2</sub>O<sub>5</sub>, TiO<sub>2</sub>, Na<sub>2</sub>O, and perhaps  $\epsilon_{\text{HF}}$  beginning at 2280 mbsl and extending upward to the top of zone 3 at 2233 mbsl (Figure 16). H<sub>2</sub>O content increases continuously over all of zone 3; i.e., its increase in the upper ~50 m is a continuation of the overall increase in the zone. FeO\* is unchanged, Al<sub>2</sub>O<sub>3</sub> (and perhaps CaO) increases slightly, and SiO<sub>2</sub> may decrease slightly from 2280 to 2233 mbsl. Sulfur may also increase slightly near the top of zone 3, but the change, if it occurs, is not obviously restricted to the upper ~50 m. Finally, the degree of fractionation increases (i.e., the MgO content decreases) in the upper ~50 m of zone 3. Note, however, that although incompatible components such as H<sub>2</sub>O, TiO<sub>2</sub>, P<sub>2</sub>O<sub>5</sub>, etc. all increase progressively toward the top of this ~50 m interval, after adjustment for fractionation (e.g., to 7% MgO), they are all roughly constant in this interval [Seaman *et al.*, 2004]. After such correction for fractionation, some components (e.g., H<sub>2</sub>O, S) are unchanged relative to the underlying zone 3 samples, whereas others (e.g., K<sub>2</sub>O, TiO<sub>2</sub>, Na<sub>2</sub>O, P<sub>2</sub>O<sub>5</sub>, F) are enriched by up to about 30%. No whole rocks from this interval have been analyzed, so all data on this excursion come from glass analyses.

[78] The compositions of the glasses in the 2233–2280 mbsl interval are shown with distinctive green symbols on all figures. These glasses are compositionally distinct from other low-SiO<sub>2</sub> HSDP2 glasses, particularly in their trend toward alkalic/transitional compositions, their systematically more fractionated nature, and their elevated concentrations of some incompatible elements (which, as discussed by Seaman *et al.* [2004], cannot be explained by low-pressure fractionation of the more typical low-SiO<sub>2</sub> magmas). Moreover, the comparisons with glasses from other Hawaiian volcanoes (Figure 11) show that only one glass from the literature (from Mahukona [Clague and

Moore, 1991]) overlaps in composition the HSDP2 glasses from this excursion. In addition, one glass from Haleakala is similar in the concentrations of all oxides other than TiO<sub>2</sub>, and several Loihi glasses come close to those from this excursion, although the two sets of glasses are distinct in their CaO, Al<sub>2</sub>O<sub>3</sub>, H<sub>2</sub>O, and TiO<sub>2</sub> contents. Similarly, despite considerable scatter, Figure 12 shows that glasses from the 2233–2280 mbsl excursion are also distinguishable, particularly in CaO, Al<sub>2</sub>O<sub>3</sub>, Na<sub>2</sub>O, and TiO<sub>2</sub>, from whole rocks from other Hawaiian volcanoes.

[79] Baker *et al.* (manuscript in preparation, 2004a) show that the concentrations of most highly to moderately incompatible minor and trace elements in glass from the 2233–2280 mbsl excursion (including Na<sub>2</sub>O, K<sub>2</sub>O, P<sub>2</sub>O<sub>5</sub>, and TiO<sub>2</sub> from this work) can be modeled by a decrease in the degree of melting of ~30% (i.e., from about 10 to 7%) relative to the underlying low-SiO<sub>2</sub> zone 3 glasses. The slightly higher Al<sub>2</sub>O<sub>3</sub> contents of glasses from the excursion are in the expected direction given such decrease in melt fraction; the near constancy in FeO\* would require that the average pressure of melting did not change significantly. One difficulty for this hypothesis is that CaO is not lower in the 2233–2280 mbsl interval, even though this would be expected with decreasing degrees of melting with a lherzolitic residue, but this may not be surprising given that the inferred change in degree of melting is relatively small; alternatively, CO<sub>2</sub> could play a role in keeping the CaO content high. Note that although a lower degree of melting successfully accounts for most chemical differences between glasses from this interval and the underlying zone 3 glasses, there must be a component of source region variability accompanying the decrease in melt fraction given the constancy in H<sub>2</sub>O content across 2280 mbsl and the increase in  $\epsilon_{\text{HF}}$  from 2280 to 2233 mbsl [Blichert-Toft *et al.*, 2003].

[80] The excursion at the top of zone 3 is clearly an unusual event in the evolutionary history sampled by the HSDP2 core. The lower degrees of melting inferred for this ~50 m interval, the evolution toward transitional and more fractionated compositions with decreasing depth in the interval, the abrupt termination of the excursion, and the significantly different high-SiO<sub>2</sub> tholeiitic compositions of the samples overlying the excursion are all reminiscent of the end of shield building at the top of the Mauna Kea section in the core (i.e., at 245 mbsl). The upward progression toward more

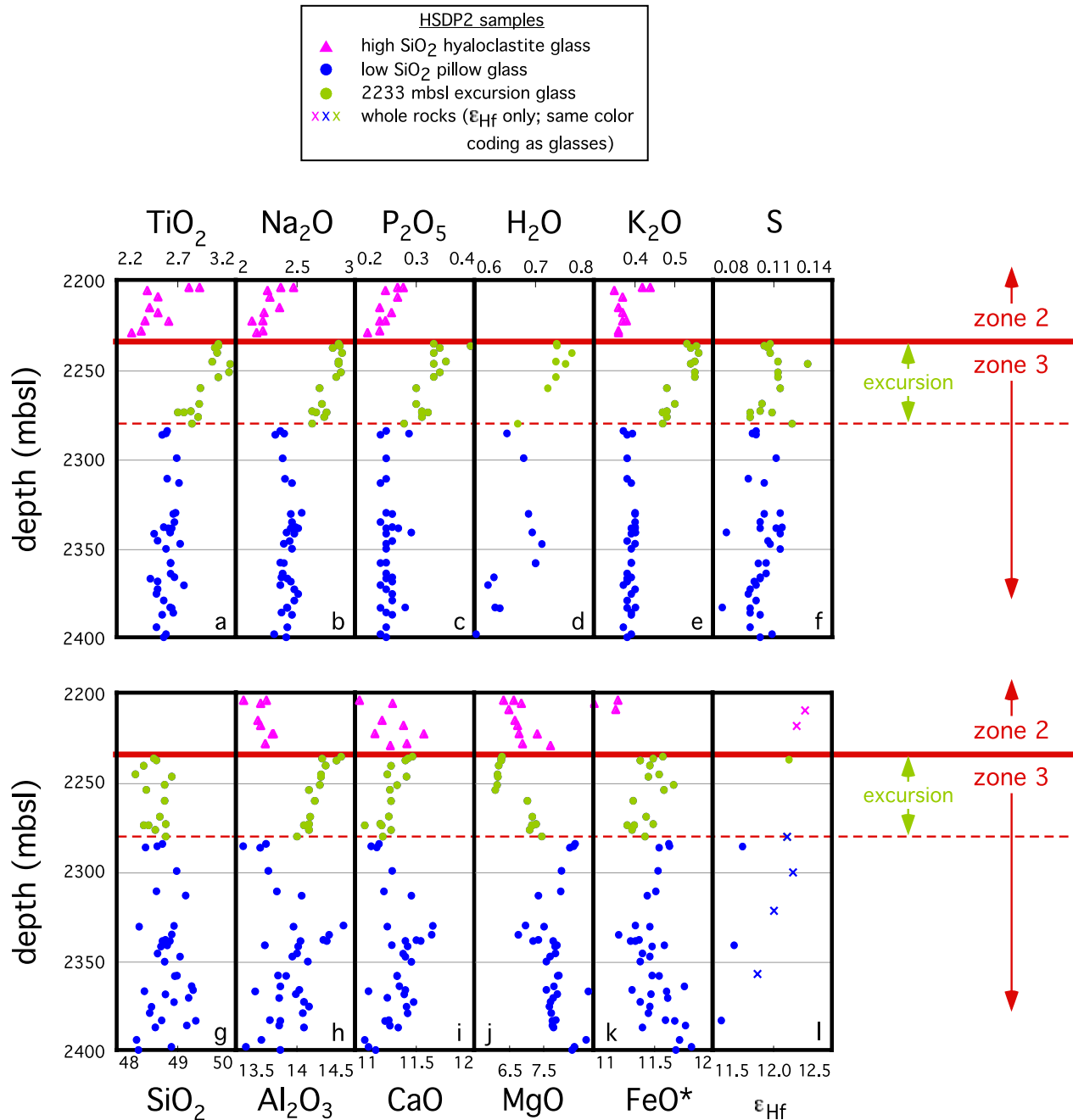


**Figure 16.** Depth (mbsl) versus concentrations of various oxides and S (wt.%) and  $\epsilon_{\text{Hf}}$  [Blichert-Toft *et al.*, 2003] in pillow-rim glasses (circles) at the top of zone 3 and hyaloclastite glasses (triangles) at the bottom of zone 2. Also shown are  $\epsilon_{\text{Hf}}$  values for whole rocks (crosses) over the same depth interval. The “2233–2280 mbsl excursion” refers to the 2233–2280 mbsl depth interval. Color coding is explained in the legend. (a)  $\text{TiO}_2$ ; (b)  $\text{Na}_2\text{O}$ ; (c)  $\text{P}_2\text{O}_5$ ; (d)  $\text{K}_2\text{O}$ ; (e)  $\text{H}_2\text{O}$ ; (f) S; (g)  $\text{SiO}_2$ ; (h)  $\text{Al}_2\text{O}_3$ ; (i)  $\text{CaO}$ ; (j)  $\text{MgO}$ ; (k)  $\text{FeO}^*$ ; and (l)  $\epsilon_{\text{Hf}}$ .

fractionated compositions is also seen at the top of the subaerial Mauna Kea section [Frey *et al.*, 1990] and is consistent with a declining magma flux. Moreover, as shown in Figure 7, there are continuous changes in isotopic ratios over all of zone 3 (i.e., decreases in  $^3\text{He}/^4\text{He}$  and  $^{87}\text{Sr}/^{86}\text{Sr}$  and

increases in  $\epsilon_{\text{Nd}}$ ) that are similar in direction and magnitude to the changes observed over the entire subaerial section. Note that  $\epsilon_{\text{Hf}}$  behaves differently, with a variation over zone 3 that is comparable in magnitude but opposite in sign to the variation in the upper 150 m of the Mauna Kea section; as

pointed out by *Huang and Frey* [2003], the inverse correlation between  $\epsilon_{\text{Nd}}$  and  $\epsilon_{\text{Hf}}$  observed at the top of the Mauna Kea section is anomalous. In any case, the end of Mauna Kea's shield building and zone 3 both have similar long-term variations in  $^3\text{He}/^4\text{He}$ ,  $^{87}\text{Sr}/^{86}\text{Sr}$ , and  $\epsilon_{\text{Nd}}$ , culminating in a narrow zone of transitional to alkalic lavas attributable to decreasing melt fraction and melt flux. We speculate in sections 8 and A6 as to what this excursion and the boundary between zones 2 and 3 may signify.

## 7. Excursion to CaO-K<sub>2</sub>O-Rich Glasses at 1765–1810 mbsl

[81] The second geochemical excursion occurs in the 1765–1810 mbsl depth interval; this interval was subdivided into eleven units (7 hyaloclastites, 3 massives, and 1 sandstone) during on-site core logging. The low-SiO<sub>2</sub> glasses defining this excursion are all from hyaloclastites. Sandwiched between the low-SiO<sub>2</sub> glasses in this depth interval are three unremarkable high-SiO<sub>2</sub> glasses from 1782–1793 mbsl; the 1782–1793 mbsl depth range is dominated by three massive units, and although two of these high-SiO<sub>2</sub> glasses are from hyaloclastites and only one is from a massive unit, all three are plausibly associated with the massive units from this depth interval.

[82] The compositions of the low-SiO<sub>2</sub> glasses in the 1765–1810 mbsl interval are shown with distinctive cyan symbols on all figures. Although their silica contents are in the range of the other low-SiO<sub>2</sub> glasses, these glasses are compositionally distinct from other low-SiO<sub>2</sub> HSDP2 glasses, particularly in their elevated K<sub>2</sub>O and CaO contents (Figure 17). They are less fractionated than most other glasses (all have >6.8% MgO), and they have lower Al<sub>2</sub>O<sub>3</sub> and FeO\* contents than other low-SiO<sub>2</sub> HSDP2 glasses at the same MgO content. They are also unusual in that their elevated K<sub>2</sub>O contents are not accompanied by elevated P<sub>2</sub>O<sub>5</sub> or TiO<sub>2</sub>, and their Na<sub>2</sub>O contents are lower than those of most other low-SiO<sub>2</sub> glasses. Finally, the trace element pattern of the single high-CaO glass analyzed by Baker et al. (manuscript in preparation, 2004a) is distinctive, with significant enrichments in Ba, K, and Pb and depletions in Ta, Nb, Hf, Zr, and heavy rare earth elements relative to elements of similar compatibility when normalized to typical low-SiO<sub>2</sub> magmas.

[83] Figure 18 (see also Figures A2 and 11) compares the HSDP2 glasses with HSDP whole rocks

and with whole rock analyses of Mauna Kea tholeiites and tholeiitic Hawaiian glasses from the literature. The rocks most like the high CaO-K<sub>2</sub>O glasses from ~1800 mbsl are the subaerial Hamakua tholeiites. This is emphasized particularly by Figure 18d, in which the high CaO and K<sub>2</sub>O of these glasses is seen to overlap precisely a subset of the Hamakua tholeiites. However, a key feature of the high CaO-K<sub>2</sub>O glasses from ~1800 mbsl is that the enrichment in K<sub>2</sub>O is not accompanied by enrichments in Na<sub>2</sub>O, P<sub>2</sub>O<sub>5</sub>, or TiO<sub>2</sub>. In contrast, although the Hamakua tholeiites share the characteristic of not being enriched in Na<sub>2</sub>O, they are enriched in P<sub>2</sub>O<sub>5</sub> and TiO<sub>2</sub>. Consequently, as shown in Figures 18a–18c, although the two magma types overlap in K<sub>2</sub>O/Na<sub>2</sub>O, the CaO-K<sub>2</sub>O-rich glasses have significantly higher K<sub>2</sub>O/P<sub>2</sub>O<sub>5</sub> and K<sub>2</sub>O/TiO<sub>2</sub> than the Hamakua tholeiites. Nevertheless, in the ways in which glasses defining the ~1800 mbsl excursion are most distinctive (elevated CaO and K<sub>2</sub>O contents), the Hamakua tholeiites are an excellent match. It is interesting that these distinctive characteristics appear in a single pulse in the submarine section, then only reappear in the waning stages of the lifetime of the Mauna Kea volcano.

[84] Although they are rare, lavas with similar (but again not precisely overlapping) compositions have appeared in several other Hawaiian volcanoes. For example, as shown in Figure 17, a few Kilauea, Hualalai, and Loihi tholeiitic whole rocks and several Loihi tholeiitic glasses are also enriched in K<sub>2</sub>O and CaO. The Loihi glasses are the closest match and they are also systematically Al<sub>2</sub>O<sub>3</sub>-poor, but they nevertheless differ from the ~1800 mbsl glasses (e.g., they are typically higher in FeO\* (Figure 11), and they have lower K<sub>2</sub>O/Na<sub>2</sub>O ratios (Figure 18)). Perhaps the most interesting comparison is to the K<sub>2</sub>O-rich (up to 2–3% K<sub>2</sub>O) samples recently discovered on the submarine flanks of Kilauea and thought to represent a magmatic component of the early submarine history of Kilauea [*Sisson et al.*, 2002]. Although these Kilauea samples are highly alkalic and thus not directly comparable to the glasses from this excursion (which we would refer to as transitional based on their norms), both rock types have elevated CaO contents and elevated K<sub>2</sub>O/P<sub>2</sub>O<sub>5</sub>, K<sub>2</sub>O/TiO<sub>2</sub>, and K<sub>2</sub>O/Na<sub>2</sub>O ratios.

[85] The enrichment of the glasses at the ~1800 mbsl excursion relative to other low-SiO<sub>2</sub> HSDP glasses in K<sub>2</sub>O without enrichment in other incompatible elements such as Na<sub>2</sub>O, TiO<sub>2</sub>, and

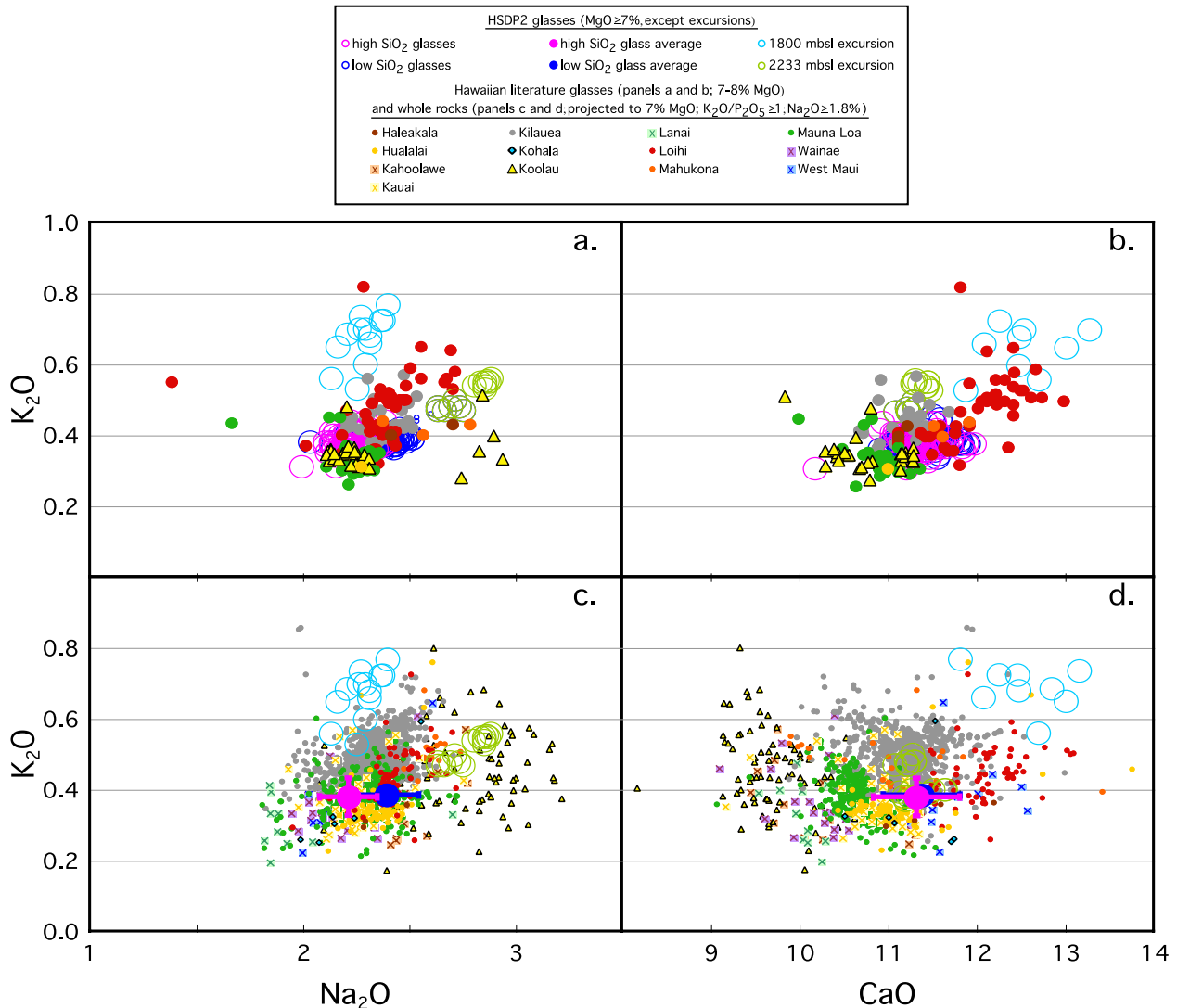


**Figure 17.**  $\text{Na}_2\text{O}$  versus  $\text{K}_2\text{O}$  and  $\text{CaO}$  versus  $\text{K}_2\text{O}$  (wt.%) for glasses from the HSDP2 core ( $\geq 7\%$  MgO; excepting excursions) compared with tholeiitic glasses (7–8% MgO) from other Hawaiian volcanoes from the literature (Figures 17a and 17b) and with whole rock analyses of tholeiitic lavas from other Hawaiian volcanoes from the literature (Figures 17c and 17d) projected to 7% MgO as described in Appendix A4. In order to minimize the effects of alteration, whole rock analyses with  $\text{K}_2\text{O}/\text{P}_2\text{O}_5 < 1$  or  $\text{Na}_2\text{O} < 1.8\%$  were excluded from the compilation. Symbols and color coding are explained in the legend; large filled pink and blue circles in Figures 17c and 17d are the means of the high- and low- $\text{SiO}_2$  glasses with  $\geq 7\%$  MgO; error bars are  $\pm 2$  sigma. See captions to Figure 11 and Figure 12 for references to literature analyses.

$\text{P}_2\text{O}_5$  and the overall trace element pattern with its enrichments in Ba and Pb and depletions in Ta, Nb, Hf, and Zr cannot plausibly be produced from the same source that produced the more abundant low- $\text{SiO}_2$  HSDP glasses. The trace element pattern is best understood as due to enrichment in fluids and/or melts coming off a subducting slab [e.g., Weaver, 1991; Pearce and Parkinson, 1993], and this may thus indicate the presence of material recycled from an ancient arc

or mantle wedge among the sources of HSDP magmas.

## 8. Magmatic Diversity in the HSDP2 Core

### 8.1. General Considerations

[86] The conventional wisdom about Hawaiian volcanoes, derived from Macdonald [1968], was

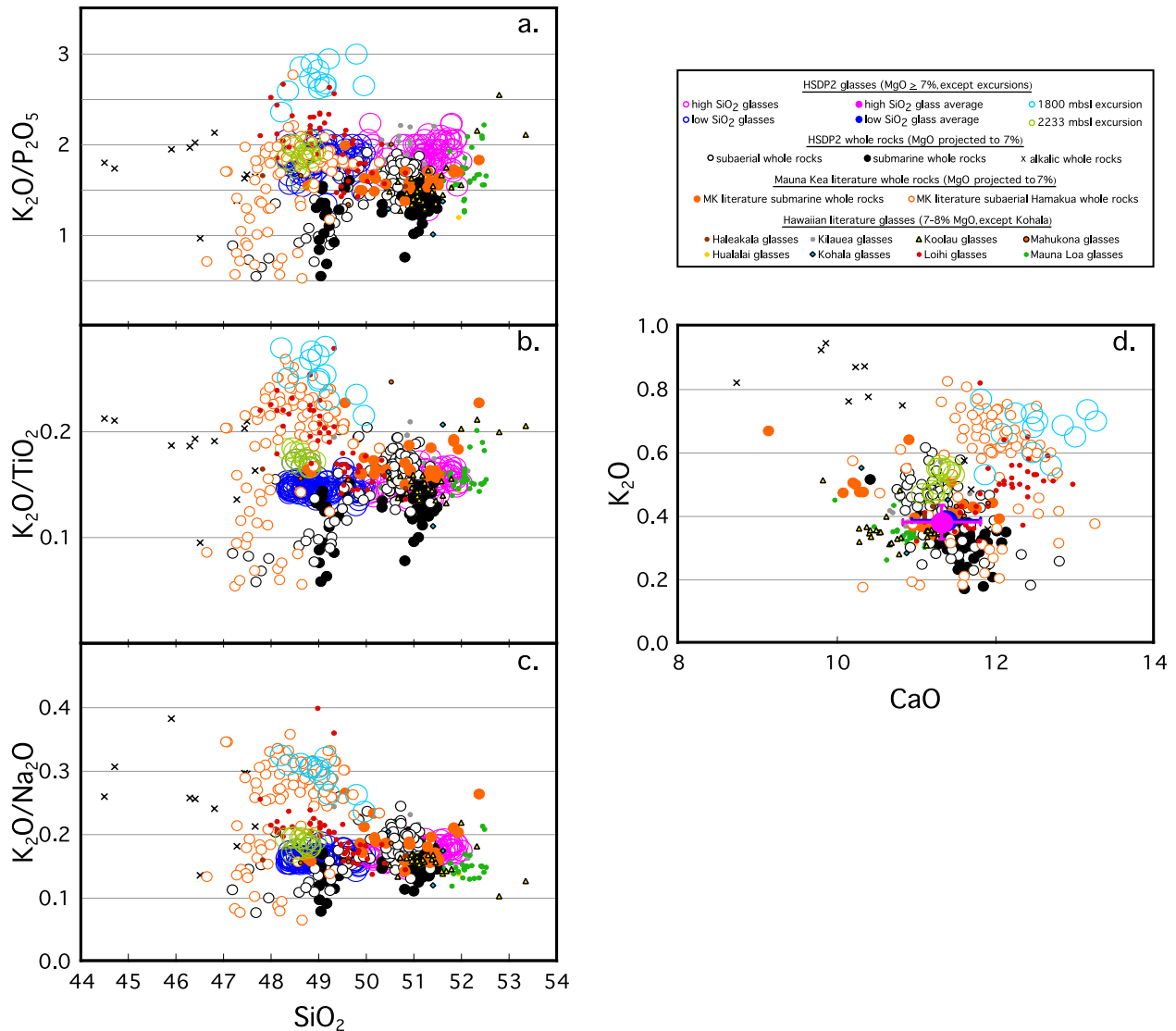


**Figure 18.**  $\text{SiO}_2$  (wt.%) versus (a)  $\text{K}_2\text{O}/\text{P}_2\text{O}_5$ , (b)  $\text{K}_2\text{O}/\text{Na}_2\text{O}$ , and (c)  $\text{K}_2\text{O}/\text{TiO}_2$  and (d)  $\text{CaO}$  versus  $\text{K}_2\text{O}$  (all wt.% or weight ratios) in glasses from the HSDP2 core ( $\geq 7\%$  MgO; excepting excursions) and in whole rocks from the HSDP1 and HSDP2 cores compared with whole rock analyses of tholeiitic Mauna Kea lavas from the literature and tholeiitic glasses with 7–8% MgO from other Hawaiian volcanoes (except glasses from Kohala, all of which have  $< 7\%$  MgO). Whole rock compositions have all been projected to 7% MgO as described in Appendices A1 and A3. Symbols and color coding are explained in the legend. See captions to Figures 9 and 11 for the sources of the glass and whole rock analyses from the literature.

that their output was monotonously tholeiitic over most of their history, only changing, either continuously or in fits and starts, at the end of the lifetime of the volcano to alkaline compositions. With the discovery of alkaline lavas on the Loihi seamount, still in an early phase of its growth [Moore *et al.*, 1982], and recent characterization of the early history of Kilauea exposed on its submarine flank [Lipman *et al.*, 2002], the conventional wisdom has been modified to include an early alkaline phase, a

tholeiitic phase encompassing most of the volumetric output of the volcano, culminating in diverse alkaline lavas at the end of the volcano's life. Moreover, it has been generally assumed that the compositional distinctiveness of the tholeiites from each volcano (e.g., the silica contents and isotopic ratios that typically “fingerprint” the tholeiites of a given Hawaiian volcano [Tatsumoto, 1978; Garcia *et al.*, 1989; Frey and Rhodes, 1993; Frey *et al.*, 1994; Hauri, 1996]) persisted over most of its

lifetime. Although largely based on speculation, since most of the output of Hawaiian volcanoes was hidden from view either due to having been erupted under water, covered by later lavas, or subsided beyond the reach of easy sampling, this conventional view was consistent with available information. Moreover, it was also consistent with the existence of a relatively shallow magma chamber at depths of a few kilometers below the summit [Ryan *et al.*, 1981; Klein *et al.*, 1987] and the possibility of deeper chambers as well [Wright, 1971; Clague, 1987; West *et al.*, 1988; Garcia *et al.*, 1998]; such chambers would effectively mix incoming magmas, so even if the input were variable, mixing in the magma chambers would dampen high frequency or abrupt changes in the input and perhaps eliminate them entirely [Albarède, 1993; Pietruszka and Garcia, 1999a]. Only with diminished magma flux at the end of the lifetime of the volcano, leading to the elimination of these magma chambers [Clague, 1987; Frey *et al.*, 1990], might high-frequency variations in the character of mantle-derived magmas be directly expressed in erupted magmas.

[87] Recent studies have modified the conventional view. For example, detailed studies of drill cores, submarine samples, and subaerial lavas with improved stratigraphic control indicate that even in the shield-building phase of a Hawaiian volcano's output there are shifts in chemical and isotopic composition on timescales of  $10^1$ – $10^4$  years that cannot be attributed to high-level fractionation and must involve variations in source chemistry and/or processes [e.g., Kurz and Kammer, 1991; Dzurisin *et al.*, 1995; Kurz *et al.*, 1995; Rhodes and Hart, 1995; Pietruszka and Garcia, 1999a; Mukhopadhyay *et al.*, 2003]. Similarly, the hypothesis of a concentrically zoned plume over which an individual volcano moves over its lifetime has led to the expectation of gradual, long-term variations in at least the isotopic characteristics of the output of individual Hawaiian volcanoes [e.g., Hauri *et al.*, 1994; Kurz *et al.*, 1995; DePaolo *et al.*, 2001]. Finally, investigations of melt inclusions in phenocrysts in Hawaiian tholeiites have also, as has been observed in a wide range of volcanic environments, demonstrated considerable variability in trace element patterns inherited from mantle sources; note, however, that this variability is not expressed in the lavas that transport these phenocrysts, supporting the notion that magma chambers are efficient at homogenizing variations in mantle-derived magmas before eruption [Sobolev *et al.*, 2000]. Despite these demonstrations of variations in the

compositions of magmas exiting the mantle, the theme of dominantly constant or slowly shifting tholeiitic magmas over most of the shield-building phase of an individual volcano's lifetime has remained an essential part of our understanding of Hawaiian volcanism, in large part due to the expectation of efficient mixing in magma chambers.

[88] Rocks from the HSDP2 core, however, suggest a different view. For example, the submarine section is characterized by considerable variability in major element and trace element geochemistry and in radiogenic isotope ratios. These shifts in chemistry can be gradual (e.g., over the entire 300 m depth range of zone 2, or over the ~50 m of the excursion at the top of zone 3) or discontinuous (e.g., the upper and lower boundaries of zone 3 at 2233 and 2481 mbsl, or the excursion at 1765–1810 mbsl). Although we consider the possibility that these variations reflect the output of several volcanoes (see section A6), in this section we adopt the assumption that the samples represent the output of a single volcano, Mauna Kea, and consider how the observed variations in magma composition can be understood in the context of current ideas of melt generation beneath Hawaii.

## 8.2. Do Compositional Variations in HSDP2 Samples Indicate Abrupt Chemical Variations in the Output of the Mauna Kea Volcano?

[89] The abrupt changes at 2481 mbsl from high-SiO<sub>2</sub> magma to low-SiO<sub>2</sub> magma and then back again at 2233 mbsl to high-SiO<sub>2</sub> magma must signify major changes in source composition and/or processes. Likewise, the differences between the high-SiO<sub>2</sub> magmas at the bottom of zone 2 and the low-SiO<sub>2</sub> magmas at its top must also reflect significant differences in their sources. The isolated occurrences of low-SiO<sub>2</sub> magma deeper than ~500 mbsl in the subaerial section, the spikes in <sup>3</sup>He/<sup>4</sup>He seen at ~830 mbsl and below [Kurz *et al.*, 2004], the narrow interval of low-SiO<sub>2</sub> magma at 1350–1400 mbsl, and the excursion to high-CaO-K<sub>2</sub>O, low-SiO<sub>2</sub> magmas in the 1765–1810 mbsl interval all indicate that this variability can occur over relatively short depth intervals (the shortest depth interval between sampled high- and low-SiO<sub>2</sub> glasses is between hyaloclastites at 1929.1 and 1930.7 mbsl). It is important to emphasize, however, that these transitions between magma types could in principle have taken place over long time intervals yet be abrupt as functions of

depth if the core contains significant hiatuses in deposition.

[90] Without considerably more information on the age versus depth relationship in the core than is currently available, the continuity of deposition in the core and thus the timescales of the abrupt variations in magma composition that we observe cannot be quantified. We have, however, examined the core for indirect evidence of variations in deposition rate and possible depositional hiatuses. The arrows in Figure 19 show the depths of thick zones of fine-grained and bedded hyaloclastites and sediments in the core. Although no sedimentological studies of the core have been undertaken, it is plausible that these fine-grained zones represent time periods in which largely reworked rather than freshly erupted material was deposited at the drill site. Although not all such bedded zones correspond to chemical “events” in the core, every zone boundary (i.e., the boundaries between zones 1 and 2, 2 and 3, and 3 and 4), the upper and lower boundaries of the 1765–1810 “excursion,” and the boundaries of the “sub-zone” in zone 4 over which sulfur decreases systematically [Seaman *et al.*, 2004] all coincide with such fine-grained, bedded intervals. More work on the sedimentology of the hyaloclastites is required, but we speculate that the correspondence between the occurrence of thick, fine-grained, bedded intervals and chemical “events” in the core signifies that these intervals represent time intervals over which freshly erupted magma was either not delivered (or was delivered at lower than the average rate) to the drill site.

[91] Although we thus suggest on the basis of Figure 19 that major chemical boundaries in the core (i.e., between adjacent occurrences of high- and low-SiO<sub>2</sub> glasses) may represent intervals with low accumulation rates of fresh lava at the drill site, we have no basis for estimating the duration of these intervals. The only constraint we have is that the time represented by the transitions from one magma type to the other must be  $\ll 150$  Kyr, the approximate time interval of the entire sampled submarine section (Sharp and DePaolo, manuscript in preparation, 2004). Likewise, we have no direct information on the time intervals represented by the low-SiO<sub>2</sub> magmas of zone 3 or the continuous transition from high- to low-SiO<sub>2</sub> magma that occurs over zone 2, but we can estimate durations of  $\sim 15$  Kyr in both cases on the basis of the continuous age-depth relationship of Sharp and DePaolo (manuscript in preparation, 2004). At higher levels in the core (i.e., in zone 1), abrupt,

short-duration episodes of low-SiO<sub>2</sub> magmas occur within a dominantly high-SiO<sub>2</sub> magmatic interval; these intervals are on the order of 50 m in extent, corresponding to time intervals of  $\sim 3$  Kyr, again assuming a continuous age-depth relationship. Note that Rhodes and Hart [1995], Pietruszka and Garcia [1999a], and Mukhopadhyay *et al.* [2003] have documented significant correlated isotopic and chemical variability among Mauna Loa, Kilauea, and Kauai magmas, respectively, on time-scales as short as  $\leq 10^1$ – $10^2$  years.

### 8.3. What are the Expected Timescales for Variations in Magmatic Output of Hawaiian Volcanoes?

[92] What insights do these estimates of timescales of major chemical variability as short or shorter than a few thousands to tens of thousands of years give into magmatic processes during shield building of Hawaiian volcanoes? Consider first the case of an ascending plume that has a sharp horizontal boundary (i.e., a step function) between distinctive source rocks entering the melting zone. Since melting is generally believed to take place over a depth interval of several tens of kilometers, such a sharp source boundary would be expected to be expressed gradually in the average magmatic output of the melting zone if melts from different levels mix on ascent. Suppose, for example, that the melting zone were  $\sim 60$  km in height and the ascent rate for the plume is  $\sim 30$ – $100$  cm/yr [e.g., Watson and McKenzie, 1991; Ribe and Christensen, 1999]. In this case, it would take  $\sim 50,000$ – $200,000$  years for the horizontal boundary to pass through the melting zone and consequently for the complete transition from one magma type to another. Given the estimated age-depth relationship in the HSDP2 core, this would correspond to a depth interval of on the order of a kilometer, clearly inconsistent with the abrupt changes we observe between magma types, even accounting for the existence of hiatuses at their boundaries. Even if mixing did not occur between melts from above and below the assumed horizontal boundary (i.e., melts from across the boundary between sources were able to retain their identities en route to the surface), one would expect alternations of the two magma types such that the average output of the volcano would shift gradually over the  $10^5$  year timescale required for the boundary to pass through the melting zone.

[93] An alternative geometry for source heterogeneity is implicit in the concentrically zoned plume

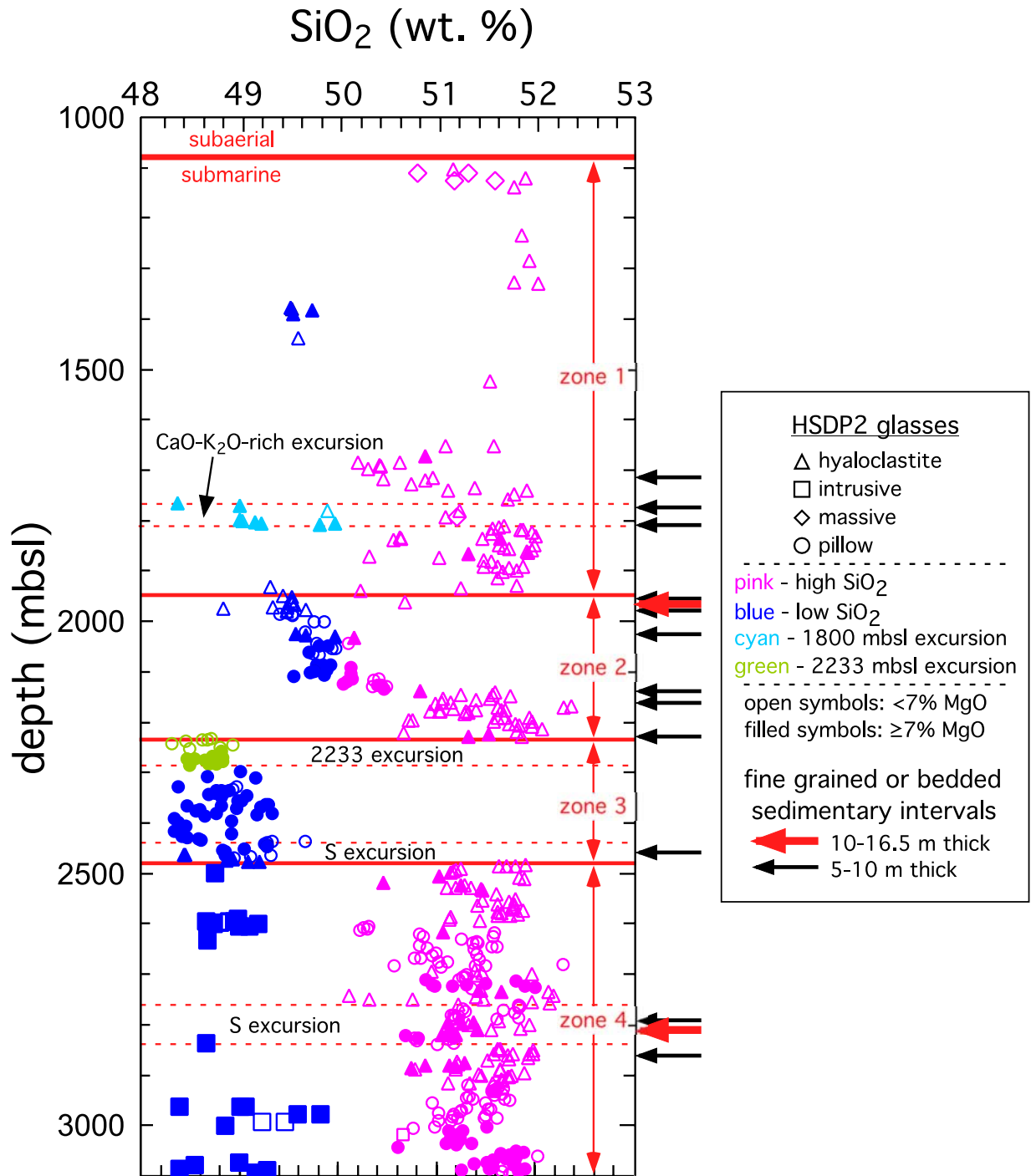


**Figure 19.** Depth (mbsl) versus SiO<sub>2</sub> content of glasses in the submarine section of the HSDP2 core; symbols and color coding are explained in the legend. Horizontal, solid red lines show divisions of the core into subaerial samples and zones 1–4 (see section 4.2). Dashed red lines show locations of “excursions” (see sections 6 and 7); the excursions in S content are described by *Seaman et al.* [2004]. Arrows at the right of the figure indicate the midpoints of intervals of fine-grained (clasts < 2–4 mm) and/or bedded sedimentary units. Red arrows indicate 10–16.5 m thick intervals; black arrows indicate 5–10 m thick intervals. Some thick sequences of fine-grained hyaloclastite roughly coincide with major geochemical boundaries: e.g., a 5.4 m thick sequence overlies the zone 3 pillow sequence; fine-grained sequences at 1956 (5.3 m thick), 1966 (11.9 m thick), and 1980 (8.2 m thick) mbsl occur near the top of zone 2; and the CaO-K<sub>2</sub>O-rich excursion in zone 1 is bounded near its top (1777 mbsl; 5.2 m thick) and bottom (1811 mbsl; 5.0 m thick) by fine-grained sediments.

envisioned by many authors working on Hawaiian magmas [e.g., *Hauri et al.*, 1994, 1996; *Kurz et al.*, 1995; *DePaolo et al.*, 2001; *Dixon and Clague*, 2001; *Blichert-Toft et al.*, 2003; *Eisele et al.*, 2003; *Kurz et al.*, 2004]. In this case, the plume is homogeneous in the vertical dimension but has vertical boundaries between contrasting source regions. In this case, the characteristic timescale for the transition from magmas from one source type to those from the second source type would be the time it takes for the zone of melt sampling for a Hawaiian volcano (e.g., a  $\sim 25$  km radius circular melt sampling zone such as that assumed by *DePaolo and Stolper* [1996]) to pass over the vertical boundary between source types. Assuming a plate velocity of  $\sim 10$  cm/yr, the transition between magmas from distinct vertical zones would again be on the order of  $10^5$  years (although shorter timescales would result if the heterogeneities were close to an inner or outer edge of the sampling circle). The chemical and isotopic transition that occurs over most of the subaerial part of the core (see Figure 8) is gradual and corresponds to a  $10^5$  year timescale, and thus is consistent with the passage of the sampling zone of the Mauna Kea volcano over a vertical boundary between concentric zones in the plume [e.g., *DePaolo et al.*, 1996; *Kurz et al.*, 1996; *Eisele et al.*, 2003; *Huang and Frey*, 2003].

[94] Although the end-members of horizontal and vertical boundaries between heterogeneities described in the previous two paragraphs are oversimplified descriptions of the distribution and orientation of boundaries between contrasting source regions, they demonstrate that the timescales for variation in the average output of heterogeneous source regions are expected to be much longer than those associated with the significant chemical variations observed in the submarine portion of the HSDP2 core. The variations observed in the HSDP2 core therefore require some other explanation, and there are many possibilities to account for short duration variations in the compositions of magmas delivered from the mantle to the volcanic plumbing system. For example, *Spiegelman and Kelemen* [2003] showed how complexities in the mechanism of melt migration into high porosity conduits and the temporal evolution of conduit geometry can result, even for adiabatic melting of homogeneous sources, in highly variable melts exiting conduits at the top of the zone of melt generation. Alternatively, a distribution of heterogeneities at many scales in an ascending plume could generate melts and deliver

them in a highly heterogeneous fashion in time and space due to their contrasting chemistries and the complex productivity functions of heterogeneities embedded within an overall adiabatic upwelling system [e.g., *Hirschmann and Stolper*, 1996; *Phipps Morgan*, 1999]. Related to this, *Reiners* [2002] proposed that deep, high degree melts of productive heterogeneities (e.g., pyroxenites) could alternate with shallower melts from less productive peridotite, with the timescale of  $\leq 10^2$  years for switching from dominantly shallow to deep melts. It is also possible to envision instabilities in the high-level plumbing system of a volcanic edifice: for example, structural changes (e.g., landslides, earthquakes) within the volcanic edifice could lead to abrupt changes in the plumbing system and the local regions from which melts in the underlying mantle are collected.

[95] We emphasize again, however, that although factors such as those listed in the previous paragraph could lead to relatively rapid shifts in the output of the mantle to the volcano, the average output of the melting zone cannot easily shift more abruptly than the simple calculations presented above suggest; i.e., all parts of the system are thought to be producing melt continuously, so although individual parts of the system can be sampled preferentially for a short time, unless significant portions of the magmatic production of the sources bypass the volcano (e.g., by underplating or intrusion), most of the magmas being produced should eventually be expressed in the magmatic output of the system. So the curious feature of the submarine section of the HSDP2 core may not be so much the variability or even the abruptness of the transitions between magma types (although these must signify hiatuses in deposition and/or the absence or bypassing of magma chambers that can dilute the effects of highly variable magma delivery), but the existence of intervals such as zone 3, in which a significant thickness of low-SiO<sub>2</sub> magma is sandwiched between largely high-SiO<sub>2</sub> magmas: i.e., where did the high-SiO<sub>2</sub> magmas that must have been being produced during the time interval represented by zone 3 go?

#### 8.4. Zone 3: How Can We Explain a Significant Interval of Low-SiO<sub>2</sub> Magma Abruptly Sandwiched Between Overlying and Underlying High-SiO<sub>2</sub> Magma?

[96] The high-SiO<sub>2</sub> hyaloclastites above and below zone 3 provide clear evidence of subaerial

eruptions spanning the time period of zone 3, and they show that there was probably an active high-level magma chamber containing dominantly high-SiO<sub>2</sub> magma before and after the eruption of the low-SiO<sub>2</sub>, zone 3 pillows. Unless the lower and upper contacts of zone 3 represent very long time intervals, it would seem implausible that this magma chamber was fully flushed twice (first in the transition from zone 4, high-SiO<sub>2</sub> magmas to zone 3, low-SiO<sub>2</sub> magmas, and then back again in the transition from zone 3 to zone 2) with no evidence of either transition. An alternative is that the high-SiO<sub>2</sub> hyaloclastites at the top of zone 4 and the base of zone 2 reflect magmas from a high-level magma chamber continuously containing high-SiO<sub>2</sub> magma, and the zone 3 pillows represent magmas that bypassed the main plumbing system and were delivered directly to the submarine flank of the volcano. The absence of high-SiO<sub>2</sub> magmas, intermediate SiO<sub>2</sub> (i.e., mixed) magmas, or degassed magmas among the samples in zone 3 are all consistent with this hypothesis. Since several of the unique geochemical signatures of zone 3 magmas reflect characteristics of their sources (see section 4.1), in the context of this hypothesis not only would the low-SiO<sub>2</sub>, zone 3 magmas have bypassed the high-level plumbing system of the volcano, they also would probably have had to bypass the dominant plumbing system of the volcano all the way from their mantle sources (see also section 5.3). Note that the intrusive glasses from zone 4 are all undegassed and nearly all are in the low-SiO<sub>2</sub> group, so they, like the zone 3 pillow magmas, may also have bypassed existing magma chambers en route to the location of the drill site. *Johnson et al.* [2002] suggested similarly that magmas feeding flank and distal eruptions on Kilauea's Puna ridge may have bypassed the volcano's shallow rift-zone plumbing system, and it could be that this is a common characteristic of Hawaiian submarine flank eruptions.

[97] An alternative explanation of these observations could be that the high-level magma chamber was stratified, such that the low-SiO<sub>2</sub>, undegassed zone 3 magmas were preferentially drawn from the deeper parts of the magma chamber that rarely mixed with high-SiO<sub>2</sub>, variably degassed magmas from shallower levels of the chamber (e.g., see *Dixon et al.* [1991] and Figure 9). Although possible (and something of this sort may be required in any case to explain the existence of undegassed, high-SiO<sub>2</sub> pillows emplaced contemporaneously with high-SiO<sub>2</sub>

hyaloclastites in zone 4, unless they also bypassed the magma chamber), this situation would not be dynamically stable since undegassed magmas are less dense than degassed magmas [*Clague et al.*, 1995] and since undegassed low-SiO<sub>2</sub> liquids would also be less dense than undegassed high-SiO<sub>2</sub> liquids of similar MgO contents given their typically higher H<sub>2</sub>O contents [*Seaman et al.*, 2004].

[98] Flank eruptions do not appear to be common on modern Hawaiian volcanoes compared to summit and rift zone eruptions. Thus flank eruptions of the sort we envision bypassing the main plumbing system of a volcano are more likely to be local rather than volcano-wide phenomena, and they seem more likely to represent individual events (e.g., from productive melting of a fertile heterogeneity) rather than long-term loci of volcanic activity comparable to volcano summits or rift zones. If this applies to zone 3, a locally high flux of low-SiO<sub>2</sub> magma could have produced a pile of pillows deposited disconformably on the magma-chamber-derived high-SiO<sub>2</sub> hyaloclastites and lava flows that make up the bulk of the volcano's flank. The formation of high-SiO<sub>2</sub> hyaloclastites would not have been affected by the deposition of zone 3 pillows (i.e., the activity of the high-level magma chamber would not have been influenced by the eruption of the zone 3 pillows), but the debris flows that formed them would have been diverted for a time around the topographic high of zone 3 pillows. This would have resulted in a hiatus in deposition at the drill site after the eruption of the zone 3 pillows ceased until debris flows built up sufficiently to overtake the topographic high, producing an abrupt transition from pillows to overlying, compositionally distinct hyaloclastites. Note that if this scenario is correct, despite its ~250 m thickness, zone 3 might be attributed to an interval of volcanic activity shorter than the ~10<sup>4</sup> years suggested on the basis of the overall age versus depth relationship of the submarine section (*Sharp and DePaolo*, manuscript in preparation, 2004).

### 8.5. The 2233–2280 mbsl Excursion at the Top of Zone 3

[99] With its shift to lower melt fractions, transitional compositions, and higher extents of fractionation (and probably diminished melt flux), the compositional excursion at the top of zone 3 has all the characteristics of the shutting down of magmatic activity at the end of shield building:

i.e., precisely the same shifts (although extending to more extreme alkalic compositions) occur at the top of the subaerial Mauna Kea HSDP2 section at depths of  $\sim 245\text{--}400$  mbsl. Moreover, several isotopic ratios ( $\epsilon_{\text{Nd}}$ ,  $^3\text{He}/^4\text{He}$ ,  $^{87}\text{Sr}/^{86}\text{Sr}$ ) shift in similar directions and over similar ranges both in zone 3 and over much of the subaerial Mauna Kea section, culminating in rapid changes to transitional or alkalic samples in the upper  $\sim 50$  m ( $\epsilon_{\text{Hf}}$  is the exception, shifting in opposite directions at the top of the Mauna Kea section and in zone 3). Thus the top of zone 3 appears to capture a winding down of magmatism comparable to the shutting down of magmatic activity that marks the end of the shield-building phase in the lifetime of a Hawaiian volcano, but it occurs well within the shield-building phase of Mauna Kea's volcanic activity. Although not accompanied by comparable changes in composition, variations in magma flux are known for Kilauea and Mauna Loa on historic and longer timescales [Lipman, 1995; Pietruszka and Garcia, 1999a], but a "failed" shutdown of a Hawaiian volcano has not been previously observed.

[100] The shift to lower degrees of melting at the end of shield building can be envisioned as the effect of the volcano moving off the plume, sampling its progressively cooler outer edges [e.g., DePaolo and Stolper, 1996; Ribe and Christensen, 1999; Feigenson et al., 2003; Huang and Frey, 2003; Rhodes and Vollinger, 2004]. It is more difficult to understand a shift to lower degrees of melting in the middle of the shield-building phase of a volcano's history without invoking ad hoc, poorly constrained scenarios. One possibility is to invoke a fertile heterogeneity in the source: such a heterogeneity would have a period of high productivity (i.e., enhanced by thermal interactions with the less productive material in which it is embedded [see Hirschmann and Stolper, 1996]), which might help to explain the relatively thick interval in zone 3 of low-SiO<sub>2</sub> magmas from 30–40 kbar. The excursion to lower melt fractions at the top of zone 3 might then result from mixing of diminishing melts from the heterogeneity (e.g., after it reaches clinopyroxene exhaustion) with lower degree melts from its surroundings [Reiners, 2002]. Alternatively, the plume feeding Mauna Kea might have broken up into "blobs," each of which had a life history ending, like an archetypical Hawaiian volcano, in a transitional or alkalic cap; a succession of such blobs passing through the melting zone could result in the occurrence of such cycles (though muted) in the output of a single volcano. A period of diminished productivity between blobs

could result in a hiatus that might explain the abruptness of the upper boundary of zone 3, although the absence of an alkalic "startup" phase (e.g., such as is observed at Loihi) at the base of zone 2 would imply that such magmas, if they existed, did not reach the drill site. This alternative envisions zone 3 as a volcano-wide phenomenon that would be observable as a time-stratigraphic horizon if other sites were drilled into the Mauna Kea volcano.

[101] Whatever its explanation, the excursion at the top of zone 3 represents an unprecedented feature of the HSDP2 core, demonstrating an internal boundary in the tholeiitic section of a type previously thought to be associated uniquely with the end of a volcano's lifetime. Note finally that if the shift to transitional magmas is, as we infer, associated with decreased magma flux, the shape of the age versus depth curve in the core is likely to be more complex than a simple linear or continuous concave down curve (see Sharp and DePaolo, manuscript in preparation, 2004).

## 8.6. Gradual Transition From High- to Low-SiO<sub>2</sub> Magmas in Zone 2

[102] We emphasized in section 4.2 the gradual transition from high- to low-SiO<sub>2</sub> magmas extending over the  $\sim 280$  m from the base to the top of zone 2. Assuming two discrete magma series (i.e., a high-SiO<sub>2</sub> and a low-SiO<sub>2</sub> series, but note that the lower SiO<sub>2</sub> magmas from the top of the zone are all part of the CaO-Al<sub>2</sub>O<sub>3</sub>-rich group; see section 4.6), this transition would have to reflect varying proportions of the two distinct parental magmas in the mixed magmas erupted at the drill site. We consider here the possibility that this gradual transition reflects the residence time of magma in a magma chamber. In particular, we model the system as a perfectly mixed magma chamber of fixed size (i.e., input at its base is matched by output from its top) initially filled with high-SiO<sub>2</sub> magma. We then suppose that the input to the magma chamber changed abruptly to low-SiO<sub>2</sub> magma due to unspecified changes (e.g., variability in conduit geometry, enhanced melting of embedded heterogeneities, etc.). The temporal variation of the output of the magma chamber is then a simple function of the ratio of the magma flux to the size of the magma chamber.

[103] Figure 20 shows the results of such a model assuming the initial SiO<sub>2</sub> content of the high-SiO<sub>2</sub> magma in the chamber was 52.0%, the low-SiO<sub>2</sub>

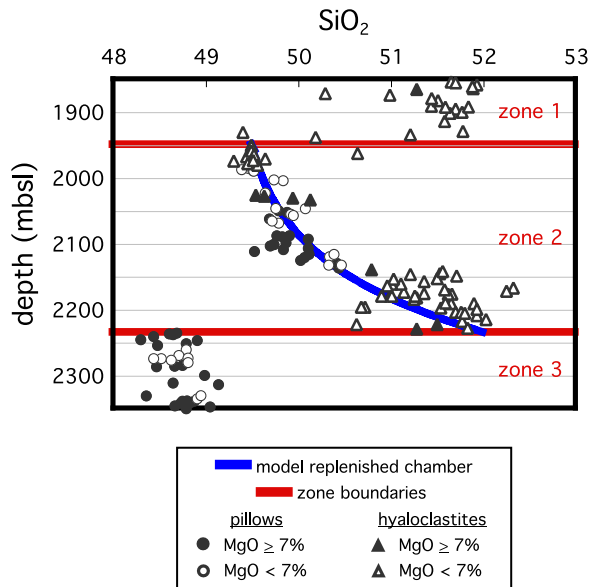


**Figure 20.** Close-up of  $\text{SiO}_2$  versus depth (mbsl) illustrating the progressive change in silica content from the bottom of the top of zone 2. The curve describes the output of magma from a constant volume, perfectly mixed magma chamber into which magma of a constant  $\text{SiO}_2$  content is continuously input at a fixed flux; the constant volume assumption requires that the perfectly mixed magma exits the chamber at the same rate at which magma enters the chamber. The parameters of the fitted curve are an initial  $\text{SiO}_2$  content of the magma in the chamber of 52.0%, 49.3%  $\text{SiO}_2$  in the magma entering the chamber, a magma chamber radius of  $\sim 1.9$  km, a magma flux of  $0.1 \text{ km}^3/\text{yr}$  [e.g., Lipman, 1995], and an age difference between the top and bottom of zone 2 of  $\sim 16$  Kyr (Sharp and DePaolo, manuscript in preparation, 2004).

magma entering the chamber had 49.3%  $\text{SiO}_2$ , and the age difference between the top and bottom of zone 2 is  $\sim 16$  Kyr (on the basis of the depth-age relationship of Sharp and DePaolo (manuscript in preparation, 2004)). The model trend provides an excellent match to the concave upward variation of  $\text{SiO}_2$  content with depth. Assuming a magma flux of  $\sim 0.1 \text{ km}^3/\text{yr}$  [e.g., Lipman, 1995], the implied radius of a spherical magma chamber based on this model is  $\sim 1.9$  km. This is a reasonable size for a high-level Hawaiian magma chamber [e.g., Ryan et al., 1981; Pietruszka and Garcia, 1999b], suggesting that the gradual change from high- to low- $\text{SiO}_2$  magmas over the depth interval of zone 2 can be reasonably explained by mixing processes in a high-level magma chamber.

[104] Note that this model requires a magma chamber already filled with high- $\text{SiO}_2$  magma at

the start of the zone 2 interval. Given the abruptness of the boundary between zones 2 and 3, this implies either a hiatus between the top of zone 3 and the bottom of zone 2 (i.e., an equivalent amount of time would have been required to replace with high- $\text{SiO}_2$  magma the low- $\text{SiO}_2$  magma present in the magma chamber at the time corresponding to the top of zone 3, but no magmas corresponding to this transition are present in the drill core), or that low- $\text{SiO}_2$  zone 3 magmas bypassed the magma chamber as we suggested in section 8.4. However, even if the low- $\text{SiO}_2$  magmas from zone 3 bypassed the magma chamber, the model developed here requires that both high- and low- $\text{SiO}_2$  magmas were supplied to a single magma chamber during the time period represented by zone 2.

[105] The transition at the top of zone 2 from low- to high- $\text{SiO}_2$  magma is not as abrupt as the opposite transition at its base, extending over  $\sim 30$  m (corresponding to  $\sim 2$  Kyr assuming the smooth depth-age relationship of Sharp and DePaolo (manuscript in preparation, 2004)). This is nevertheless relatively sharp, especially given the mode of formation of hyaloclastites, which collect fragmental material near the shoreline and slump periodically (i.e., even sharp transitions in magma composition would typically be broadened to at least the thickness at the drill site of the debris flow that captured the abrupt transition). If the gradual transition in zone 2 reflects the existence of a relatively large well-mixed magma chamber as we suggest here, the abrupt zone 2 upper boundary would be difficult to understand unless it represents a hiatus in deposition at the drill site; i.e., it would be difficult to replace the low- $\text{SiO}_2$  magma in such a well-mixed chamber with high- $\text{SiO}_2$  magma on the timescale of  $\sim 10^3$  years required by the 30 m transition from the top of zone 2 to the base of zone 1 if the rate of deposition were constant unless the magma flux to the magma chamber increased by about an order of magnitude. As shown in Figure 19, the boundary between zones 1 and 2 corresponds to the position of a thick zone of fine-grained, bedded sediments and hyaloclastites and is thus consistent with this boundary representing a period of low deposition at the drill site. An alternative explanation of the shift from low- $\text{SiO}_2$  to high- $\text{SiO}_2$  glasses at the zone 1-zone 2 boundary might be that the zone 1 magmas immediately above the boundary bypassed the magma chamber. However, we consider this unlikely since zone 1 and zone 2 samples are all hyaloclastites or degassed pillows that we infer degassed subaerially

and thus might have had difficulty avoiding a high-level magma chamber.

## 9. Summary and Conclusions

[106] 1. The lower  $\sim 2000$  m of the section drilled by the Hawaii Scientific Drilling Project in 1999 is submarine and contains a considerable amount of glass. Nearly all the submarine glasses are tholeiitic, but in contrast to what is typically observed in subaerially exposed Hawaiian tholeiites, the glasses from the HSDP2 core span a significant range ( $\sim 48$ – $52.5\%$ ) of  $\text{SiO}_2$  contents. The  $\text{SiO}_2$  contents are bimodally distributed, particularly among pillow glasses, with modes at  $\sim 48.5$ – $49$  and  $51$ – $52\%$ . Among undegassed glasses, there is no compositional overlap between the high- and low- $\text{SiO}_2$  glasses: i.e., all glasses with intermediate silica contents are degassed. Focusing on glasses with  $\geq 7\%$   $\text{MgO}$ , the low- $\text{SiO}_2$  group is higher in  $\text{Al}_2\text{O}_3$ ,  $\text{FeO}^*$ ,  $\text{Na}_2\text{O}$ , and  $\text{TiO}_2$  than the high- $\text{SiO}_2$  group. The two groups are indistinguishable in  $\text{CaO}$ ,  $\text{K}_2\text{O}$ , or  $\text{P}_2\text{O}_5$ . Restricting the comparison to undegassed glasses,  $\text{H}_2\text{O}$  is slightly higher and S perhaps slightly lower in the low- $\text{SiO}_2$  glasses.

[107] 2. The high- and low- $\text{SiO}_2$  glass groups are also evident among whole rocks from the HSDP2 core. High- and low- $\text{SiO}_2$  whole rocks and glasses are generally distinguishable using isotopic ratios (e.g.,  $^3\text{He}/^4\text{He}$ ,  $\epsilon_{\text{Nd}}$ ,  $^{176}\text{Hf}/^{177}\text{Hf}$ ,  $^{206}\text{Pb}/^{204}\text{Pb}$ , and  $^{87}\text{Sr}/^{86}\text{Sr}$ ) and certain trace element ratios (e.g.,  $\text{Zr}/\text{Nb}$ ), demonstrating that sorting of the glasses into these groups is not artificial and that petrogenesis of the two groups involved compositionally distinguishable mantle sources.

[108] 3. On the basis of the distributions of high- and low- $\text{SiO}_2$  glasses with depth, the submarine section of the core is divided into four zones. In zone 1 (1079– $\sim 1950$  mbsl), most samples are high- $\text{SiO}_2$  hyaloclastites and massive lavas, but there are narrow intervals of low- $\text{SiO}_2$  hyaloclastites. Zone 2 ( $\sim 1950$ – $2233$  mbsl), a zone of degassed pillows and hyaloclastites, displays a continuous decrease in silica content from bottom to top. In zone 3 ( $2233$ – $2481$  mbsl), nearly all samples are undegassed low- $\text{SiO}_2$  pillows. In zone 4 ( $2481$ – $3098$  mbsl), samples are mostly high- $\text{SiO}_2$  undegassed pillows and degassed hyaloclastites. This zone also contains most of the intrusive units

in the core, none of which are degassed and most of which are low- $\text{SiO}_2$ .

[109] 4. Comparison of HSDP2 glasses to tholeiitic samples from other studies of Mauna Kea confirms that the low- $\text{SiO}_2$  HSDP2 glasses are a distinctive, previously unrecognized Mauna Kea magma type, although they are most similar chemically to the Hamakua tholeiites from the subaerially exposed late stages of shield building. One deep dredge sample ( $>3$  kmbsl) from the Hilo ridge is similar to the low- $\text{SiO}_2$  HSDP2 samples. The high- $\text{SiO}_2$  HSDP2 glasses are similar to samples dredged from the deeper parts of the Hilo ridge.

[110] 5. Comparison of HSDP2 glasses to tholeiitic samples from other Hawaiian volcanoes shows that although each volcano has distinctive features, the high- $\text{SiO}_2$  HSDP2 glasses generally fall on trends defined by other Hawaiian volcanoes, especially in  $\text{FeO}^*$ - $\text{SiO}_2$  and  $\text{CaO}$ - $\text{SiO}_2$  space. The high- $\text{SiO}_2$  HSDP2 glasses are most similar to samples from Kilauea and from the recently identified main-shield phase of Koolau. In contrast, the low- $\text{SiO}_2$  HSDP2 glasses form a distinctive group falling off the compositional trends versus  $\text{SiO}_2$  defined by most other Hawaiian magmas; in particular they have lower  $\text{CaO}$ ,  $\text{Al}_2\text{O}_3$ ,  $\text{TiO}_2$ , and probably  $\text{K}_2\text{O}$  than other Hawaiian magmas at similar  $\text{SiO}_2$  contents. Although there are differences, the low- $\text{SiO}_2$  HSDP2 glasses are most similar to those from Loihi.

[111] 6. Phase equilibrium data suggest that parental magmas of the low- $\text{SiO}_2$  suite could have been produced by partial melting of fertile lherzolite at  $30$ – $40$  kbar. Although the high- $\text{SiO}_2$  parents could have equilibrated with harzburgite at  $15$ – $20$  kbar, they could neither have been produced simply by higher degrees of melting of the sources of the low- $\text{SiO}_2$  parents nor by mixing of known high-silica (e.g., dacitic) partial melts of pyroxenite or eclogite with the low- $\text{SiO}_2$  parents. Our hypothesis for the relationship between these magma types is that as they ascended from their sources, low- $\text{SiO}_2$  magmas interacted chemically and thermally with overlying peridotites, resulting in dissolution of orthopyroxene and clinopyroxene and precipitation of olivine, thereby generating high- $\text{SiO}_2$  magmas. As this assimilation process proceeded, it would first have exhausted clinopyroxene from the lherzolite, explaining the equilibration of the high- $\text{SiO}_2$  parent liquid with a harzburgitic assemblage at  $15$ – $20$  kbar; ultimately, this process

could lead to dunitic channels in the overlying peridotite.

[112] 7. In addition to the abundant high- and low-SiO<sub>2</sub> glasses, there is a group of glasses with slightly elevated CaO, Al<sub>2</sub>O<sub>3</sub>, and SiO<sub>2</sub> relative to the main group of low-SiO<sub>2</sub> glasses. Most if not all of the glasses with these characteristics are from zone 2. This group of glasses cannot be generated by low-pressure fractionation of the more abundant low-SiO<sub>2</sub> magmas or by variable degrees of melting of the same sources that produced the low-SiO<sub>2</sub> magmas. We propose that the differences between the more abundant low-SiO<sub>2</sub> glasses and these high CaO-Al<sub>2</sub>O<sub>3</sub> glasses reflect involvement of pyroxene-rich lithologies (e.g., pyroxenite, eclogite, and/or clinopyroxene-rich peridotites) in their petrogenesis.

[113] 8. Low-SiO<sub>2</sub> glasses from the top of zone 3 (2233–2280 mbsl) are more alkaline, more fractionated, and incompatible-element-enriched relative to other glasses from zone 3. Glass compositions in this interval are generally consistent with a decrease of up to several tens of percent in the degree of partial melting relative to the other zone 3 glasses. This excursion at the top of zone 3 toward transitional, trace element-enriched compositions is abruptly terminated and overlain by high-SiO<sub>2</sub> magma; this is reminiscent of the end of shield building at the top of the Mauna Kea section in the core where alkaline Mauna Kea lavas are discomformably overlain by Mauna Loa lavas. An upward progression toward more fractionated compositions is also seen both at the top of the subaerial Mauna Kea section and at the top of zone 3 and is consistent with declining magma flux. Thus the excursion at the top of zone 3 has characteristics of the shutting down of magmatic activity at the end of shield building, but the presence of such a trend in the middle of the shield-building tholeiitic phase of a Hawaiian volcano has not been previously observed.

[114] 9. Low-SiO<sub>2</sub> glasses at ~1800 mbsl are distinguished by their elevated K<sub>2</sub>O and CaO contents. They are on average less fractionated than other glasses, and they have lower Al<sub>2</sub>O<sub>3</sub> and FeO\* contents than other low-SiO<sub>2</sub> HSDP2 glasses at the same MgO content. They are also unusual in that their elevated K<sub>2</sub>O contents are not accompanied by elevated P<sub>2</sub>O<sub>5</sub> or TiO<sub>2</sub> and their Na<sub>2</sub>O contents are lower than those of most other low-SiO<sub>2</sub> glasses. Among other Mauna Kea samples, the subaerial Hamakua tholeiites are most similar. The sources of the CaO-K<sub>2</sub>O-rich glasses were clearly distinct from those of all other HSDP2

lavas; these differences may reflect enrichments in fluids and/or melts coming off a subducting slab, perhaps indicating the presence of materials recycled from an ancient arc or mantle wedge among the sources of HSDP magmas.

[115] 10. Abrupt compositional changes over narrow depth intervals are observed at many places in the HSDP2 core, signifying major changes in source composition and/or processes. All of the zone boundaries and several other compositional changes in the core correspond to thick intervals of fine-grained and bedded hyaloclastites. These intervals may represent periods in which largely reworked rather than freshly erupted material was deposited at the drill site, suggesting that major compositional changes in the core occur across depositional hiatuses. Nevertheless, the HSDP2 core documents major chemical variability over timescales  $\leq 10^3$ – $10^4$  years during shield building. Possibilities for explaining such rapid variations in the compositions of erupted magmas include instabilities and temporal evolution of conduit geometries in mantle sources; distributions of heterogeneities at many scales in an ascending plume; and instabilities in the high-level plumbing system of the volcanic edifice that could lead to abrupt changes in the regions from which magmas in the underlying mantle are collected.

[116] 11. There are several factors that could contribute to the abrupt boundaries and considerable thickness of zone 3, the low-SiO<sub>2</sub> interval at 2233–2481 mbsl. The high-SiO<sub>2</sub> hyaloclastites above and below this zone could reflect well-mixed magmas from a high-level magma chamber while the zone 3 pillows represent melts that for an interval of  $\sim 10^4$  years bypassed the main plumbing system, delivering deep magma directly to the flanks of the volcano. Although zone 3 represents a substantial depth interval, it could have been produced during a period of anomalous magma flux that produced a topographic high at the drill site around which high-SiO<sub>2</sub>, hyaloclastite-forming debris flows were diverted for a time. After the pulse of low-SiO<sub>2</sub> pillow lavas ended, a hiatus in deposition at the site would follow until dominantly high-SiO<sub>2</sub> debris flows built up sufficiently to overtop the topographic high, producing an abrupt transition from pillows to overlying, compositionally distinct hyaloclastites at the drill site.

[117] 12. There is a gradual transition from high- to low-SiO<sub>2</sub> magmas extending over the  $\sim 280$  m from the base to the top of zone 2. Assuming these

magmas represent the output of a well-mixed magma chamber initially filled with high-SiO<sub>2</sub> magma into which low-SiO<sub>2</sub> magma was delivered, a magma supply rate of 0.1 km<sup>3</sup>/yr, and that zone 2 spans ~15 Kyr, this transition can be modeled quantitatively if the magma chamber had a radius of ~2 km.

## Appendix A

### A1. Comparison of the Compositions of HSDP Glasses and Whole Rocks

[118] In this section we compare the compositions of our HSDP2 glass samples with whole rock data on samples from the HSDP2 [Rhodes and Vollinger, 2004] and HSDP1 [Rhodes, 1996] cores. Aspects of this comparison were discussed in section 4.3.

[119] A complication in dealing with whole rock analyses of Hawaiian lavas is that they span a wide range of MgO contents, reflecting magma mixing and/or the accumulation of olivine phenocrysts/xenocrysts in basaltic liquids [e.g., Clague *et al.*, 1995; Rhodes, 1995; Rhodes and Vollinger, 2004]. For comparison with our glass analyses, which span a much narrower and generally lower range of MgO contents, we adjusted the whole rock analyses in an effort to deal with these effects. We did this by first converting all Fe<sub>2</sub>O<sub>3</sub> to FeO and all trace element concentrations to oxide weight percents and then normalizing each whole rock analysis (Rhodes [1996] for the pilot hole and Rhodes and Vollinger [2004] for HSDP2) to 100%. We then plotted the normalized whole rock data on MgO-SiO<sub>2</sub> and MgO-Al<sub>2</sub>O<sub>3</sub> variation diagrams. When viewed in this way, the separation of the whole rocks into high- and low-SiO<sub>2</sub> groups is apparent, particularly for the HSDP2 samples, and each sample was assigned to one or the other group. For each oxide, best-fit lines versus MgO were then calculated (excluding alkalic samples, defined as those with an alkalinity greater than zero [Carmichael *et al.*, 1974]) either for the entire data set or separately for the high- and low-SiO<sub>2</sub> data sets. Individual whole rock analyses were then projected to 7% MgO using one of the best-fit slopes: SiO<sub>2</sub> and Al<sub>2</sub>O<sub>3</sub> concentrations were projected to 7% MgO using the separate fits to the high- and low-SiO<sub>2</sub> groups because the differences between the groups are well defined for these oxides. For all other oxides, projections to 7% MgO were done using a single best fit to the entire

data set (again excluding the alkalic samples) because the differences between the groups are less well defined. For alkalic samples, projections to 7% MgO were done using the low-SiO<sub>2</sub> fits for SiO<sub>2</sub> and Al<sub>2</sub>O<sub>3</sub> and the fits to the combined high- and low-SiO<sub>2</sub> groups for all other oxides.

[120] Figure 8 shows SiO<sub>2</sub> content and alkalinity versus depth for our suite of glasses from the HSDP2 core and whole rocks from the HSDP1 and HSDP2 cores. As described in section 4.3, it is clear from this comparison that the glass data and the whole rock data are similar in the regions in which they overlap. The only interval in which there is a discrepancy is zone 1, in which the high-SiO<sub>2</sub> hyaloclastite glasses tend to be ~0.5% higher in SiO<sub>2</sub> than the whole rock analyses. This could be an artifact of the projection to 7% MgO, which introduces uncertainty, or to some small but systematic differences in composition. Note also that the whole rock sample from a hyaloclastite just above the excursion at 1765–1810 mbsl (sample SR675-6.90 at 1739.3 mbsl), although low in SiO<sub>2</sub>, does not share any of the unusual compositional characteristics (e.g., high CaO and K<sub>2</sub>O; see section 7) of the glasses from this excursion, apparently representing an additional, distinct occurrence of low-SiO<sub>2</sub> magmas in zone 1. Although all but two of the 28 intrusive glasses analyzed by us (all of which were from deeper than 2500 mbsl and consequently in zone 4) are low-SiO<sub>2</sub> samples, of the five intrusive units analyzed as whole rocks, only one is a low-SiO<sub>2</sub> magma; two of the intrusives analyzed as whole rocks are from zone 1, and both are high-SiO<sub>2</sub> magmas. Finally, although 13 of the 14 whole rock analyses of massive lavas are (like the glasses from massive units included in this study) high-SiO<sub>2</sub> samples from zone 1, one whole rock analysis of a massive sample in the reference suite from zone 4 (unit 298) has low SiO<sub>2</sub>.

[121] Figure A1 uses SiO<sub>2</sub> variation diagrams to compare concentrations of several oxides in the HSDP2 glasses (all with ≥7% MgO) with whole rock analyses from the HSDP1 and HSDP2 cores. The glass and whole rock data sets define similar characteristics for the high- and low-SiO<sub>2</sub> groups. The elevations in FeO\* and P<sub>2</sub>O<sub>5</sub> in the whole rocks relative to the glasses appear to reflect small but systematic differences in these oxides between the whole rocks and the glass data obtained at the University of Hawaii. The larger scatter in the whole rocks for some oxides could reflect several factors. For example, the projection scheme we have used to adjust the whole rock data to 7%

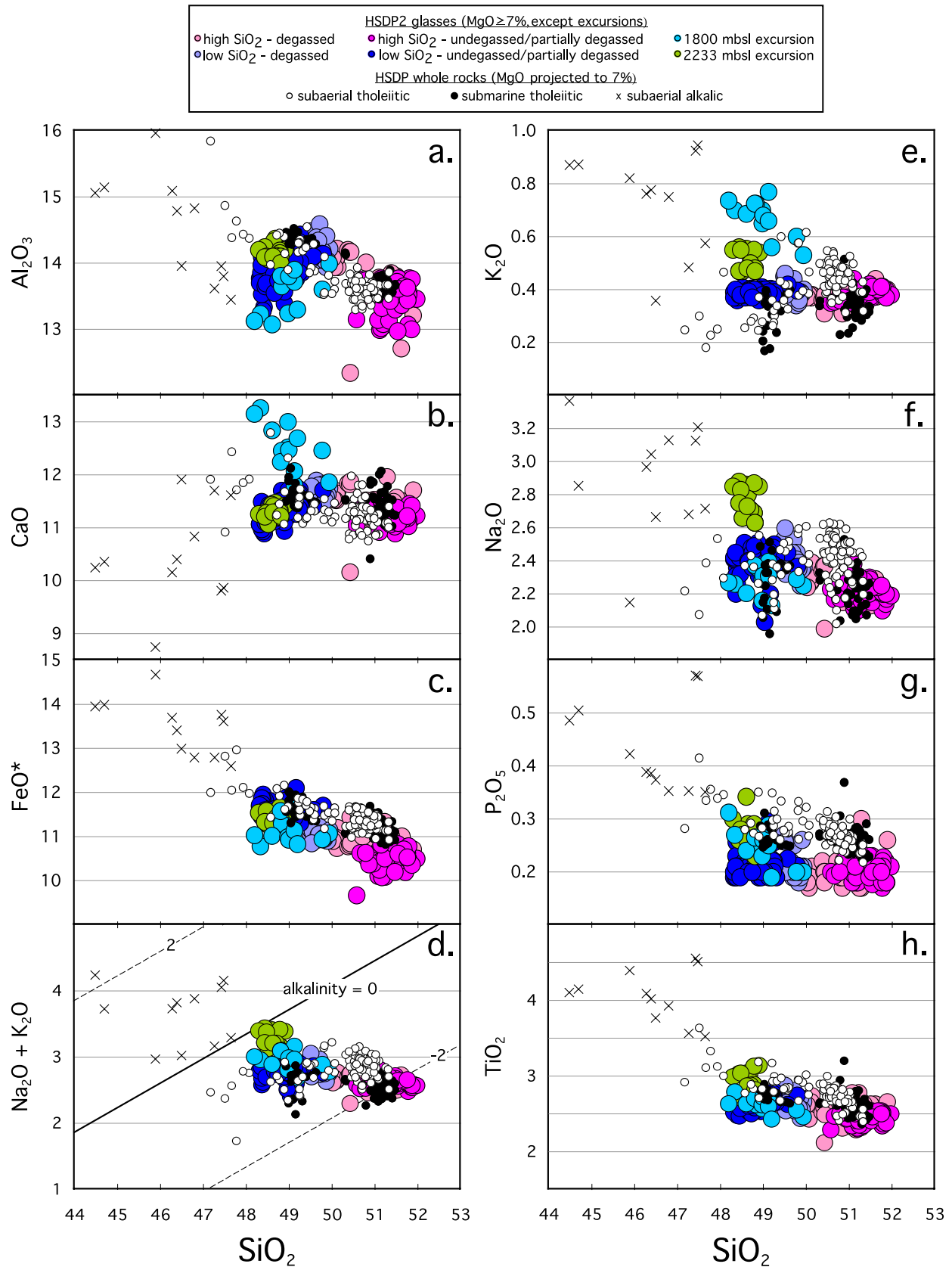


Figure A1

MgO assumes that all sources of compositional variation in samples with MgO contents >7% are strictly parallel in composition space, yet this is certainly not the case since a variety of processes (e.g., accumulation and fractionation of olivine, accumulation and fractionation of other phases, and magma mixing) are all known to influence Hawaiian whole rocks [e.g., *Clague et al.*, 1995; *Rhodes*, 1995; *Rhodes and Vollinger*, 2004]. Although some whole rocks have MgO contents near 7% and thus the effects of projection are small, in most cases the projection must be done over a significant distance in MgO and the potential for uncertainty is large. In addition, although every effort was made in the sampling of the whole rocks from the core to avoid altered material, the groundmass and olivines of many of the rocks were altered, and infilled vesicles and fractures could not always be avoided [*Hawaii Scientific Drilling Project*, 2000]. Thus some of the whole rocks are inevitably compromised to unknown and variable extents by the effects of alteration. This is probably the cause of the variable K<sub>2</sub>O and Na<sub>2</sub>O contents of many of the whole rocks [*Chen and Frey*, 1985; *Garcia*, 1996; Baker et al., manuscript in preparation, 2004a], but CaO, Al<sub>2</sub>O<sub>3</sub>, and SiO<sub>2</sub> are also influenced by the presence of zeolites and other alteration phases in vesicles and fractures as well as by leaching during alteration [*Lipman et al.*, 1990].

## A2. Isotopic and Trace Element Ratios in the High- and Low-SiO<sub>2</sub> Groups

[122] Isotopic and trace element characteristics of whole rocks and glasses are shown versus depth in Figure 7, color coded by compositional group. The main points of this comparison and especially the distinctions between the high- and low-SiO<sub>2</sub> groups are discussed in section 4.1. We point out briefly here two other features of these data as they relate to zones 2 and 3 defined in section 4.2. (1) The continuous trend from high- to low-SiO<sub>2</sub> samples from bottom to top of zone 2 is also expressed in the isotopic and trace element ratios shown in Figure 7. (2) The subtle decrease in SiO<sub>2</sub> upward from the base of zone 3 to ~2280 mbsl is accompanied by decreases in <sup>3</sup>He/<sup>4</sup>He (Figure 7a) and an increase in ε<sub>Nd</sub> (Figure 7b). <sup>176</sup>Hf/<sup>177</sup>Hf

in glasses from this study also increase in this depth interval, but the whole rocks do not precisely overlap the trend defined by the glasses (Figure 7c). <sup>87</sup>Sr/<sup>86</sup>Sr (Figure 7d) and Zr/Nb (Figure 7f) both decrease slightly over this interval of zone 3, but insufficient data are available for Pb isotopes to discern a trend (Figure 7e). Only one isotopic analysis, for <sup>176</sup>Hf/<sup>177</sup>Hf, is available for the “excursion” at 2233–2280 mbsl, but it suggests a continuation over the depth interval of the excursion of the increase in <sup>176</sup>Hf/<sup>177</sup>Hf observed from the base of zone 3 to 2280 mbsl. This single glass analysis also suggests that the increase in <sup>176</sup>Hf/<sup>177</sup>Hf over the ~50 m of the excursion is as large as that over the ~200 m of pillows underlying the excursion.

## A3. Comparison of HSDP2 Glasses to Mauna Kea Whole Rock Analyses and Glass Analyses in the Literature

[123] We presented briefly in section 4.4 comparisons between glass compositions from the HSDP2 core and tholeiitic glass and lava compositions from Mauna Kea and other Hawaiian volcanoes based on a survey of the literature. In this appendix we present additional aspects of the comparison between the HSDP2 glasses and analyses of Mauna Kea rocks and glasses from the literature. In the following appendix, we develop further the comparison between the HSDP2 glasses and analyses of tholeiitic whole rocks and glasses from other Hawaiian volcanoes. These comparisons provide additional context for understanding the significance of the compositional variations observed in the HSDP cores.

[124] There have over the years been many analyses of subaerial Mauna Kea lavas [e.g., *Wolfe et al.*, 1995], and more recently submarine samples have been obtained by dredging and one submersible dive [*Garcia et al.*, 1989; *Moore and Clague*, 1992; *Yang et al.*, 1994; *Holcomb et al.*, 2000]. Although most of the subaerial samples are alkalic, many of the subaerial Hamakua series lavas have alkalinities less than zero and thus are tholeiitic by our definition [see *Yang et al.*, 1994] (most of these are defined as transitional by *Wolfe et al.* [1995]), as are most of the submarine samples.

**Figure A1.** SiO<sub>2</sub> versus various oxides (wt.%) for glasses with ≥7% MgO from the HSDP2 core compared with whole rocks from the HSDP1 and HSDP2 cores [*Rhodes*, 1996; *Rhodes and Vollinger*, 2004]. Whole rock compositions have all been projected to 7% MgO as described in Appendix A1. Symbols and color coding are explained in the legend. Degassed, partially degassed, and undegassed glasses are defined in section 4.1. (a) Al<sub>2</sub>O<sub>3</sub>; (b) CaO; (c) FeO\*; (d) Na<sub>2</sub>O + K<sub>2</sub>O; (e) K<sub>2</sub>O; (f) Na<sub>2</sub>O; (g) P<sub>2</sub>O<sub>5</sub>; and (h) TiO<sub>2</sub>.

[125] As with the HSDP whole rocks, the compositions of Mauna Kea whole rocks from the literature were projected to 7% MgO on the basis of linear fits for these samples of all oxides versus MgO, although for the non-HSDP samples, the submarine and subaerial analyses were fit separately. For the purposes of this comparison, we assume that all submarine samples from the Hilo ridge (nearly all of which are from >1100 mbsl) are from Mauna Kea. The possibility that samples from deeper than 1100 mbsl on the Hilo ridge are actually samples from Kohala rather than Mauna Kea [Holcomb *et al.*, 2000] is discussed below (see section A6).

[126] Figure A2 compares glasses with  $\geq 7\%$  MgO from this study with projected whole rock analyses of HSDP samples and Mauna Kea tholeiites from the literature; subaerial whole rocks are shown as open circles and submarine whole rocks are shown as filled symbols. There is considerable scatter in the whole rock analyses for some oxides, and some of this probably reflects the same factors described above (section A1) in connection with the HSDP whole rocks. Nevertheless, there are both similarities and systematic differences between the HSDP2 glasses and these whole rocks that can be discerned from this comparison. Although not as primitive as the plotted HSDP2 glasses, all of which have  $\geq 7\%$  MgO, we also show for comparison in Figure A2 tholeiitic Mauna Kea glasses from the literature with  $>6.5\%$  MgO.

[127] The SiO<sub>2</sub> contents (projected to 7% MgO) of the submarine whole rocks from the literature (most of which are from the Hilo ridge at depths of 400–3300 mbsl) range from 48.2 to 52.0% and thus overlap nearly the full range of high- and low-SiO<sub>2</sub> glasses from the HSDP2 core. As shown in Figure 9a, SiO<sub>2</sub> contents greater and less than 50% are roughly equally abundant among the submarine whole rocks, and there is no suggestion of bimod-

ality in the distribution of their silica contents (although as for the glasses shown in Figure 10, the submarine whole rocks from off the west coast of Hawaii are generally lower in SiO<sub>2</sub> than those from the Hilo ridge; see Figure A3). Figure A2 shows that the projected concentrations of other oxides in the submarine whole rocks from the Hilo ridge are comparable to glasses ( $\geq 7\%$  MgO) and whole rocks from the HSDP2 core. This similarity would be even more apparent if rather than restricting ourselves to glasses with  $\geq 7\%$  MgO, we included the full range of glass data, which like the submarine whole rocks show a wider range in the concentrations of most oxides than the MgO-rich glasses. Note that in contrast to many of the HSDP whole rocks, the submarine whole rocks from the literature are not systematically displaced to low K<sub>2</sub>O contents (or low K<sub>2</sub>O/P<sub>2</sub>O<sub>5</sub> ratios; see Figure 18a).

[128] Although there is considerable scatter and the submarine whole rocks and glasses sampled by dredging and by submersible represent an incomplete sampling of the exposed submarine section, there is an overall trend to lower SiO<sub>2</sub> contents with shallower collection depth (Figure A3). Assuming that volcanism ended progressively later at shallower levels on Mauna Kea's rift zones (i.e., that there is a correlation between depth on the ridge and age as suggested for Mauna Loa [Moore *et al.*, 1990b]), it is plausible that the decrease in silica content observed for submarine samples from the literature corresponds to the comparable decrease observed in the upper several hundred meters of the subaerial Mauna Kea section in the HSDP1 and HSDP2 cores (although samples corresponding to the lowest silica, alkalic samples in the upper ~100 m of the HSDP subaerial sections are not represented among submarine lavas or glasses from the literature). The suggestion of a stratigraphic equivalence between the submarine lavas and glasses available from dredging and

**Figure A2.** SiO<sub>2</sub> versus various oxides (wt.%) for glasses ( $\geq 7\%$  MgO) and whole rocks from the HSDP cores [Rhodes, 1996; Rhodes and Vollinger, 2004] compared with analyses of the following Mauna Kea samples from the literature: Mauna Kea glasses with  $\geq 6.5\%$  MgO [Garcia *et al.*, 1989; Moore and Clague, 1992; Yang *et al.*, 1994]; subaerial, Hamakua series Mauna Kea tholeiitic whole rocks [Muir and Tilley, 1963; Macdonald and Katsura, 1964; Basaltic Volcanism Study Project, 1981; Frey *et al.*, 1990, 1991; Wolfe *et al.*, 1995]; and submarine Mauna Kea tholeiitic whole rocks [Moore and Clague, 1992; Yang *et al.*, 1994; Wolfe *et al.*, 1995; Norman and Garcia, 1999; Holcomb *et al.*, 2000]. Whole rock compositions have all been projected to 7% MgO as described in Appendices A1 and A3. Symbols and color coding are explained in the legend. Degassed, partially degassed, and undegassed glasses are defined in section 4.1. (a) Al<sub>2</sub>O<sub>3</sub>; (b) CaO; (c) FeO\*; (d) Na<sub>2</sub>O + K<sub>2</sub>O; (e) K<sub>2</sub>O; (f) Na<sub>2</sub>O; (g) P<sub>2</sub>O<sub>5</sub>; and (h) TiO<sub>2</sub>. Mauna Kea glass sample #22-2 [Moore and Clague, 1992] from off the west coast of Hawaii is discussed in Appendix A3 and is indicated in Figure A2b.

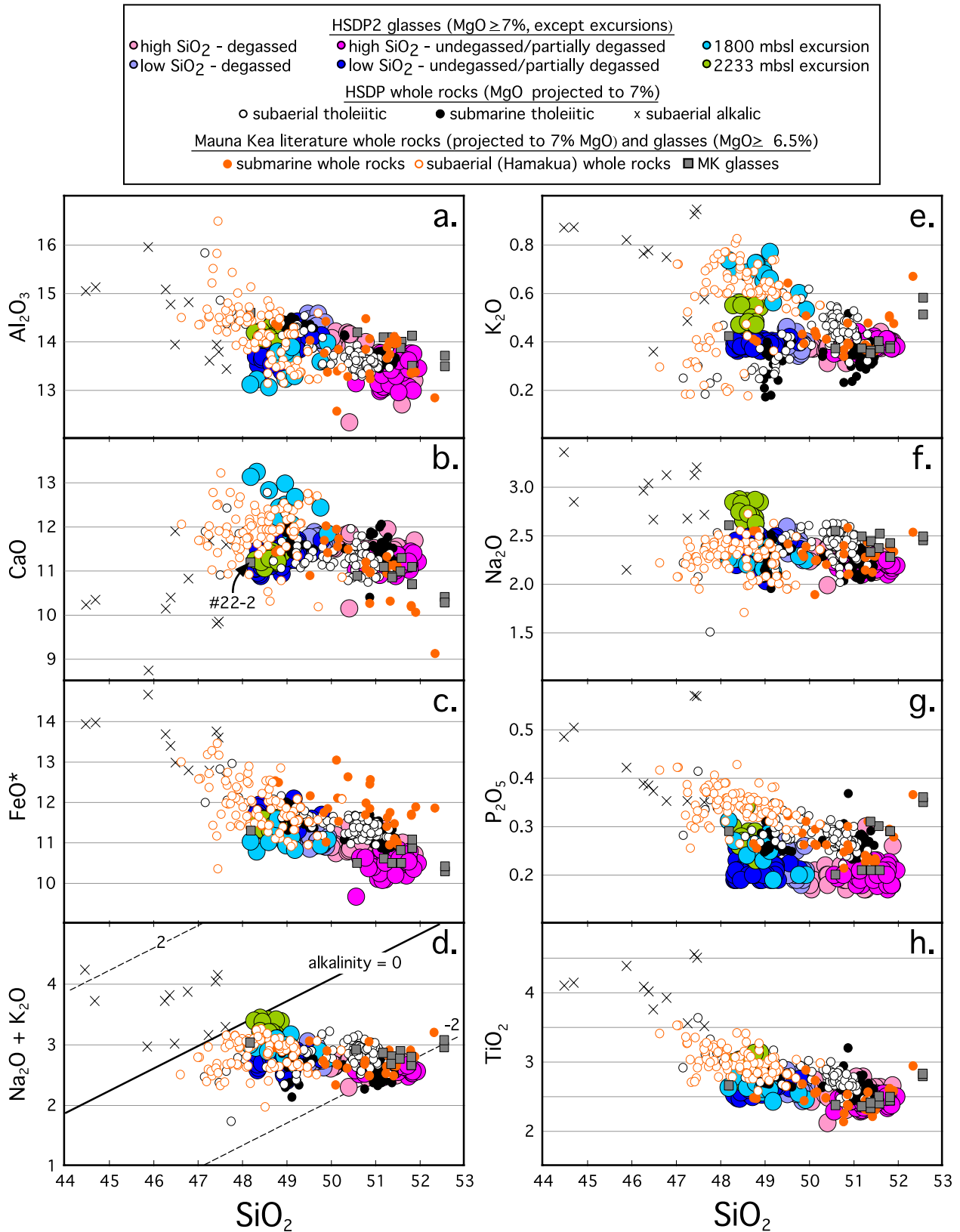
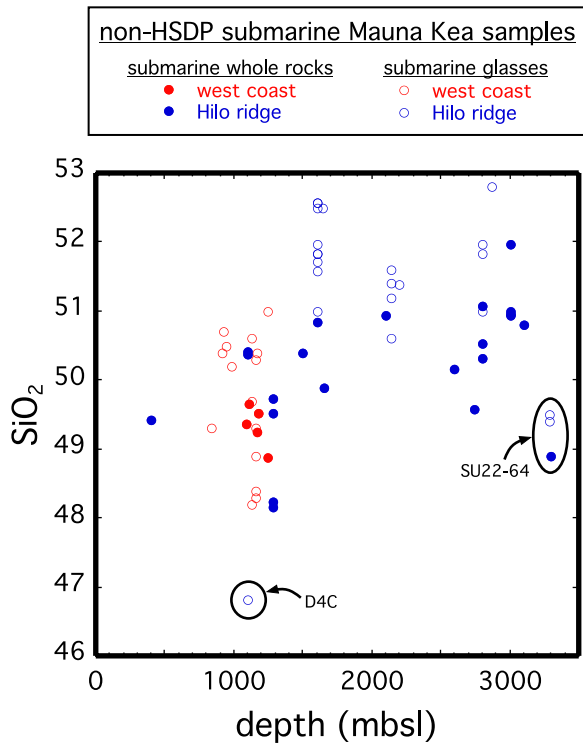


Figure A2



**Figure A3.**  $\text{SiO}_2$  contents versus depth for literature analyses of submarine whole rocks (projected to 7% MgO; see Appendix A3) and glasses from Mauna Kea. Samples are from the Hilo ridge and off the west coast of Hawaii. Hilo ridge samples SU-22-64 [Moore and Clague, 1992; Yang et al., 1994] and D4C [Holcomb et al., 2000] are discussed in Appendix A3. See caption to Figure A2 for references to other analyses. Note that not all of these samples are tholeiitic based on the alkalinity  $\leq 0$  definition used here.

submersible collections and all but the very top of the upper several hundred meters of the subaerial Mauna Kea section sampled by the HSDP is consistent not only with the progressive changes in silica content in both suites, but also with the similar ranges in silica contents and other oxides in these two sample suites and, most importantly in the context of our data, with the absence in both data sets of bimodal distributions in silica contents (in contrast to the distribution characteristic of the deeper submarine section sampled by the HSDP2 core).

[129] The subaerial tholeiites from the literature (all of which are Hamakua series lavas) overlap in silica contents with the primitive low- $\text{SiO}_2$  HSDP2 glasses (although the Hamakua tholeiites extend to lower silica contents than the HSDP2 glasses; see Figures 9 and A2). The Hamakua tholeiites are

similar to the low- $\text{SiO}_2$  HSDP2 glasses in other respects as well, but they are nevertheless a distinctive compositional group. In particular, although the  $\text{FeO}^*$  and  $\text{Al}_2\text{O}_3$  contents of the subaerial Hamakua whole rocks and the low- $\text{SiO}_2$  HSDP2 glasses are not distinguishable, relative to HSDP2 glasses at the same  $\text{SiO}_2$  contents, the Hamakua subaerial whole rocks are generally higher in CaO,  $\text{K}_2\text{O}$ , and  $\text{TiO}_2$  and similar (to somewhat lower) in  $\text{Na}_2\text{O}$ , although the scatter is such that there is overlap between the Hamakua series and the low- $\text{SiO}_2$  HSDP2 glasses for most of these oxides. At silica contents lower than the low- $\text{SiO}_2$  HSDP2 glasses (i.e., below about 48%  $\text{SiO}_2$ ), the  $\text{K}_2\text{O}$  contents of the Hamakua tholeiites range from significantly higher to significantly lower than the low- $\text{SiO}_2$  glasses; the low- $\text{K}_2\text{O}$  samples have probably been influenced by alteration [Chen and Frey, 1985; Lipman et al., 1990; Garcia, 1996]. Note that although the  $\text{P}_2\text{O}_5$  contents of the Hamakua samples are systematically higher than those of the HSDP2 glasses, they are comparable to those of the HSDP2 whole rocks, suggesting as pointed out previously that the microprobe analyses of the glasses are systematically offset relative to the whole rock analyses.

[130] Ten submarine Mauna Kea glasses from the literature have  $<50\%$   $\text{SiO}_2$  (see Figures 10a and A3); seven of these samples were recovered from relatively shallow depths (835–1160 mbsl) off the west coast of Hawaii [Moore and Clague, 1992]. Although only one such sample (#22-2) is shown in Figure A2 because the rest have  $<6.5\%$  MgO, these samples cannot be distinguished from either the low- $\text{SiO}_2$  HSDP2 glasses or the Hamakua tholeiites by any oxides. However, the CaO contents of these glasses (including #22-2, shown in Figure A2) are lower than is typical for the Hamakua samples; the CaO contents of these glasses correspond well to the low- $\text{SiO}_2$  HSDP2 submarine glasses and to the low- $\text{SiO}_2$  tholeiites found in the subaerial part of the HSDP2 section. As pointed out above, the recovery of these low- $\text{SiO}_2$  submarine glasses from relatively shallow water depths suggests that they come from near the top of the Mauna Kea section and would thus be consistent with their association with the low- $\text{SiO}_2$  tholeiites from the subaerial part of the HSDP2 core and/or the Hamakua series tholeiites. This is also the case for one alkalic glass (sample D4C with 46.8%  $\text{SiO}_2$  from Holcomb et al. [2000]; the analysis was included in a personal communication from P. Reiners) from 1100 mbsl on the Hilo

ridge (Figure A3); this sample is not shown in Figure A2 because of its low MgO content (4.7% MgO), but its alkalic nature and shallow occurrence are consistent with its being stratigraphically equivalent to post-shield Mauna Kea lavas. Note that this glass is distinguished from other low-SiO<sub>2</sub> samples discussed here by its elevated FeO\*, K<sub>2</sub>O, and TiO<sub>2</sub> contents and its low Al<sub>2</sub>O<sub>3</sub> content.

[131] Two glasses dredged from 3285 mbsl on the Hilo ridge are low in SiO<sub>2</sub> (49.4–49.5% SiO<sub>2</sub>) yet come from much deeper than other low-SiO<sub>2</sub> glasses from the Hilo ridge. Both glasses are from SU-22-64 [Moore and Clague, 1992]; they are shown in Figure A3 but not Figure A2 because they have <6.5% MgO. Yang *et al.* [1994] emphasized the anomalous nature of SU-22-64 relative to all other submarine Mauna Kea rocks and its compositional similarities to tholeiites from the subaerial Hamakua series. However, the greater depth of this sample may suggest it is older than the more abundant, shallower low-SiO<sub>2</sub> submarine Mauna Kea samples from off the west coast of Hawaii and the Hilo ridge, and thus this sample may correspond to the low-SiO<sub>2</sub> submarine magmas of the HSDP2 core (i.e., rather than to the low-SiO<sub>2</sub> magmas from the end of shield building). This sample has lower Zr/Nb, higher <sup>87</sup>Sr/<sup>86</sup>Sr, and lower <sup>143</sup>Nd/<sup>144</sup>Nd than the more abundant high-SiO<sub>2</sub> Hilo ridge samples [Yang *et al.*, 1994], characteristics shared by the submarine HSDP2 low-SiO<sub>2</sub> magmas (Figure 7). The only clear distinction between SU-22-64 and the low-SiO<sub>2</sub> submarine HSDP2 magmas is in Pb isotopes; i.e., <sup>206</sup>Pb/<sup>204</sup>Pb in SU-22-64 is higher than in other Hilo ridge samples [Yang *et al.*, 1994], whereas this ratio is low in submarine low-SiO<sub>2</sub> HSDP2 magmas relative to high-SiO<sub>2</sub> magmas (Figure 7). Despite this difference, SU-22-64 is the only Hilo ridge sample that might correspond to the abundant low-SiO<sub>2</sub> magma type of the HSDP2 core.

[132] These comparisons between the HSDP samples and Mauna Kea whole rocks and glasses from the literature illustrate the incomplete representation of the magmatic history of a Hawaiian volcano that can be obtained from its subaerial section and its submarine flanks. In particular, looking at Figures 9a and A2 one would have the impression from the subaerial whole rocks that Hamakua-like magmas dominate Mauna Kea tholeiites; however, such lavas are in fact unrepresentative of the high-SiO<sub>2</sub> magmas produced over much of the subaerial section and differ significantly from the submarine

part of the section that has so far been sampled in the HSDP2 core.

#### A4. Comparison of HSDP2 Glasses to Glasses and Whole Rocks From Other Hawaiian Volcanoes

[133] Our final comparison is between undegassed glasses with ≥7% MgO from the HSDP2 core and tholeiitic glasses and whole rocks from other Hawaiian volcanoes. The HSDP2 glass analyses are compared to tholeiitic glasses from the literature with similar MgO contents (Figure 11) and to tholeiitic whole rocks projected to 7% MgO (Figure 12). Glass data from the following volcanoes are shown: Haleakala, Hualalai, Kilauea, Koolau, Loihi, Mahukona, and Mauna Loa; all glasses plotted have 7–8% MgO. Whole rock data are shown for the following volcanoes: Haleakala, Hualalai, Kahoolawe, Kauai, Kilauea, Kohala, Koolau, Lanai, Loihi, Mahukona, Mauna Loa, Wainae, and West Maui. For the whole rocks, analyses of tholeiitic lavas for each volcano were fit to lines versus MgO for each oxide and each individual analysis was then projected on a line of this slope back to 7% MgO.

[134] The data arrays shown in Figures 11 and 12 show that despite overall similarities between Hawaiian volcanoes, there are few simple or universal trends among the tholeiites of these volcanoes. For example, as described in section 4.4, Loihi tholeiitic glasses have SiO<sub>2</sub> contents (and FeO\*, Na<sub>2</sub>O, and TiO<sub>2</sub> contents; Figure 11) that overlap precisely with those of the low-SiO<sub>2</sub> HSDP2 glasses, but they are distinctly lower in some oxides (Al<sub>2</sub>O<sub>3</sub>, H<sub>2</sub>O) and often somewhat higher in other components (CaO, K<sub>2</sub>O, P<sub>2</sub>O<sub>5</sub>, and S). These differences are also observed in the projected whole rock compositions, although with considerably more scatter (Figure 12). Likewise, Kilauea glasses are mostly at the low end of the range of silica contents of the high-SiO<sub>2</sub> HSDP2 glasses, and in many respects they are the closest match among lavas from other volcanoes to the high-SiO<sub>2</sub> group of HSDP2 glasses. However, K<sub>2</sub>O and P<sub>2</sub>O<sub>5</sub> contents of Kilauea glasses tend to be higher than those of either HSDP2 group; the elevations in K<sub>2</sub>O and P<sub>2</sub>O<sub>5</sub> (and TiO<sub>2</sub>) are particularly apparent in Kilauea whole rocks.

[135] Mauna Loa whole rocks and glasses (which are similar to most of the Hualalai samples) have silica contents overlapping the high end of the range of high-SiO<sub>2</sub> HSDP2 glasses, but there is not a monotonic sequence from low-SiO<sub>2</sub>

HSDP2 → high-SiO<sub>2</sub> HSDP2 → Mauna Loa/Hualalai for most oxides. For example, although the Al<sub>2</sub>O<sub>3</sub> contents of the high-SiO<sub>2</sub> HSDP2 glasses are lower than those of the low-SiO<sub>2</sub> samples, glasses from Mauna Loa and Hualalai are as high in Al<sub>2</sub>O<sub>3</sub> as the low-SiO<sub>2</sub> HSDP2 samples rather than lower as would be expected if they continued the trend with SiO<sub>2</sub> defined by the two groups of HSDP2 glasses. Similarly, Mauna Loa and Hualalai samples would be expected to have lower Na<sub>2</sub>O contents if they continued the trend defined by the low- to high-SiO<sub>2</sub> HSDP glasses, but their Na<sub>2</sub>O contents are indistinguishable from the high-SiO<sub>2</sub> HSDP2 group.

[136] *Hauri* [1996] noted that FeO content decreases continuously with increasing SiO<sub>2</sub> content in Hawaiian whole rocks corrected to a bulk Mg/(Mg + Fe<sup>+2</sup>) value of 0.77 (via olivine addition or subtraction), with Loihi defining the low-SiO<sub>2</sub> end of the trend and Koolau defining the high-SiO<sub>2</sub> end. There is indeed a well-defined negatively sloped trend in FeO\*-SiO<sub>2</sub> space on which the HSDP2 glasses, other Hawaiian glasses, and Hawaiian whole rocks all fall (Figures 11c and 12c).

[137] There is also a negatively sloped trend in CaO-SiO<sub>2</sub> among most Hawaiian tholeiites (Figures 11b and 12b). However, although the high-SiO<sub>2</sub> HSDP glasses fall on the CaO-SiO<sub>2</sub> trend defined by other Hawaiian tholeiites, most low-SiO<sub>2</sub> HSDP glasses have CaO contents essentially identical to the high-SiO<sub>2</sub> group and thus fall off this trend (Figures 11b and 12b); in other words, the HSDP2 glasses with <50% SiO<sub>2</sub> define a positively sloped “dogleg” off the negatively sloped CaO-SiO<sub>2</sub> trend defined by samples from other Hawaiian volcanoes and HSDP2 glasses with >50% SiO<sub>2</sub>. Note, however, that the glasses with elevated CaO and Al<sub>2</sub>O<sub>3</sub> contents (see section 4.6) do fall on the overall trend of Hawaiian lavas. Low-SiO<sub>2</sub> glasses and whole rocks from Haleakala and Mahukona and whole rocks from West Maui fall on the same dogleg in CaO-SiO<sub>2</sub> space, and the alkalic subaerial lavas from the HSDP2 core and from the Hamakua volcanics (not shown) extend this trend to even lower CaO and SiO<sub>2</sub> contents. In contrast, however, tholeiitic whole rocks and tholeiitic and alkalic (not shown) glasses from Loihi and alkalic glasses from the North Arch (not shown) do not deviate from the overall CaO-SiO<sub>2</sub> trend of Hawaiian lavas, and they overlap with each other (and with Hamakua tholeiites) at the low-silica

end of the trend (Figures 11, 12, and A2). Finally, we note that the low-SiO<sub>2</sub> HSDP2 glasses also define doglegs in SiO<sub>2</sub>-Al<sub>2</sub>O<sub>3</sub> and SiO<sub>2</sub>-TiO<sub>2</sub> space (i.e., they define positively sloped arrays at an angle to the overall negatively sloped trends of Hawaiian whole rocks and glasses, which include the high-SiO<sub>2</sub> HSDP2 glasses); no other Hawaiian glasses or whole rocks show such trends, even those that have positively sloped trends in CaO-SiO<sub>2</sub> space.

[138] There are also rough negative correlations in K<sub>2</sub>O, Na<sub>2</sub>O, and TiO<sub>2</sub> versus SiO<sub>2</sub> defined by most of the glass groups shown in Figure 11, although one or more volcanoes fall off each trend. The whole rock data shown in Figure 12 support the trend in TiO<sub>2</sub> defined by the glasses, but not those in Na<sub>2</sub>O and K<sub>2</sub>O. However, K<sub>2</sub>O and Na<sub>2</sub>O in Hawaiian whole rocks are susceptible to the effects of alteration [*Chen and Frey*, 1985; *Lipman et al.*, 1990; *Garcia*, 1996], and thus systematics in the glass data are probably more reliable. The deviation of the highest-SiO<sub>2</sub> Koolau samples from the overall negative trend in Na<sub>2</sub>O-SiO<sub>2</sub> space is significant. There are no simple trends in Al<sub>2</sub>O<sub>3</sub> or P<sub>2</sub>O<sub>5</sub> versus SiO<sub>2</sub> among Hawaiian tholeiitic glasses or whole rocks, although the low Al<sub>2</sub>O<sub>3</sub> contents of Loihi samples and high Al<sub>2</sub>O<sub>3</sub> contents of the highest-SiO<sub>2</sub> Koolau samples pointed out in section 4.4 are striking.

## A5. Petrogenesis of Hamakua Tholeiites

[139] *Yang et al.* [1996a], *Feigenson et al.* [2003], and *Huang and Frey* [2003] suggested that the alkaline and low-SiO<sub>2</sub> lavas from near the top of the Mauna Kea section can be understood as lower degree, higher pressure partial melts from sources similar (except in isotopic ratios) to those that produced the high-SiO<sub>2</sub> liquids from deeper in the subaerial and submarine parts of the section. Similarly, *Frey et al.* [1991] suggested an increase in the degree of partial melting in the sequence from subaerial Hamakua alkaline lavas, to subaerial Hamakua tholeiites, to the high-SiO<sub>2</sub> submarine lavas known at the time. The continuous, generally negatively sloped trends in all oxides other than CaO from subaerial alkalic lavas, through the Hamakua tholeiites, to the high-SiO<sub>2</sub> HSDP glasses and whole rocks (Figure A2) are consistent with this hypothesis. The sequence from low-CaO alkaline lavas (both from HSDP and Hamakua lavas), to high-CaO Hamakua tholeiites,

to low CaO, high-SiO<sub>2</sub> magmas is likewise consistent with such a trend provided the Hamakua tholeiites were generated roughly at the point of clinopyroxene exhaustion and the high-SiO<sub>2</sub> magmas equilibrated with harzburgitic residues. Moreover, alkaline HSDP lavas and Hamakua tholeiites are enriched in K<sub>2</sub>O, P<sub>2</sub>O<sub>5</sub>, TiO<sub>2</sub>, and Na<sub>2</sub>O relative to high-SiO<sub>2</sub> HSDP magmas roughly in the order of increasing compatibility. Previous efforts to explain the elevated CaO contents in Hamakua tholeiites relative to higher SiO<sub>2</sub> Mauna Kea lavas (which in other respects can be explained by lower degrees of melting than the high-SiO<sub>2</sub> submarine lavas) have appealed to higher CO<sub>2</sub> contents in their sources [Frey and Rhodes, 1993; Yang *et al.*, 1996a]. This may indeed be a factor, although it would be unnecessary if the last equilibration of the high-SiO<sub>2</sub> magmas was with harzburgitic rather than lherzolitic residua.

[140] An alternative to this view of the high-level alkaline magmas and Hamakua tholeiites as single stage melts produced by lower degrees of melting than the more abundant underlying high-SiO<sub>2</sub> magmas is that mantle-melt interaction (see section 5.3) is stronger and proceeds to shallower levels in the main shield-building phase of the volcano, but wanes with decreasing melt flux as the volcano moves off the hot spot. The trend from high-SiO<sub>2</sub> magmas to Hamakua tholeiites and alkaline lavas as volcanism winds down might thus reflect diminishment of or deepening of the effects of melt-mantle interactions with the end of shield-building, leading to progressively deeper, lower degree melts showing less of the SiO<sub>2</sub> enrichment characteristic of progressively shallower resorption of overlying lherzolites and harzburgites.

[141] We pointed out above (Appendix A3) that the Hamakua tholeiites and the low-SiO<sub>2</sub> HSDP2 submarine glasses are similar in several respects. The relatively small chemical differences between these two low-SiO<sub>2</sub> tholeiitic series could be largely accounted for by the Hamakua series representing lower degrees of lherzolite melting at similar to higher mean pressures of melting than the low-SiO<sub>2</sub> HSDP2 magmas. This could explain the similar to slightly higher Al<sub>2</sub>O<sub>3</sub>, FeO\*, K<sub>2</sub>O, P<sub>2</sub>O<sub>5</sub>, and TiO<sub>2</sub> of the Hamakua lavas relative to the low-SiO<sub>2</sub> HSDP2 magma series. The greater enrichments in Hamakua lavas relative to the low-SiO<sub>2</sub> HSDP2 magmas in K<sub>2</sub>O and P<sub>2</sub>O<sub>5</sub> relative to TiO<sub>2</sub> (Figure A2) are also consistent with the higher compatibility of TiO<sub>2</sub>. However, the similar to lower Na<sub>2</sub>O contents and generally higher CaO

contents of the Hamakua tholeiites can not be simply explained in this way.

## A6. Multiple Volcanoes?

[142] We consider here briefly the possibility that the contrasting high- and low-SiO<sub>2</sub> magmas encountered in the HSDP2 core represent not the variable output of the Mauna Kea volcano, but rather the alternation of a relatively homogeneous, high-SiO<sub>2</sub> output of Mauna Kea and the low-SiO<sub>2</sub> output of another volcano. This possibility was not considered likely in the design of the HSDP project because it is difficult to envision how submarine lavas from Kohala, Hualalai, or Mauna Loa, the other volcanoes known to be active over the time period represented in the upper part of the submarine section [Moore and Clague, 1992; Holcomb *et al.*, 2000; Baker *et al.*, manuscript in preparation, 2004b] could reach the drill site. In the cases of Kohala and Hualalai, the Mauna Kea edifice was expected on the basis of simple geometric considerations to have blocked access of their lavas to the drill site. The same is true for Mauna Loa lavas, which have only reached the drill site at a high level on the flank of Mauna Kea in the past ~100 Ka and largely because of the influence of Kilauea [Baker *et al.*, manuscript in preparation, 2004b]. Nevertheless, the histories of Hawaiian volcanoes and their interactions are not sufficiently well known to rule out more complex volcanic geometries than have been envisioned or the possibility of entirely unknown volcanic systems on the island of Hawaii. The suggestion of Holcomb *et al.* [2000] that the Hilo ridge at depths below 1100 mbsl is part of Kohala rather than Mauna Kea emphasizes the possibility of unanticipated volcanic geometries.

[143] The first possibility we consider is that the high-SiO<sub>2</sub> pillows and hyaloclastites in zone 4 are Mauna Kea magmas, but that these are overlain by the low-SiO<sub>2</sub> magmas of zone 3, which are nearly all pillows from another volcano; the dominantly high-SiO<sub>2</sub> magmas of zones 1 and 2 would again represent Mauna Kea lavas. Although difficult to test, this hypothesis has several interesting features: (1) The abrupt transitions from high- to low-SiO<sub>2</sub> magmas seen in the HSDP core would be natural consequences of alternating outputs of different volcanoes. (2) The shift toward lower degrees of melting and transitional lavas in the upper ~50 m of zone 3 could be explained by the end of shield building of the unknown volcano. Moreover, as

discussed sections 6 and 8.5), a discontinuous shift to high-SiO<sub>2</sub> magmas above a transition from tholeiitic to alkaline lavas is precisely the signature of the unconformity between Mauna Kea and Mauna Loa lavas encountered near the top of HSDP core (i.e., at ~245 mbsl), and it would be reasonable to interpret the similar pattern at the top of zone 3 in similar terms as an unconformity between lavas from different volcanoes. (3) Most of the intrusive units occur below zone 3 and most of these are low-SiO<sub>2</sub> magmas. This would be consistent with the invasion of the Mauna Kea volcanic edifice by magmas from another source. (4) The decreasing abundance of low-SiO<sub>2</sub> magmas with time above zone 3 would be consistent with a declining flux from the unknown volcano above the excursion at the top of zone 3 that signals the end of shield building, although the tholeiitic rather than alkaline character of low-SiO<sub>2</sub> magmas above zone 3 is inconsistent with this. (5) The gradual transition from high- to low-SiO<sub>2</sub> magmas in zone 2 requires in the context of the two-volcano hypothesis that magmas from both volcanoes can pass through the same magma chamber. “Capture” of Mauna Loa magmas by Kilauea has been inferred [Rhodes *et al.*, 1989], so although this suggestion may seem strange, it would not be unprecedented.

[144] A second possibility is that some lavas sampled deep in the HSDP2 core are from Kohala rather than from Mauna Kea. *Holcomb et al.* [2000] proposed that the Hilo ridge at water depths >1100 mbsl is not a rift zone of Mauna Kea, as its geometry has suggested, but rather an elongated rift zone of Kohala. This proposal was based originally on the correlation of the terrace at 1100 mbsl with a Kohala terrace, but *Holcomb et al.* [2000] showed that the isotopic characteristics of the lavas from this terrace are similar to known Kohala lavas. Moreover, as reviewed by *Smith et al.* [2002], recent gravity data suggest that the Hilo ridge and Mauna Kea may not be related, and magnetic data suggest that the deeper parts of the Hilo ridge are reversely magnetized and therefore older than 780 Ka, consistent with Kohala but not with Mauna Kea.

[145] Since the HSDP2 drill site is only ~16 km from Mauna Kea’s east rift, if the Hilo ridge is in fact composed of Kohala lavas below a particular depth, then we would expect to encounter Kohala lavas at depth in the HSDP cores as well. The expected depth of this transition can be estimated

by first projecting uphill along the trace of the Hilo ridge through the 1100 m terrace that *Holcomb et al.* [2000] suggest represents the ancient shoreline and surface of Kohala, and then passing a line perpendicular to the Hilo ridge trace downhill to the drill site. Assuming subaerial slopes of ~5° parallel to the Hilo ridge and ~6° perpendicular to the ridge and a submarine slope of ~12° perpendicular to the ridge, the depth of the ancient Kohala surface at the location of the HSDP2 drill hole can be estimated to be ~3400 mbsl.

[146] Although this calculation is at best a rough estimate, it suggests a position of the putative transition to Kohala lavas deeper than the maximum depth of the HSDP2 core. We nevertheless consider the possibility that some of the deepest HSDP2 samples are from Kohala. We first reemphasize that most of the Hilo ridge submarine whole rocks and glasses from deeper than the supposed Kohala transition at 1100 mbsl on the ridge correspond closely to the high-SiO<sub>2</sub> glasses and whole rocks that occur in the HSDP cores (see Figures 10a, A2, and A3). Since the shallow high-SiO<sub>2</sub> HSDP glasses and whole rocks (i.e., from zone 1 or the lower parts of the subaerial section) are surely Mauna Kea lavas, this close correspondence is an argument against the deeper parts of the Hilo ridge being Kohala. Moreover, the high-SiO<sub>2</sub> HSDP2 glasses from zone 4 are so similar to the Mauna Kea glasses from zone 1 (Figure 6), there is no basis for suggesting that the deeper HSDP2 glasses are not from Mauna Kea as well. Although one might argue that the low-SiO<sub>2</sub> magmas of zones 3 and 4 could be identified with Kohala, if so, the rarity of such magmas deep on the Hilo ridge would argue against the hypothesis of *Holcomb et al.* [2000] that the deep Hilo ridge surface is covered by Kohala lavas. *Rhodes and Vollinger* [2004] also briefly addressed the possibility that the low-SiO<sub>2</sub> magmas were from Kohala and noted the lack of chemical correspondence between the low-SiO<sub>2</sub> magma type and known Kohala lavas. Finally, as shown in Figure A4, the isotopic characteristics of HSDP samples are unambiguously distinct from Kohala tholeiites and overlap with subaerial Mauna Kea lavas. Since the correspondence of samples from the Hilo ridge to the isotopic field for subaerial Kohala tholeiites was considered to be the key test for these dredged samples having come from Kohala rather than Mauna Kea, we conclude that the HSDP samples fail this test. Although the HSDP core may ultimately encounter Kohala

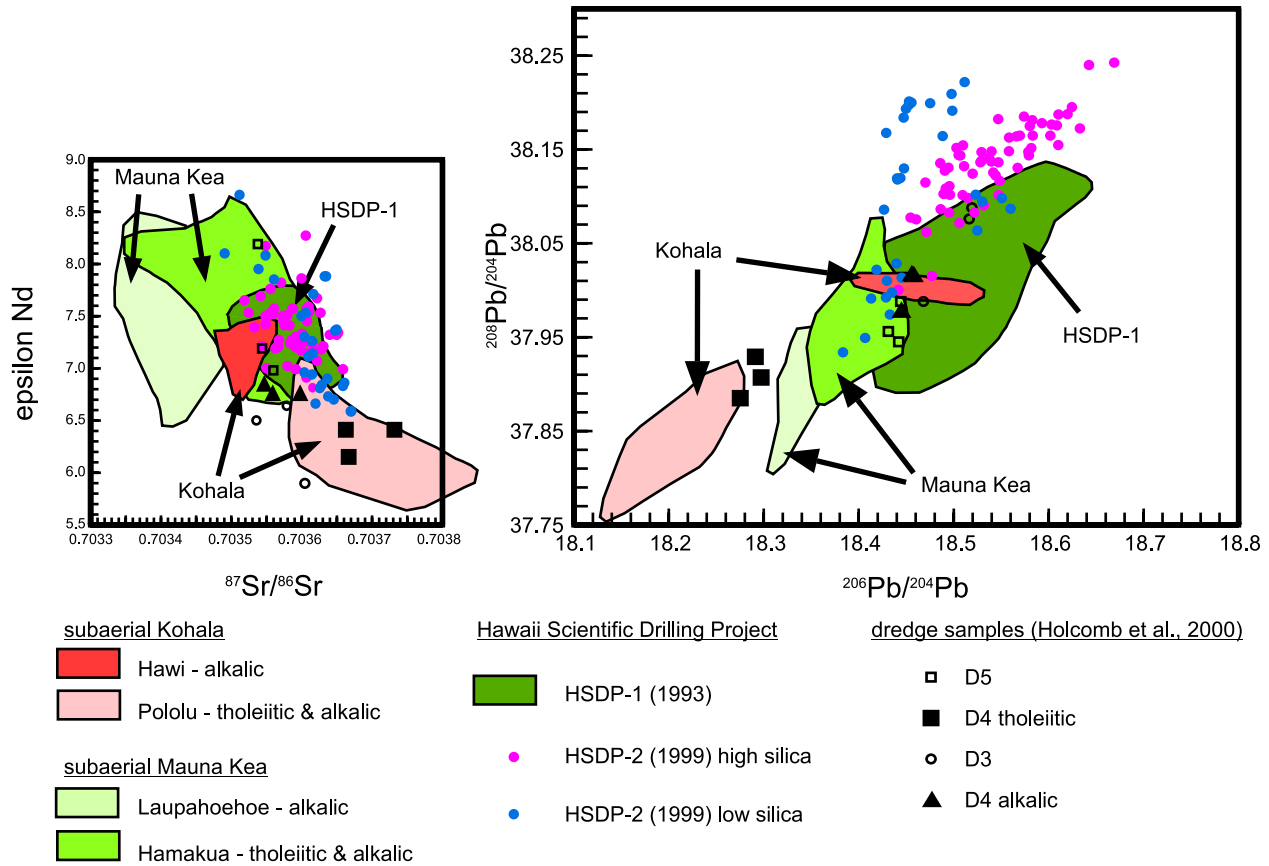


**Figure A4.** Pb, Nd, and Sr isotopic ratios of HSDP samples compared with previous studies of Mauna Kea and Kohala lavas. Note that the HSDP lavas are all distinct from the field for tholeiitic samples from Kohala. The correspondence of the D4 dredges with this Kohala field was used by *Holcomb et al.* [2000] to argue that the deeper parts of the Hilo ridge were from Kohala, not Mauna Kea. Independent of the validity of this argument in the case of the Hilo ridge samples, these data are not supportive of the deeper parts of the HSDP2 core having encountered Kohala lavas.

lavas, it appears not to have done so at levels shallower than 3098 mbsl.

[147] In conclusion, we emphasize how difficult it will be to distinguish between the possibility that HSDP2 core sampled the output of two distinct volcanoes or the alternative that the Mauna Kea volcano has sampled heterogeneous, rapidly changing magmas from the upwelling mantle plume. At this point, all we can do is to keep both possibilities open, while noting that the multiple volcano hypothesis is not being actively pursued in the interpretations of the HSDP chemical and isotopic results.

## Acknowledgments

[148] We thank the entire Hawaii Scientific Drilling Project team for their assistance, but in particular Don DePaolo and Don Thomas for their roles in the leadership of the project. This work was supported by NSF grants EAR-9528594

(Caltech) and EAR-9528534 (University of Hawaii) and by The International Continental Scientific Drilling Program (ICDP). Caltech Division of Geological and Planetary Science contribution number 8937. University of Hawaii SOEST contribution number 6353.

## References

- Albarède, F. (1993), Residence time analysis of geochemical fluctuations in volcanic series, *Geochim. Cosmochim. Acta*, 57, 615–621.
- Albarède, F. (1996), High-resolution geochemical stratigraphy of Mauna Kea flows from the Hawaii Scientific Drilling Project core, *J. Geophys. Res.*, 101, 11,841–11,853.
- Anderson, A. T., and T. L. Wright (1972), Phenocrysts and glass inclusions and their bearing on oxidation and mixing of basaltic magmas, Kilauea volcano, Hawaii, *Am. Mineral.*, 57, 188–216.
- Armstrong, J. T. (1988), Quantitative analysis of silicate and oxide minerals: Comparison of Monte Carlo, ZAF and  $\phi(\rho z)$  procedures, in *Microbeam Analysis—1988*, edited by D. E. Newbury, pp. 239–246, San Francisco Press, San Francisco, Calif.

- Asimow, P. D. (2002), Steady-state mantle-melt interactions in one dimension: II. Thermal interactions and irreversible terms, *J. Petrol.*, *43*, 1707–1724.
- Asimow, P. D., and E. M. Stolper (1999), Steady-state mantle-melt interactions in one dimension: I. Equilibrium transport and melt focusing, *J. Petrol.*, *40*, 475–494.
- Baker, M. B., S. Alves, and E. M. Stolper (1996), Petrography and petrology of the Hawaii Scientific Drilling Project lavas: Inferences from olivine phenocryst abundances and compositions, *J. Geophys. Res.*, *101*, 11,715–11,727.
- Basaltic Volcanism Study Project (1981), *Basaltic Volcanism on the Terrestrial Planets*, 1286 pp., Pergamon, New York.
- Blichert-Toft, J., D. Weis, C. Maerschalk, A. Agranier, and F. Albarède (2003), Hawaiian hot spot dynamics as inferred from the Hf and Pb isotope evolution of Mauna Kea volcano, *Geochem. Geophys. Geosyst.*, *4*(2), 8704, doi:10.1029/2002GC000340.
- Bryce, J., and D. J. DePaolo (2000), Sr and Nd variations in Mauna Kea lavas: Preliminary results from analyses from the 1999 Hawaii Scientific Drilling Project, *Eos Trans. AGU*, *81*(48), Fall Meet. Suppl., Abstract V12C-01.
- Budahn, J. R., and R. A. Schmitt (1985), Petrogenetic modeling of Hawaiian tholeiitic basalts: A geochemical approach, *Geochim. Cosmochim. Acta*, *49*, 67–87.
- Burkhard, D. J. M. (2001), Crystallization and oxidation of Kilauea basalt glass: Processes during reheating experiments, *J. Petrol.*, *42*, 507–527.
- Byers, C., M. Garcia, and D. Muenow (1985), Volatiles in pillow rim glasses from Loihi and Kilauea volcanoes, *Geochim. Cosmochim. Acta*, *49*, 1887–1896.
- Carmichael, I. S. E., F. J. Turner, and F. Verhoogen (1974), *Igneous Petrology*, 739 pp., McGraw-Hill, New York.
- Chen, C. Y., and F. A. Frey (1985), Trace-element and isotopic geochemistry of lavas from Haleakala volcano, East Maui, Hawaii: Implications for the origin of Hawaiian basalts, *J. Geophys. Res.*, *90*, 8743–8768.
- Clague, D. A. (1987), Hawaiian xenolith populations, magma supply rates, and development of magma chambers, *Bull. Volcanol.*, *49*, 577–587.
- Clague, D. A., and J. G. Moore (1991), Geology and petrology of Mahukona volcano, Hawaii, *Bull. Volcanol.*, *53*, 159–172.
- Clague, D. A., R. T. Holcomb, J. M. Sinton, R. S. Detrick, and M. E. Torresan (1990), Pliocene and Pleistocene alkalic flood basalts on the seafloor north of the Hawaiian Islands, *Earth Planet. Sci. Lett.*, *98*, 175–191.
- Clague, D. A., W. S. Weber, and J. E. Dixon (1991), Picritic glasses from Hawaii, *Nature*, *353*, 553–556.
- Clague, D. A., J. G. Moore, J. E. Dixon, and W. B. Friesen (1995), Petrology of submarine lavas from Kilauea's Puna ridge, Hawaii, *J. Petrol.*, *36*, 299–349.
- Clague, D. A., A. S. Davis, J. L. Bischoff, J. E. Dixon, and R. Geyer (2000), Lava bubble-wall fragments formed by submarine hydrovolcanic: Explosions on Loihi seamount and Kilauea volcano, *Bull. Volcanol.*, *61*, 437–449.
- Clague, D. A., J. G. Moore, and A. S. Davis (2002), Volcanic breccia and hyaloclastite in blocks from the Nuanu and Wailau landslides, Hawaii, in *Hawaiian Volcanoes: Deep Underwater Perspectives*, edited by E. Takahashi et al., pp. 279–296, AGU, Washington, D. C.
- Davis, M. G., M. O. Garcia, and P. Wallace (2003), Volatiles in glasses from Mauna Loa volcano, Hawaii: Implications for magma degassing and contamination, and growth of Hawaiian volcanoes, *Contrib. Mineral.*, 570–591.
- DePaolo, D. J., and E. M. Stolper (1996), Models of Hawaiian volcano growth and plume structure: Implications of results from the Hawaii Scientific Drilling Project, *J. Geophys. Res.*, *101*, 11,643–11,654.
- DePaolo, D. J., E. Stolper, and D. Thomas (1996), The Hawaii Scientific Drilling Project: Summary of preliminary results, *GSA Today*, *6*, 1–8.
- DePaolo, D. J., J. G. Bryce, A. Dodson, D. L. Shuster, and B. M. Kennedy (2001), Isotopic evolution of Mauna Loa and the chemical structure of the Hawaiian plume, *Geochem. Geophys. Geosyst.*, *2*, Paper number 2000GC000139.
- Dixon, J. E., and D. A. Clague (2001), Volatiles in basaltic glasses from Loihi seamount, Hawaii: Evidence for a relatively dry plume component, *J. Petrol.*, *42*, 627–654.
- Dixon, J. E., and E. M. Stolper (1995), An experimental study of water and carbon dioxide solubilities in mid-ocean ridge basaltic liquids, Part II: Applications to degassing, *J. Petrol.*, *36*, 1633–1646.
- Dixon, J. E., D. A. Clague, and E. M. Stolper (1991), Degassing history of water, sulfur, and carbon in submarine lavas from Kilauea volcano, Hawaii, *J. Geol.*, *99*, 371–394.
- Dzurisin, D., J. P. Lockwood, T. J. Casadevall, and M. Rubin (1995), The Uwekahuna ash member of the Puna Basalt: Product of violent phreatomagmatic eruptions at Kilauea volcano, Hawaii, between 2800 and 2100 <sup>14</sup>C years ago, *J. Volcanol. Geotherm. Res.*, *66*, 163–184.
- Eggs, S. M. (1992), Petrogenesis of Hawaiian tholeiites: 2. Aspects of dynamic melt segregation, *Contrib. Mineral. Petrol.*, *110*, 398–410.
- Eisele, J., W. Abouchami, S. J. G. Galer, and A. W. Hofmann (2003), The 320 kyr Pb isotope evolution of Mauna Kea lavas recorded in the HSDP-2 drill core, *Geochem. Geophys. Geosyst.*, *4*(5), 8710, doi:10.1029/2002GC000339.
- Falloon, T. J., and D. H. Green (1988), Anhydrous partial melting of peridotite from 8 to 35 kb and the petrogenesis of MORB, *J. Petrol.*, special lithosphere issue, 379–414.
- Feigenson, M. D., L. L. Bolge, M. J. Carr, and C. T. Herzberg (2003), REE inverse modeling of HSDP2 basalts: Evidence for multiple sources in the Hawaiian plume, *Geochem. Geophys. Geosyst.*, *4*(2), 8706, doi:10.1029/2001GC000271.
- Frey, F. A., and J. M. Rhodes (1993), Intershield geochemical differences among Hawaiian volcanoes: Implications for source compositions, melting process and magma ascent paths, *Philos. Trans. R. Soc. London, Ser. A*, *342*, 121–136.
- Frey, F. A., W. S. Wise, M. O. Garcia, H. West, S. T. Kwon, and A. Kennedy (1990), Evolution of Mauna Kea volcano, Hawaii: Petrologic and geochemical constraints on post-shield volcanism, *J. Geophys. Res.*, *95*, 1271–1300.
- Frey, F. A., M. O. Garcia, W. S. Wise, A. Kennedy, P. Gurrriet, and F. Albarède (1991), The evolution of Mauna Kea volcano, Hawaii: Petrogenesis of tholeiitic and alkalic basalts, *J. Geophys. Res.*, *96*, 14,347–14,375.
- Frey, F. A., M. O. Garcia, and M. F. Roden (1994), Geochemical characteristics of Koolau volcano—Implications of inter-shield geochemical differences among Hawaiian volcanoes, *Geochim. Cosmochim. Acta*, *58*, 1441–1462.
- Garcia, M. (1996), Petrography and olivine and glass chemistry of lavas from the Hawaii Scientific Drilling Project, *J. Geophys. Res.*, *101*, 11,701–11,713.
- Garcia, M. O., and M. G. Davis (2001), Submarine growth and internal structure of ocean island volcanoes based on submarine observations of Mauna Loa volcano, Hawaii, *Geology*, *29*, 163–166.
- Garcia, M. O., D. Muenow, K. E. Aggrey, and J. R. O'Neil (1989), Major element, volatile, and stable isotopic geochemistry of Hawaiian submarine tholeiitic glasses, *J. Geophys. Res.*, *94*, 10,525–10,538.

- Garcia, M. O., M. D. Kurz, and D. W. Muenow (1990), Mahukona—The missing Hawaiian volcano, *Geology*, *18*, 1111–1114.
- Garcia, M. O., B. A. Jorgenson, J. J. Mahoney, E. Ito, and A. J. Irving (1993), An evaluation of temporal geochemical evolution of Loihi summit lavas: Results from Alvin submersible dives, *J. Geophys. Res.*, *98*, 537–550.
- Garcia, M. O., D. J. P. Foss, H. B. West, and J. J. Mahoney (1995a), Geochemical and isotopic evolution of Loihi volcano, Hawaii, *J. Petrol.*, *36*, 1647–1674.
- Garcia, M. O., T. P. Hulsebosch, and J. M. Rhodes (1995b), Olivine-rich submarine basalts from the southwest rift zone of Mauna Loa volcano: Implications for magmatic processes and geochemical evolution, in *Mauna Loa Revealed: Structure, Composition, History, and Hazards*, edited by J. M. Rhodes and J. P. Lockwood, pp. 219–239, AGU, Washington, D. C.
- Garcia, M. O., K. H. Rubin, M. D. Norman, J. M. Rhodes, D. W. Graham, D. W. Muenow, and K. Spencer (1998), Petrology and geochronology of basalt breccia from the 1996 earthquake swarm of Loihi seamount, Hawaii: Magmatic history of its 1996 eruption, *Bull. Volcanol.*, *59*, 577–592.
- Grove, T. L., and T. C. Juster (1989), Experimental investigations of low-Ca pyroxene stability and olivine-pyroxene-liquid equilibria at 1-atm in natural basaltic and andesitic liquids, *Contrib. Mineral. Petrol.*, *103*, 287–305.
- Haskins, E. H., and M. O. Garcia (2004), Scientific drilling reveals geochemical heterogeneity within the Koolau shield, Hawaii, *Contrib. Mineral. Petrol.*, *147*, 162–188.
- Hauri, E. (1996), Major-element variability in the Hawaiian mantle plume, *Nature*, *382*, 415–419.
- Hauri, E. H., J. A. Whitehead, and S. R. Hart (1994), Fluid dynamic and geochemical aspects of entrainment in mantle plumes, *J. Geophys. Res.*, *99*, 24,275–24,300.
- Hauri, E. H., J. C. Lassiter, and D. J. DePaolo (1996), Osmium isotope systematics of drilled lavas from Mauna Loa, Hawaii, *J. Geophys. Res.*, *101*, 11,793–11,806.
- Hawaii Scientific Drilling Project (2000), *Core Logs and Summarizing Data*, edited by C. Seaman, M. O. Garcia, and E. Stolper, Calif. Inst. of Technol., Pasadena.
- Hawaii Scientific Drilling Project (2001), Deep drilling into a Hawaiian volcano, *Eos Trans. AGU*, *82*(13), 149, 154–155.
- Hawkins, J., and J. Melchior (1983), Petrology of basalts from Loihi seamount, Hawaii, *Earth Planet. Sci. Lett.*, *66*, 356–368.
- Helz, R. T., N. G. Banks, C. Heliker, C. A. Neal, and E. W. Wolfe (1995), Comparative geothermometry of recent Hawaiian eruptions, *J. Geophys. Res.*, *100*, 17,637–17,657.
- Hirose, K., and I. Kushiro (1993), Partial melting of dry peridotites at high pressures: Determination of compositions of melts segregated from peridotite using aggregates of diamond, *Earth Planet. Sci. Lett.*, *114*, 477–489.
- Hirschmann, M. M., and E. M. Stolper (1996), A possible role for garnet pyroxenite in the origin of the “garnet signature” in MORB, *Contrib. Mineral. Petrol.*, *124*, 185–208.
- Hirschmann, M. M., T. Kogiso, M. B. Baker, and E. M. Stolper (2003), Alkalic magmas generated by partial melting of garnet pyroxenite, *Geology*, *31*, 481–484.
- Hofmann, A. W., and K. P. Jochum (1996), Source characteristics derived from very incompatible trace elements in Mauna Loa and Mauna Kea basalts, Hawaii Scientific Drilling Project, *J. Geophys. Res.*, *101*, 11,831–11,839.
- Hofmann, A. W., M. D. Feigenson, and I. Raczek (1984), Case studies on the origin of basalt: III. Petrogenesis of the Mauna Ulu eruption, Kilauea, 1969–1971, *Contrib. Mineral. Petrol.*, *88*, 24–35.
- Holcomb, R. T., B. K. Nelson, P. W. Reiners, and N. L. Sawyer (2000), Overlapping volcanoes: The origin of Hilo ridge, Hawaii, *Geology*, *28*, 547–550.
- Honda, M., I. McDougall, D. B. Patterson, A. Doulgeris, and D. A. Clague (1993), Noble-gases in submarine pillow basalt glasses from Loihi and Kilauea, Hawaii—A solar component in the Earth, *Geochim. Cosmochim. Acta*, *57*, 859–874.
- Huang, S., and F. A. Frey (2003), Trace element abundances of Mauna Kea basalt from phase 2 of the Hawaii Scientific Drilling Project: Petrogenetic implications of correlations with major element content and isotopic ratios, *Geochem. Geophys. Geosyst.*, *4*(6), 8711, doi:10.1029/2002GC000322.
- Jackson, M. C., F. A. Frey, M. O. Garcia, and R. A. Wilmoth (1999), Geology and geochemistry of basaltic lava flows and dikes from the trans-Koolau tunnel, O’ahu, Hawaii’i, *Bull. Volcanol.*, *60*, 381–401.
- Jambon, A., and J. L. Zimmermann (1990), Water in oceanic basalts—Evidence for dehydration of recycled crust, *Earth Planet. Sci. Lett.*, *101*, 323–331.
- Jarosewich, E., J. A. Nelen, and J. A. Norberg (1979), Electron microprobe reference samples for mineral analyses, *Smithson. Contrib. Earth Sci.*, *22*, 68–72.
- Johnson, K. T. M., J. R. Reynolds, D. Vonderhaar, D. K. Smith, and L. S. L. Kong (2002), Petrological systematics of submarine basalt glasses from the Puna ridge, Hawaii’i: Implications for rift zone plumbing and magmatic processes, in *Hawaiian Volcanoes: Deep Underwater Perspectives*, edited by E. Takahashi et al., pp. 143–159, AGU, Washington, D. C.
- Kelemen, P. B. (1986), Assimilation of ultramafic rock in subduction-related magmatic arcs, *J. Geol.*, *94*, 829–843.
- Kelemen, P. B. (1990), Reaction between ultramafic rock and fractionating basaltic magma. 1. Phase-relations, the origin of calc-alkaline magma series, and the formation of discordant dunite, *J. Petrol.*, *31*, 51–98.
- Kelemen, P. B., K. T. M. Johnson, R. J. Kinzler, and A. J. Irving (1990), High-field-strength element depletions in arc basalts due to mantle-magma interaction, *Nature*, *345*, 521–524.
- Kelemen, P. B., N. Shimizu, and V. J. M. Salters (1995), Extraction of mid-ocean-ridge basalt from the upwelling mantle by focused flow of melt in dunite channels, *Nature*, *375*, 747–753.
- Kent, A. J. R., D. A. Clague, M. Honda, E. M. Stolper, I. D. Hutcheon, and M. D. Norman (1999), Widespread assimilation of a seawater-derived component at Loihi seamount, Hawaii, *Geochim. Cosmochim. Acta*, *63*, 2749–2761.
- Kinzler, R. (1997), Melting of mantle peridotite at pressures approaching the spinel to garnet transition: Application to mid-ocean ridge basalt petrogenesis, *J. Geophys. Res.*, *102*, 853–874.
- Kinzler, R. J., and T. L. Grove (1985), Crystallization and differentiation of Archean komatiite lavas from northwest Ontario: Phase equilibria and kinetic studies, *Am. Mineral.*, *70*, 40–51.
- Klein, F. W., R. Y. Koyanagi, J. S. Nakata, and W. R. Tanigawa (1987), The seismicity of Kilauea’s magma system, *U.S. Geol. Surv. Prof. Pap.*, *1350*, 1019–1185.
- Kogiso, T., and M. M. Hirschmann (2001), Experimental study of clinopyroxenite partial melting and the origin of ultra-calcic melt inclusions, *Contrib. Mineral. Petrol.*, *142*, 347–360.
- Kress, V. C., and I. S. E. Carmichael (1991), The compressibility of silicate liquids containing Fe<sub>2</sub>O<sub>3</sub> and the effect of

- composition, temperature, oxygen fugacity and pressure on their redox states, *Contrib. Mineral. Petrol.*, *108*, 82–92.
- Kurz, M. D., and D. P. Kammer (1991), Isotopic evolution of Mauna Loa volcano, *Earth Planet. Sci. Lett.*, *103*, 257–269.
- Kurz, M. D., T. C. Kenna, D. P. Kammer, J. M. Rhodes, and M. O. Garcia (1995), Isotopic evolution of Mauna Loa volcano: A view from the submarine southwest rift zone, in *Mauna Loa Revealed: Structure, Composition, History, and Hazards*, edited by J. M. Rhodes and J. P. Lockwood, pp. 289–306, AGU, Washington, D. C.
- Kurz, M. D., T. C. Kenna, J. C. Lassiter, and D. J. DePaolo (1996), Helium isotopic evolution of Mauna Kea volcano: First results from the 1-km drill core, *J. Geophys. Res.*, *101*, 11,781–11,791.
- Kurz, M. D., J. Curtice, D. E. Lott III, and A. Solow (2004), Rapid helium isotopic variability in Mauna Kea shield lavas from the Hawaiian Scientific Drilling Project, *Geochem. Geophys. Geosyst.*, *5*, Q04G14, doi:10.1029/2002GC000439.
- Kushiro, I. (1996), Partial melting of a fertile mantle peridotite at high pressures: An experimental study using aggregates of diamond, in *Earth Processes: Reading the Isotopic Code*, *Geophys. Monogr. Ser.*, vol. 95, edited by A. Basu and S. Hart, pp. 109–122, AGU, Washington, D. C.
- Lassiter, J. C., and E. H. Hauri (1998), Osmium-isotope variations in Hawaiian lavas: Evidence for recycled oceanic lithosphere in the Hawaiian plume, *Earth Planet. Sci. Lett.*, *164*, 483–496.
- Lassiter, J. C., E. H. Hauri, P. W. Reiners, and M. O. Garcia (2000), Generation of Hawaiian post-erosional lavas by melting of a mixed lherzolite/pyroxenite source, *Earth Planet. Sci. Lett.*, *178*, 269–284.
- Lipman, P. W. (1995), Declining growth of Mauna Loa during the last 100,000 years: Rates of lava accumulation vs. gravitational subsidence, in *Mauna Loa Revealed: Structure, Composition, History, and Hazards*, edited by J. M. Rhodes and J. P. Lockwood, pp. 45–80, AGU, Washington, D. C.
- Lipman, P. W., J. M. Rhodes, and G. B. Dalrymple (1990), The Ninole basalt—Implications for the structural evolution of Mauna Loa volcano, Hawaii, *Bull. Volcanol.*, *53*, 1–19.
- Lipman, P. W., T. W. Sisson, T. Ui, J. Naka, and J. R. Smith (2002), Ancestral submarine growth of Kilauea volcano and instability of its south flank, in *Hawaiian Volcanoes: Deep Underwater Perspectives*, edited by E. Takahashi et al., pp. 161–191, AGU, Washington, D. C.
- Longhi, J. (2002), Some phase equilibrium systematics of lherzolite melting: I, *Geochem. Geophys. Geosyst.*, *3*(3), 1020, doi:10.1029/2001GC000204.
- Longhi, J., and V. Pan (1988), A reconnaissance study of phase boundaries in low-alkali basaltic liquids, *J. Petrol.*, *29*, 115–147.
- Macdonald, G. A. (1968), Composition and origin of Hawaiian lavas, *Mem. Geol. Soc. Am.*, *116*, 477–522.
- Macdonald, G. A., and T. Katsura (1964), Chemical composition of Hawaiian lavas, *J. Petrol.*, *5*, 82–133.
- Mangan, M. T., C. C. Heliker, T. N. Mattox, J. P. Kauahikaua, and R. T. Helz (1995), Episode-49 of the Puu-Oo Kupaianaha eruption of Kilauea volcano—Breakdown of a steady-state eruptive era, *Bull. Volcanol.*, *57*, 127–135.
- Moore, J. G., and D. A. Clague (1987), Coastal lava flows from Mauna Loa and Hualalai volcanoes, Kona, Hawaii, *Bull. Volcanol.*, *49*, 752–764.
- Moore, J. G., and D. A. Clague (1992), Volcano growth and evolution of the island of Hawaii, *Bull. Geol. Soc. Am.*, *104*, 1471–1484.
- Moore, J. G., D. A. Clague, and W. R. Normark (1982), Diverse basalt types from Loihi seamount, Hawaii, *Geology*, *10*, 88–92.
- Moore, J. G., D. J. Fornari, and D. A. Clague (1985), Basalts from the 1877 submarine eruption of Mauna Loa, Hawaii: New data on the variation of palagonitization rate with temperature, *U.S. Geol. Surv. Bull.*, *1663*, 1–11.
- Moore, J. G., D. A. Clague, K. R. Ludwig, and R. K. Mark (1990a), Subsidence and volcanism of the Haleakala ridge, Hawaii, *J. Volcanol. Geotherm. Res.*, *42*, 273–284.
- Moore, J. G., W. R. Normark, and B. J. Szabo (1990b), Reef growth and volcanism on the submarine southwest rift zone of Mauna Loa, Hawaii, *Bull. Volcanol.*, *52*, 375–380.
- Moore, J. G., W. B. Bryan, M. H. Beeson, and W. R. Normark (1995), Giant blocks in the South Kona landslide, Hawaii, *Geology*, *23*, 125–128.
- Muir, I. D., and C. E. Tilley (1963), Contributions to the petrology of Hawaiian basalts: II. The tholeiitic basalts of Mauna Loa and Kilauea, *Am. J. Sci.*, *261*, 111–128.
- Mukhopadhyay, S., J. C. Lassiter, K. A. Farley, and S. W. Bogue (2003), Geochemistry of Kauai shield-stage lavas: Implications for the chemical evolution of the Hawaiian plume, *Geochem. Geophys. Geosyst.*, *4*(1), 1009, doi:10.1029/2002GC000342.
- Naka, J., T. Kanamatsu, P. W. Lipman, T. W. Sisson, N. Tsuboyama, J. K. Morgan, J. R. Smith, and T. Ui (2002), Deep-sea volcanoclastic sedimentation around the southern flank of Hawaii, in *Hawaiian Volcanoes: Deep Underwater Perspectives*, edited by E. Takahashi et al., pp. 29–50, AGU, Washington, D. C.
- Navon, O., and E. Stolper (1987), Geochemical consequences of melt percolation: The upper mantle as a chromatographic column, *J. Geol.*, *95*, 285–307.
- Norman, M. D., and M. O. Garcia (1999), Primitive magmas and source characteristics of the Hawaiian plume: Petrology and geochemistry of shield picrites, *Earth Planet. Sci. Lett.*, *168*, 27–44.
- Norman, M. D., M. O. Garcia, V. S. Kamenetsky, and R. L. Nielsen (2002), Olivine-hosted melt inclusions in Hawaiian picrites: Equilibration, melting, and plume source characteristics, *Chem. Geol.*, *183*, 143–168.
- Pearce, J. A., and I. J. Parkinson (1993), Trace element models for mantle melting: Application to volcanic arc petrogenesis, in *Magmatic Processes and Plate Tectonics*, edited by H. M. Prichard et al., *Geological Soc. Spec. Publ.*, *76*, 373–403.
- Petermann, M., and M. M. Hirschmann (2003), Anhydrous partial melting experiments on MORB-like eclogite: Phase relations, phase compositions and mineral/melt partitioning of major elements at 2–3 GPa, *J. Petrol.*, 2173–2201.
- Phipps Morgan, J. (1999), Isotope topology of individual hot-spot basalt arrays: Mixing curves or melt extraction trajectories?, *Geochem. Geophys. Geosyst.*, *1*, Paper number 1999GC000004.
- Pietruszka, A. J., and M. O. Garcia (1999a), A rapid fluctuation in the mantle source and melting history of Kilauea volcano inferred from the geochemistry of its historical summit lavas (1790–1982), *J. Petrol.*, *40*, 1321–1342.
- Pietruszka, A. J., and M. O. Garcia (1999b), The size and shape of Kilauea volcano's summit magma storage reservoir: A geochemical probe, *Earth Planet. Sci. Lett.*, *167*, 311–320.
- Putirka, K. (1999), Clinopyroxene + liquid equilibria to 100 kbar and 2450 K, *Contrib. Mineral. Petrol.*, *135*, 151–163.
- Quane, S. L., M. O. Garcia, H. Guillou, and T. P. Hulsebosch (2000), Magmatic history of the east rift zone of Kilauea

- volcano, Hawaii based on drill core from SOH 1, *J. Volcanol. Geotherm. Res.*, *102*, 319–338.
- Reiners, P. W. (2002), Temporal-compositional trends in intraplate basalt eruptions: Implications for mantle heterogeneity and melting processes, *Geochem. Geophys. Geosyst.*, *3*(2), 1011, doi:10.1029/2001GC000250.
- Rhodes, J. M. (1995), The 1852 and 1868 Mauna Loa picrite eruptions: Clues to parental magma compositions and the magmatic plumbing system, in *Mauna Loa Revealed: Structure, Composition, History, and Hazards*, edited by J. M. Rhodes and J. P. Lockwood, pp. 241–262, AGU, Washington, D.C.
- Rhodes, J. M. (1996), Geochemical stratigraphy of lava flows sampled by the Hawaii Scientific Drilling Project, *J. Geophys. Res.*, *101*, 11,729–11,746.
- Rhodes, J. M., and S. R. Hart (1995), Episodic trace element and isotopic variations in historical Mauna Loa lavas: Implications for magma and plume dynamics, in *Mauna Loa Revealed: Structure, Composition, History, and Hazards*, edited by J. M. Rhodes and J. P. Lockwood, pp. 263–288, AGU, Washington, D.C.
- Rhodes, J. M., and M. J. Vollinger (2004), Composition of basaltic lavas sampled by phase-2 of the Hawaii Scientific Drilling Project: Geochemical stratigraphy and magma types, *Geochem. Geophys. Geosyst.*, *5*, Q03G13, doi:10.1029/2002GC000434.
- Rhodes, J. M., K. P. Wenz, C. A. Neal, J. W. Sparks, and J. P. Lockwood (1989), Geochemical evidence for invasion of Kilauea's plumbing system by Mauna Loa magma, *Nature*, *337*, 257–260.
- Ribe, N. M., and U. R. Christensen (1999), The dynamical origin of Hawaiian volcanism, *Earth Planet. Sci. Lett.*, *171*, 517–531.
- Ribe, N. M., and M. D. Smooke (1987), A stagnation point flow model for melt extraction from a mantle plume, *J. Geophys. Res.*, *92*, 6437–6443.
- Ryan, M. P., R. Y. Koyanagi, and R. S. Fiske (1981), Modeling the three-dimensional structure of macroscopic magma transport systems: Application to Kilauea volcano, Hawaii, *J. Geophys. Res.*, *86*, 7111–7129.
- Salters, V. J. M., J. E. Longhi, and M. Bizimis (2002), Near mantle solidus trace element partitioning at pressures up to 3.4 GPa, *Geochem. Geophys. Geosyst.*, *3*(7), 1038, doi:10.1029/2001GC000148.
- Schiano, P., J. M. Eiler, I. D. Hutcheon, and E. M. Stolper (2000), Primitive CaO-rich, silica-undersaturated melts in island arcs: Evidence for the involvement of clinopyroxene-rich lithologies in the petrogenesis of arc magmas, *Geochem. Geophys. Geosyst.*, *1*, Paper number 1999GC000032.
- Seaman, C., S. Sherman, M. O. Garcia, M. Baker, B. Balta, and E. Stolper (2004), Volatiles in glasses from the HSDP2 drill core, *Geochem. Geophys. Geosyst.*, *5*, doi:10.1029/2003GC000596, in press.
- Sherman, S. B., M. O. Garcia, and E. Takahashi (2002), Major element geochemistry of glasses in turbidites as source indicators: Implications for the Nu'uau and Wailau giant submarine landslides, in *Hawaiian Volcanoes: Deep Underwater Perspectives*, edited by E. Takahashi et al., pp. 263–277, AGU, Washington, D. C.
- Shinozaki, K., Z.-Y. Ren, and E. Takahashi (2002), Geochemical and petrological characteristics of Nuuanu and Wailau landslide blocks, in *Hawaiian Volcanoes: Deep Underwater Perspectives*, edited by E. Takahashi et al., pp. 297–310, AGU, Washington, D. C.
- Sims, K. W. W., D. J. DePaolo, M. T. Murrell, W. S. Baldrige, S. J. Goldstein, and D. A. Clague (1995), Mechanisms of magma generation beneath Hawaii and mid-ocean ridges: Uranium/thorium and samarium/neodymium isotopic evidence, *Science*, *267*, 508–512.
- Sisson, T. W., P. W. Lipman, and J. Naka (2002), Submarine alkali through tholeiitic shield-stage development of Kilauea volcano, Hawai'i, in *Hawaiian Volcanoes: Deep Underwater Perspectives*, edited by E. Takahashi et al., pp. 193–219, AGU, Washington, D. C.
- Smith, J. R., K. Satake, J. K. Morgan, and P. Lipman (2002), Submarine landslides and volcanic features on Kohala and Mauna Kea volcanoes and the Hana ridge, Hawaii, in *Hawaiian Volcanoes: Deep Underwater Perspectives*, edited by E. Takahashi et al., pp. 11–28, AGU, Washington, D. C.
- Sobolev, A. V., A. W. Hofmann, and I. K. Nikogosian (2000), Recycled oceanic crust observed in 'ghost plagioclase' within the source of Mauna Loa lavas, *Nature*, *404*, 986–990.
- Spiegelman, M., and P. B. Kelemen (2003), Extreme chemical variability as a consequence of channelized melt transport, *Geochem. Geophys. Geosyst.*, *4*(7), 1055, doi:10.1029/2002GC000336.
- Stracke, A., V. J. M. Salters, and K. W. W. Sims (1999), Assessing the presence of garnet-pyroxenite in the mantle sources of basalts through combined hafnium-neodymium-thorium isotope systematics, *Geochem. Geophys. Geosyst.*, *1*, Paper number 1999GC000013.
- Takahashi, E., and K. Nakajima (2002), Melting processes in the Hawaiian plume: An experimental study, in *Hawaiian Volcanoes: Deep Underwater Perspectives*, edited by E. Takahashi et al., pp. 403–418, AGU, Washington, D. C.
- Tanaka, R., E. Nakamura, and E. Takahashi (2002), Geochemical evolution of Koolau volcano, Hawaii, in *Hawaiian Volcanoes: Deep Underwater Perspectives*, edited by E. Takahashi et al., pp. 311–332, AGU, Washington, D. C.
- Tatsumoto, M. (1978), Isotopic composition of lead in oceanic basalt and its implications to mantle evolution, *Earth Planet. Sci. Lett.*, *38*, 63–87.
- Thy, P. (1995), Low-pressure experimental constraints on the evolution of komatiites, *J. Petrol.*, *36*, 1529–1548.
- Thy, P., G. E. Lofgren, and P. Imsland (1991), Melting relations and the evolution of the Jan Mayen magma system, *J. Petrol.*, *32*, 303–332.
- Thy, P., C. E. Leshner, and M. S. Fram (1998), Low-pressure experimental constraints on the evolution of basaltic lavas from Site 917, southeast Greenland continental margin, in *Proc. Ocean Drill. Program Sci. Results*, *152*, 359–372.
- Thy, P., C. E. Leshner, and J. D. Mayfield (1999), Low-pressure melting studies of basalt and basaltic andesite from the southeast Greenland continental margin and the origin of dacites at Site 917, in *Proc. Ocean Drill. Program Sci. Results*, *163*, 95–112.
- Tilley, C. E., and J. H. Scoon (1960), Differentiation of Hawaiian basalts—Some variants in lava suites of dated Kilauean eruptions, *J. Petrol.*, *1*, 47–55.
- Toplis, M. J., and M. R. Carroll (1995), An experimental study of the influence of oxygen fugacity on Fe-Ti oxide stability, phase relations, and mineral-melt equilibria in ferro-basaltic systems *J. Petrol.*, *36*, 1137–1170.
- Tormey, D. R., T. L. Grove, and W. B. Bryan (1987), Experimental petrology of normal MORB near the Kane fracture zone: 22°–25°N, mid-Atlantic ridge, *Contrib. Mineral. Petrol.*, *96*, 121–139.
- Wagner, T. P., and T. L. Grove (1998), Melt/harzburgite reaction in the petrogenesis of tholeiitic magma from Kilauea volcano, Hawaii, *Contrib. Mineral. Petrol.*, *131*, 1–12.

- Walter, M. J. (1998), Melting of garnet peridotite and the origin of komatiite and depleted lithosphere, *J. Petrol.*, *39*, 29–60.
- Wang, K., T. Plank, J. D. Walker, and E. I. Smith (2002), A mantle melting profile across the Basin and Range, SW USA, *J. Geophys. Res.*, *107*(B1), 2017, doi:10.1029/2001JB000209.
- Wang, Z., N. E. Kitchen, and J. M. Eiler (2003), Oxygen isotope geochemistry of the second HSDP core, *Geochem. Geophys. Geosyst.*, *4*(8), 8712, doi:10.1029/2002GC000406.
- Watson, S., and D. McKenzie (1991), Melt generation by plumes: A study of Hawaiian volcanism, *J. Petrol.*, *32*, 501–537.
- Weaver, B. L. (1991), The origin of ocean island basalt end-member compositions: Trace element and isotopic constraints, *Earth Planet. Sci. Lett.*, *104*, 381–397.
- West, H. B., M. O. Garcia, F. A. Frey, and A. Kennedy (1988), Nature and cause of compositional variation among the alkalic cap lavas of Mauna Kea volcano, Hawaii, *Contrib. Mineral. Petrol.*, *100*, 383–397.
- Wolfe, E. W., W. S. Wise, and G. B. Dalrymple (1995), Geology and petrology of Mauna Kea volcano, Hawaii: A study of postshield volcanism, *U.S. Geol. Surv. Prof. Pap.*, *1557*.
- Wright, T. L. (1971), Chemistry of Kilauea and Mauna Loa lava in space and time, *U.S. Geol. Surv. Prof. Pap.*, *735*.
- Wright, T. L., and R. T. Helz (1996), Differentiation and magma mixing on Kilauea's east rift zone: A further look at the eruptions of 1955 and 1960. 2. The 1960 lavas, *Bull. Volcanol.*, *57*, 602–630.
- Yang, H.-J., F. A. Frey, M. O. Garcia, and D. A. Clague (1994), Submarine lavas from Mauna Kea volcano, Hawaii: Implications for Hawaiian shield-stage processes, *J. Geophys. Res.*, *99*, 15,577–15,594.
- Yang, H.-J., F. A. Frey, J. M. Rhodes, and M. O. Garcia (1996a), Evolution of Mauna Kea volcano: Inferences from lava compositions recovered in the Hawaii Scientific Drilling Project, *J. Geophys. Res.*, *101*, 11,747–11,767.
- Yang, H.-J., R. J. Kinzler, and T. L. Grove (1996b), Experiments and models of anhydrous, basaltic olivine-plagioclase-augite saturated melts from 0.001 to 10 kbar, *Contrib. Mineral. Petrol.*, *124*, 1–18.